Coarse-graining Dendritic Macromolecules: from Conformations to Phase Behaviour

Inaugural-Dissertation

zur
Erlangung des Doktorgrades der
Mathematisch-Naturwissenschaftlichen Fakultät
der Heinrich-Heine-Universität Düsseldorf

vorgelegt von

INGO O. GÖTZE

aus Neuss

Düsseldorf, 13. Mai 2005

Gedruckt mit der Genehmigung der
Mathematisch-Naturwissenschaftlichen Fakultät
der Heinrich-Heine-Universität Düsseldorf

Referent:	Prof. C. N. Likos, Ph. D.
Korreferenten:	Prof. Dr. R. Egger Prof. Dr. G. Gompper

Tag der mündlichen Prüfung: 27.06.2005

This thesis is based on the following original papers:

Chapter 3
Conformations of Flexible Dendrimers: A Simulation Study
Götze, I. O.; Likos, C. N. *Macromolecules* **2003**, *36*, 8189.

Chapter 4 and Appendix
Tunable effective interactions between dendritic macromolecules
Götze, I. O.; Harreis, H. M.; Likos, C. N. *J. Chem. Phys.* **2004**, *120*, 7761.

Chapter 5
Microscopic and coarse-grained correlation functions of concentrated dendrimer solutions
Götze, I. O.; Likos, C. N. *J. Phys.: Condens. Matter* **2005**, *17*, S1777.

Chapter 6
Macro-phase and Micro-phase Separation in Dendrimer Mixtures
Götze, I. O.; Archer, A. J.; Likos, C. N. *J. Chem. Phys.* **2005** in preparation.

Abstract

In this thesis we examine the behaviour of dendritic macromolecules at various levels of description, ranging from the conformations of isolated dendrimers to the macroscopic phase behaviour of dendrimer mixtures and bridging thereby the length scales from nanometer to centimetres. Starting at the monomer level, we introduce a very simple coarse-grained model, termed ‘bead-thread’ model, and analyse, by employing monomer-resolved Monte Carlo simulations, the radial monomer density distributions and the form factors of isolated dendrimers for various generation numbers and flexibility. Here, we observe dense-core density profiles due to backfolding of the end monomers. By comparing the results to those of a more complex, well-established model, we find a clear insensitivity to model details. Moreover, the validity of this simple model is confirmed by comparison to the form factor from experimental scattering data. We then proceed to determine, by means of simulations that employ the bead-thread model, the effective interaction potential between the centres of mass of two dendrimers. The resulting potentials can be cast in a Gaussian form, whose strength and range can be tuned by variation of the generation number and the flexibility of the spacers. Based on the isolated dendrimer density profiles, the simulational results are corroborated by density functional theory, in which the connectivity of the monomers is approximated by an external confining potential holding the monomer beads together. The simplicity of the bead-thread model allows monomer-resolved simulation of large systems containing many dendrimers. Concomitantly, we perform ‘effective simulations’ considering the dendrimers as point particles interacting by means of the previously calculated effective interaction potentials. Comparison of both approaches enables a test of the so-called factorisation approximation, which is widely used for derivation of the structure factor from experimental scattering data. Here, we find that for high densities, uncritical application of this approximation leads to incorrect results. Furthermore, we test the validity of the pair potential approximation, where it turns out that the effects of many-body forces are small and they become weaker as the dendrimer flexibility increases. Finally, employing effective interactions enables us to investigate the behaviour of two-component dendrimer mixtures by means of an accurate density functional approach. To this end, we use the Gaussian potentials obtained from monomer-resolved simulations for dendrimers of different generation number and flexibility. Depending on the dendrimers’ architecture, we find either macroscopic demixing or micro-phase separation and pattern formation under confinement. We supplement our study with simulations performed employing the effective potentials, finding good agreement with theory.

Zusammenfassung

Die vorliegende Arbeit befaßt sich mit dem Verhalten dendritischer Makromoleküle auf verschiedenen Ebenen der Beschreibung – von den Konformationen isolierter Dendrimere bis hin zum makroskopischen Phasenverhalten von Dendrimermischungen, wobei Längenskalen von Nanometern bis Zentimeter überbrückt werden. Wir beginnen auf der Ebene der Monomere und führen ein sehr einfaches vergröbertes Modell ein. Für dieses bestimmen wir mit Hilfe von monomeraufgelösten Monte-Carlo-Simulationen die radiale Segmentdichteverteilung, die aufgrund der Rückfaltung der Endmonomere ein Maximum im Zentrum des Moleküls aufweist, sowie die Formfaktoren isolierter Dendrimere verschiedener Generationen und Flexibilität. Ein Vergleich mit einem komplexeren, zur Beschreibung von Dendrimeren häufig verwendeten Modell zeigt deutlich, daß eine Unempfindlichkeit der Ergebnisse gegenüber den Details des verwendeten Modells besteht. Zudem wird die Gültigkeit des einfachen Modells durch Vergleich mit experimentellen Streudaten bekräftigt. Als nächstes bestimmen wir mittels monomeraufgelöster Simulationen die effektive Wechselwirkung zwischen den Schwerpunkten zweier Dendrimere. Wir erhalten gaußförmige Potentiale, deren Stärke und Reichweite durch die Wahl der Generationszahl und der Flexibilität des dendritischen Grundgerüsts eingestellt werden kann. Auf Basis der Dichteprofile einzelner Dendrimere untermauern wir unsere Ergebnisse durch eine Dichtefunktionaltheorie, bei der die Bindungen der Monomere durch ein externes Potential ersetzt werden, welches die Monomere zusammenhält. Die Einfachheit des eingeführten Modells ermöglicht monomeraufgelöste Simulationen größer Systeme, die aus mehreren Dendrimeren bestehen. Zugleich verwenden wir die zuvor berechneten Potentiale in effektiven Simulationen; dabei werden die Dendrimere als Punktteilchen aufgefaßt, die vermittels der effektiven Potentiale miteinander wechselwirken. Durch Vergleich beider Methoden läßt sich die bei der Bestimmung von Strukturfaktoren aus experimentellen Streudaten häufig angewandte Faktorisierungsnäherung überprüfen, wobei sich herausstellt, daß eine unkritische Anwendung derselben bei hohen Dichten zu fehlerhaften Resultaten führt. Des Weiteren untersuchen wir die Gültigkeit der Paarpotentialnäherung, mit dem Ergebnis, daß der Einfluß der Vielkörperkräfte gering ist, und mit zunehmender Flexibilität der Dendrimere abnimmt. Schließlich sind wir durch die Verwendung effektiver Wechselwirkungen in der Lage, das Verhalten zweikomponentiger Dendrimermischungen mittels Dichtefunktionaltheorie zu untersuchen. Zu diesem Zweck verwenden wir Gauß'sche Potentiale aus monomeraufgelösten Simulationen von Dendrimeren verschiedener Generationen und Flexibilität. Abhängig von der spezifischen Dendrimerarchitektur tritt dabei makroskopische Entmischung oder Mikrophasenseparation auf, und wir beobachten die Bildung von Mustern in begrenzten Systemen. Wir ergänzen unsere Untersuchungen durch effektive Simulationen, wobei gute Übereinstimmung mit der Theorie besteht.

Contents

Chapter 1

Introduction

Dendrimers are synthetic macromolecules with a tree-like[1], well-defined branched structure [1]. Due to their peculiar architecture and the flexibility in modifying it in various ways [2], dendrimers have attracted the interest of chemists and soft matter physicists, leading to an almost exponential increase in the number of publications on this topic since they have been synthesised for the first time in 1978 by Vögtle *et al.* [3] and later by Newkome *et al.* [4] and Tomalia *et al.* [5]. Simultaneously, a wealth of potential applications in miscellaneous fields of research opened up, ranging from rheology modification or chemical catalysis to medical applications, e. g. as host molecules for controlled release of pharmaceuticals, for gene transfer or as contrast agents in anticancer therapy [6–10]. Complementary to their importance in applications is their relevance as monodisperse, globular model macromolecules that form hybrids between polymeric solutions and colloidal suspensions. The aforementioned flexibility in modifying the architecture of the molecules enables to control the macroscopic behaviour of solutions at the microscopic level. Here, bridging the gap between the relevant length scales is a challenge for soft matter physicists.

In order to design dendrimers purposefully for particular applications, accurate understanding of their conformations is crucial. In this context, the question whether there are cavities inside the dendrimer, where guest molecules could be encapsulated [11], is of special interest. In this respect, the equilibrium structure of flexible, neutral dendrimers, i. e., the radial density distribution of the monomers within the macromolecule, has been discussed controversially for a long time [12–17]: the two-dimensional rendition of the dendrimer's shape shown in Figure 1.1 suggests a structure with internal voids and with a dense shell, whereas backfolding of the branches leads to an increase of the monomer density in the centre of the molecule (dense-core model). We shall return to this question in chapter 3.

---

[1] The term "dendrimer" is composed of the Greek words for 'tree' and 'part', *dendron* ($\delta\acute{\epsilon}\nu\delta\rho o\nu$) and *meros* ($\mu\acute{\epsilon}\rho o\varsigma$) respectively.

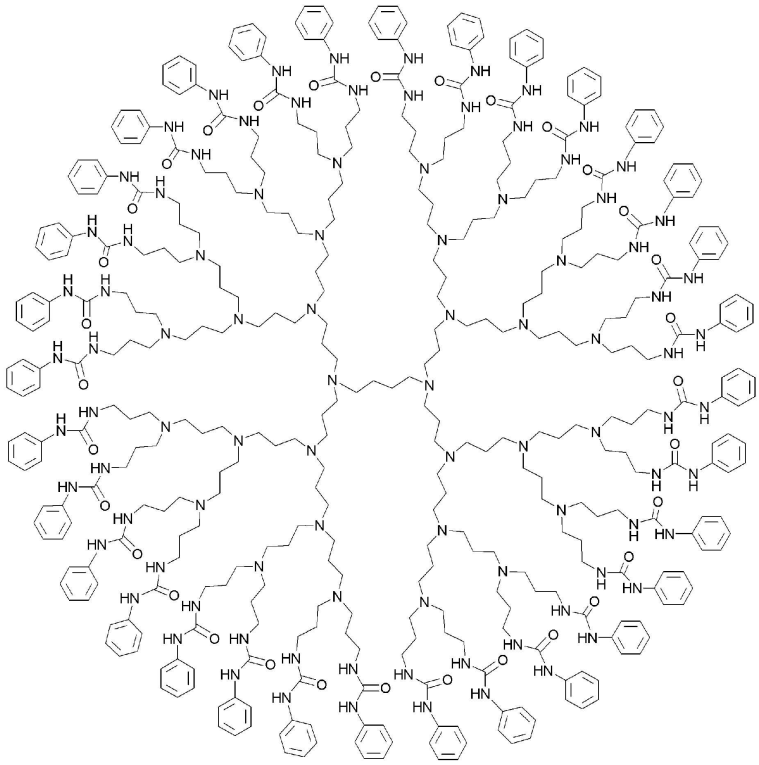

Figure 1.1: Chemical structure of a dendrimer of fourth generation (courtesy of Matthias Ballauff).

Similar to other complex materials [18–20], dendrimers can be characterised by a hierarchy of different length scales, as illustrated in Fig. 1.2. Although in principle possible, simulations at the atomistic level, in which detailed force fields for the individual atoms are employed, are restricted in practical use to very small systems due to their demand for computational resources [21–25]. It is thus desirable to develop a model, which is simple enough to be simulated by standard techniques and at the same time also sufficiently realistic to capture the salient features of the dendrimers' behaviour at the mesoscopic level.

At length scales of the order of a few Ångström, details of the chemical bondings are important (Fig. 1.2 d)). But for many problems, as for example the conformational characteristics of the dendritic backbone, it is sufficient to look upon the macromolecule at larger, coarse-grained level, where the fluctuating positions of the individual atoms comprising the dendrimer are irrelevant. Here, several atoms can be grouped together to effective monomers (Fig. 1.2 c)), and microscopic details are mapped to this coarse-grained model [18, 20]. For flexible dendrimers, the steric repulsion and the bonding interactions of these groups can be modeled by means of

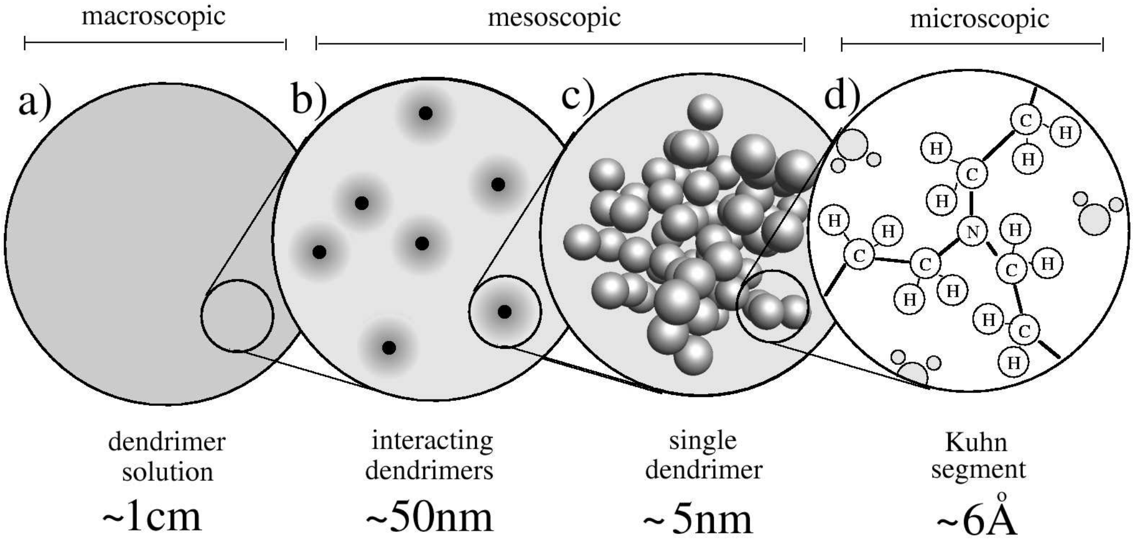

Figure 1.2: Schematic illustration of the varios length scales in dendrimer solutions.

simple, radially symmetric pair potentials. As the influence of the solvent molecules is also included in the effective monomer-monomer interaction, the number of particles which have to be considered is decreased drastically. Concomitantly, in spite of all those simplifications, atomistic and coarse grained simulations of isolated dendrimers lead to very similar results for the radial density distribution [24, 25]. The reduction of the number of particles and degrees of freedom in coarse-grained models allows efficient simulations of systems large enough for investigating intermolecular statistical quantities.

Considering solutions of dendrimers, one can go even one step further in coarse-graining: here, the dominant length scale is the size of the dendrimer. Indeed, in order to study macroscopic samples, it is inevitable to make simplifications due to the huge number of the involved particles. Since the trajectories of the individual fluctuating monomers are unimportant for the questions under consideration, it is pertinent to choose one effective coordinate that represents the whole macromolecule (for example the centre of mass). By tracing out the monomer degrees of freedom, an effective pair interaction potential with respect to the centres of the macromolecules can be derived [19]. In a dendrimer solution the individual macromolecules feature different conformations due to fluctuations of the monomers, resulting in an almost spherical statistical intramolecular monomer distribution. For the statistical behaviour of the macromolecules only the average over all conformations and orientations of the interacting dendrimers has to be taken into account, provided no phases with orientational order appear. Hence, the interaction between the macromolecules can be described by a radially symmetric potential (Fig. 1.2 b)), although a dendrimer is a complex, structured object. Once this effective interaction is known, the phase behaviour of the solution can be predicted by means of theory or simulations, regarding the macromolecules as point particles interacting via this potential. Thus, effective interactions are a powerful tool to bridge the length scales and to extract macroscopic properties from microscopic details.

As outlined before, simplifications are unavoidable when investigating macroscopic properties of soft matter systems; this holds for the development of appropriate models as well as for analytical theories based upon the same. Due to the loss of details associated with the procedure of coarse graining and approximations made in theories, consistency with experiments and other levels of description has to be checked carefully. When comparing theoretical results to experiments, discrepancies can arise from an inadequate underlying model, an inaccurate theory, or both. Here, computer simulations play an important role as they can provide exact results (within certain limitations) for a given model [26, 27]. Comparison of the simulational results to those of experiments constitutes a test of the employed model. On the other hand, comparison to theoretical predictions provides the opportunity to test the validity of a theory. The latter may, in turn, yield results beyond the scope of simulations, which are restricted to small particle numbers. Moreover, simulations can help to interpret experimental data, as it will be demonstrated in chapter 5.4.

The main purpose of this work is to find appropriate descriptions for dendrimers at various levels of coarse graining. At first, the use of a very simple monomer-resolved coarse grained model is justified by means of simulations and comparison to experimental data. This model is utilised in the next step of coarse graining in order to derive the effective interactions. The latter are then employed in simulations and for theoretical predictions of concentrated solutions and dendrimer mixtures.

The rest of this work is organised as follows: In chapter 2, quantities characterising the dendrimers are presented. Moreover, a very simple coarse grained model describing neutral flexible dendrimers in athermal solvents is introduced. This model is employed in Monte Carlo (MC) simulations in chapter 3. By comparing the static conformational properties of isolated dendrimers to the standard coarse grained model of Murat and Grest [28] and to experimental scattering data, the use of this simple model is established, which provides an increased performance in MC simulations and thus allows study of larger systems. In chapter 4, the effective interaction of dendrimers is calculated by means of simulations and density functional theory (DFT). The resulting pair potentials can be tuned by changing microscopic parameters. By comparing results of simulations employing the effective pair interaction to those of monomer-resolved simulations at various concentrations, the significance of many-body effects in concentrated solutions is examined in chapter 5. In addition, the monomer-resolved simulations also provide a test of the validity of the oft-used factorisation approximation to the total scattering intensity into a product of the form- and scattering factors. In chapter 6, the effective interactions are employed to investigate the behaviour of dendrimer mixtures by means of theory and simulations, revealing interesting properties such as demixing, micro-phase separation or pattern formation under confinement, depending on microscopic properties related to the dendrimers' architecture. Finally, in chapter 7 a summary and conclusions are presented.

Chapter 2

Basics

In this chapter, we introduce the fundamental quantities that characterise dendrimers and solutions of the same. We also present a simple coarse grained model ('bead-thread model') whose properties are subject of the next chapters of this study. Further, we give a brief overview over Monte Carlo (MC) simulations.

2.1 Terminology

In the synthesis of dendrimers, a stepwise iterative reaction is employed [13, 17]: starting with an initiator core with f reactive sites, f linear polymer chains consisting of P segments are attached to it, forming the zeroth generation of the molecule, $g = 0$. P is referred to as the spacer length. At the end of those chains there are again functional units, where $f - 1$ new chains can be attached, forming the next generation of the dendrimer. In each reaction step, the number of generations is increased by one, and the procedure is repeated, until the terminal generation G is reached. The individual generations within a dendrimer are labelled by the generation index g, with $0 \leq g \leq G$. Thus, the various experimentally realised types of dendrimers can be specified by three numbers: the functionality f, the terminal G and the spacer length P. It is convenient to denote dendrimers as Gn, where n is a positive integer denoting the final generation number.

In this work, we focus on the usual case of trifunctional units ($f = 3$). The studied dendrimers have the architecture sketched in Figure 1.1. Here, the dendra (branches) emanate from *two* connected trifunctional units and thereby the two central monomers comprise the zeroth-order generation, $g = 0$.[1] In this architecture, the total number of monomers $N(g)$ up to the g-th generation is given by

$$N(g) = (f-1)\left[(f-1)^{g+1} - 1\right], \tag{2.1}$$

---

[1] Due to this architecture, the core has the functionality 4 instead of 3. However, none of the conclusions in this work is essentially affected by this modification in the architecture.

where $f = 3$. The total degree of polymerization is $N = N(G)$. For $G \gg 1$, the ratio of the monomers at the terminal generation, $N_{\text{end}} = N(G) - N(G-1) = (f-1)^{G+1}$ obeys the relation $N/N_{\text{end}} \to 2$, thus there are as many end-monomers as in all previous generations. This exponential growth of the number of monomers with G is a unique characteristic of the dendrimers and arises from their hierarchical, self-similar architecture. It immediately has as consequence that above a certain maximum generation no space is any more available to accommodate the self-avoiding monomers and dendrimers cannot be grown any more.

2.2 Characteristic Quantities

2.2.1 Intramolecular Properties

In this section, we introduce some important intramolecular statistical quantities which describe the average behaviour of the fluctuating monomers within one dendrimer. This dendrimer does not necessesarily have to be an *isolated* dendrimer. In presence of other dendrimers, the average over all macromolecules is taken.[2] As this average is trivial and for the sake of clarity, we define here all quantities for only one dendrimer, labelled α. The position of its centre of mass is

$$\mathbf{R}_\alpha = \frac{1}{N}\sum_{i=1}^{N}\mathbf{r}_\alpha^i, \tag{2.2}$$

whereby $\mathbf{r}_\alpha^i$ are the instantaneous positions of the N monomers comprising the dendrimer.

The Radial Monomer Density Distribution

Dendrimers are subject to internal fluctuations which entail a large number of possible conformations. For the most problems, only the average conformation of the fluctuating monomers is relevant, which can be described by the radial monomer distribution. Since our dendrimers lack a single central monomer, we are led to consider the radial monomer density distributions $\xi(r)$ with respect to their centres of mass instead. It is defined as

$$\xi(r) = \left\langle \sum_{i=1}^{N}\delta(\mathbf{r} - \mathbf{r}_\alpha^i + \mathbf{R}_\alpha)\right\rangle. \tag{2.3}$$

The process of taking configurational averages, $\langle\cdots\rangle$ in Eq. (2.3), renders the density distribution radially symmetric. The same procedure can be applied to monomers

---

[2] In that case these quantities become concentration dependent.

belonging to any chosen generation g; of particular importance are those of the terminal generation $g = G$ and their density distribution will be denoted by $\xi_{\text{end}}(r)$.

The Radius of Gyration

The size of the dendrimer can be characterised by the radius of gyration, R_g, defined as

$$R_g = \sqrt{\frac{1}{N}\left\langle \sum_{i=1}^{N} (\mathbf{r}_\alpha^i - \mathbf{R}_\alpha)^2 \right\rangle}. \tag{2.4}$$

Equation (2.4) can be directly employed to calculate R_g in simulations. Its experimental value can be extracted from the small-q behaviour of the form factor.

The Form Factor

The form factor $F(q)$ depending on the wavenumber q is a very useful quantity as it contains information on the size and shape of the molecules on the one hand and it provides a direct link with experiments on the other. Indeed, when scattering (light, x-rays or neutrons) from dilute suspensions, the coherent scattering intensity $I_S(q)$ at scattering wavevector q is proportional to the form factor $F(q)$ [29,30]. The latter is defined as [31–33]

$$F(q) = 1 + \frac{1}{N}\left\langle \sum_{i=1}^{N} \sum_{j \neq i}^{N} \exp[-i\mathbf{q} \cdot (\mathbf{r}_\alpha^i - \mathbf{r}_\alpha^j)] \right\rangle, \tag{2.5}$$

with the scattering wavevector $\mathbf{q} = \mathbf{q}_{\text{out}} - \mathbf{q}_{\text{in}}$, and $q = \frac{4\pi}{\lambda}\sin(\theta/2)$ for elastic scattering, λ being the wavelength and θ the scattering angle. The behaviour of $F(q)$ at small values of the wavenumber allows to determine experimentally the gyration radius, since it holds [32]

$$F(q) \cong N\left[1 - \frac{(qR_g)^2}{3}\right] \qquad (qR_g \ll 1). \tag{2.6}$$

By comparison of the experimental value of R_g to the simulational one, the absolute length scale in coarse grained simulations can be defined.

2.2.2 Intermolecular Properties

The following quantities characterise the dendrimers' behaviour in solutions, describing the individual molecules as a whole, represented by their centres of mass.

The Pair Correlation Function

Let $\rho = M/\Omega$ be the number density of the sample containing M dendrimers in a volume Ω. The radial pair distribution function $G(R)$ between the centres of mass is defined as

$$G(R) = \frac{1}{\rho M} \left\langle \sum_{\alpha=1}^{M} \sum_{\beta \neq \alpha}^{M} \delta\left(\mathbf{R} - \mathbf{R}_{\alpha\beta}\right) \right\rangle , \tag{2.7}$$

where $\langle \cdots \rangle$ denotes a statistical average and $\mathbf{R}_{\alpha\beta} = \mathbf{R}_\alpha - \mathbf{R}_\beta$ is the relative vector between the centres of mass of the dendrimers α and β. In a uniform system, rotational and translational invariance implies that the pair correlation function only depends on the magnitude $R = |\mathbf{R}|$ of the separation vector [34]. The pair distribution function $G(R)$ is a measure for the probability of finding two dendrimers at a distance R, relative to the probability expected for a completely random distribution at the same density [26].

The Structure Factor

Related to this quantity is the structure factor $S(\mathbf{q})$ that describes the correlations between the centres of mass in reciprocal space. In isotropic and homogeneous fluids, $S(\mathbf{q})$ is a function only of the wavenumber $q = |\mathbf{q}|$ [31] and it is given by

$$S(q) = \frac{1}{M} \left\langle \sum_{\alpha=1}^{M} \sum_{\beta=1}^{M} \exp\left[-\mathrm{i}\mathbf{q} \cdot \mathbf{R}_{\alpha\beta}\right] \right\rangle . \tag{2.8}$$

Note that $S(q)$ and $G(R)$ are related by a Fourier transformation [31]

$$S(q) = 1 + \rho \int \mathrm{d}\mathbf{R} \exp\left[-\mathrm{i}\mathbf{q} \cdot \mathbf{R}\right] \left[G(R) - 1\right] . \tag{2.9}$$

The connection to the experimental measured scattering intensity of concentrated solutions will be studied in chapter 5 in more detail.

2.3 The Model

Before introducing the bead-thread model, which will be subject of large parts of this work, we first present the well-established model of Murat and Grest [28]. The latter will be used as a reference model for the comparison of the conformational properties.

Though the bond angles and lengths of the C-C bonds building the dendritic backbone are almost fixed, they also have rotational degrees of freedom, so that after a couple of successive bonds with different orientation the information on the original direction is lost, giving rise to flexibility of the dendrimer. Hence, it is reasonable to assume connected branching points as freely jointed and having a maximum distance. Due to the steric repulsion of the monomers, there is an excluded volume, i. e., a minimum distance between branching points. Thus, the dendrimer can be represented by effective monomers (Kuhn segments) which are treated as bonded spherical beads. Hereafter, the beads are simply termed 'monomers' but one should keep in mind that these are not true monomers in the chemical sense.

Since the length scales characterising the solvent and the dissolved particles are vastly different, it is reasonable to treat the former as a continuum, leading to a reduction of complexity, as there is no need to simulate and to keep track of all those solvent molecules. All that matters is the solvent quality (a fact borrowed from polymer theory on linear chains). Therefore, the solvent is taken into account only as an effective medium and the solubility of the polymers is encapsulated in a small number of parameters, such as the excluded-volume parameter or the form of the monomer-monomer interaction potential.

In the model originally introduced by Murat and Grest, the interaction between monomers is described by a pure repulsive Lennard-Jones like potential, and the bonds by the finite-extensible-nonlinear-elastic (FENE) potential [28]. (hereafter referred to as FENE-LJ model). In detail, the potential $U_{\mathrm{mm}}(r)$ between non-bonded monomers in this model is given by

$$U_{\mathrm{mm}}(r) = \begin{cases} \phi_{\mathrm{LJ}}(r) - \phi_{\mathrm{LJ}}(r_c) & \text{for} \quad r \leq r_c; \\ 0 & \text{for} \quad r > r_c, \end{cases} \tag{2.10}$$

where $\phi_{\mathrm{LJ}}(r)$ is the standard Lennard-Jones interaction

$$\phi_{\mathrm{LJ}}(r) = 4\epsilon \left[\left(\frac{\sigma_{\mathrm{LJ}}}{r} \right)^{12} - \left(\frac{\sigma_{\mathrm{LJ}}}{r} \right)^{6} \right]. \tag{2.11}$$

The cutoff distance r_c allows for the modeling of solvents of varying quality. The choice $r_c = 2^{1/6}\sigma_{\mathrm{LJ}}$ renders the monomer-monomer interaction purely repulsive and thus suitable for an effective description of athermal solvents. Increasing r_c adds an attractive tail to the interaction. In this way, the value of the second virial coefficient B_2 of the interaction can be tuned so that good ($B_2 > 0$), poor ($B_2 < 0$) and Θ ($B_2 = 0$) solvents can be incorporated into the model. Here we compare our results with those obtained by employing [35] $r_c = 2^{1/6}\sigma_{\mathrm{LJ}}$ that models athermal solvents. Furthermore, bonded monomers are connected via a FENE potential U_{FENE}, acting in addition to U_{mm}:

$$U_{\mathrm{FENE}}(r) = \begin{cases} -15\epsilon \left(\frac{R_0}{\sigma_{\mathrm{LJ}}} \right)^2 \ln \left[1 - \left(\frac{r}{R_0} \right)^2 \right] & \text{for} \quad r \leq R_0; \\ \infty & \text{for} \quad r > R_0, \end{cases} \tag{2.12}$$

where $R_0 = 1.5\sigma_{\mathrm{LJ}}$ and $T = 1.2\epsilon/k_B$. This model was also recently employed by Harreis *et al.* [35] in an analysis of the fluctuations of G4-dendrimers and it was shown that it produces excellent agreement with small-angle neutron scattering (SANS) measurements for the form factor.

The essential features of the FENE-LJ model are a strong repulsion between monomers and a maximum bond length. An even simpler model featuring the same characteristics is defined by a Hard-Sphere interaction $V_{\mathrm{HS}}(r)$ that plays the role of $U_{\mathrm{mm}}(r)$ and ideal 'threads' with a maximum extension $(1+\delta)\sigma$ that connect the beads and whose effect is given by the interaction potential $V_{\mathrm{bond}}(r)$ below. Explicitly, we have

$$V_{\mathrm{HS}}(r) = \begin{cases} \infty & \text{for} \quad r/\sigma < 1 \\ 0 & \text{otherwise} \end{cases} \tag{2.13}$$

for non-bonded monomers and

$$V_{\mathrm{bond}}(r) = \begin{cases} \infty & \text{for} \quad r/\sigma < 1 \\ 0 & \text{for} \quad 1 < r/\sigma < 1+\delta \\ \infty & \text{for} \quad r/\sigma > 1+\delta \end{cases} \tag{2.14}$$

for bonded monomers, i.e., the hard spheres of diameter σ are surface-to-surface connected by threads of contour length $\delta\sigma$. In order to avoid the occurrence of ghost chains during the simulations, i. e., crossing of bonds, δ has to be chosen smaller than $\sqrt{2}-1 \cong 0.414$. However, when only statical problems are considered, this restriction is not necessary. This bead-thread model was employed in the recent work of Sheng *et al.* [36] who examined the dependence of the radius of gyration of dendrimers on the spacer length P and generation number, restricted to the case $\delta = 0.4$. No results for density distributions or form factors were examined, however.

In the limit $\delta = 0$, the bead-thread model reduces to tangent hard spheres, a model commonly used for simulations of polymers. Lue and Prausnitz [37] have also employed the tangent hard spheres-model to simulate dendrimers, with the difference that there the angle between two bonds at each branching site was fixed to 120°. The stiffness of the bead-thread model dendrimer can be tuned by varying the surface-to-surface thread length δ. In addition to the special choice of the potential, the flexibility of the dendrimer can also be modified by the number of spacer beads between the branching points. Here, we examine exclusively dendrimers without additional spacer beads ($P = 1$).

Figure 2.1 shows a snapshot of a typical conformation of a G4-dendrimer, generated during the simulation employing the bead-thread model.

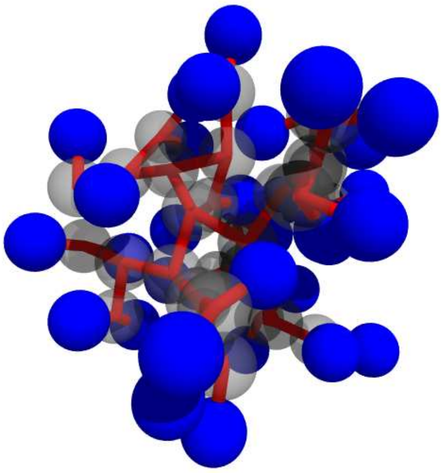

Figure 2.1: Simulation snapshot of a G4 dendrimer using the bead-thread model with $\delta = 0.10$. The blue spheres of diameter σ denote the monomers of the end groups, while all other monomers are represented by semi-transparent spheres. The bonds between the monomers are rendered as cylinders. The spread of the end-monomers inside the dendrimer can be clearly discerned.

2.4 Monte Carlo Simulations

Following references [31], [26] and [27], we give a brief introduction into Monte Carlo techniques.

Let $\mathbf{r}^N \equiv \{\mathbf{r}_1, ..., \mathbf{r}_N\}$ denote the positions of N particles with the total potential energy $V_N(\mathbf{r}^N)$. The canonical ensemle average of a function F of the particle coordinates can be written as [31]

$$\langle F \rangle = \frac{\displaystyle\int F(\mathbf{r}^N) \exp[-\beta V_N(\mathbf{r}^N)] \, d\mathbf{r}^N}{\displaystyle\int \exp[-\beta V_N(\mathbf{r}^N)] \, d\mathbf{r}^N} \quad . \tag{2.15}$$

Evaluating these $3N$ dimensional configurational integrals with standard numerical methods is practically impossible. Another approach to calculate the ensemble avarage is to generate a large number $\mathcal{N}$ of random configurations of the particles. This ‘brute force’ Monte Carlo method is inefficient, because it is likely that vast majority of the generated configurations have an extremely small Boltzmann factor and thus would yield a negligible contribution. It is thus desirable, to generate configurations more frequently in those regions of the configuration space that contribute most to the integrals in (2.15). When such a non-uniform distribution is applied, the bias introduced in the sampling is corrected by weighting the configurations appropriately. If $W(m)$ is the probability of choosing a configuration m with a total potential energy $V_N(m)$, equation (2.15) must be replaced by [31]

$$\langle F \rangle \approx \frac{\sum\limits_{m=1}^{\mathcal{N}} F(m)\exp[-\beta V_N(m)]/W(m)}{\sum\limits_{m=1}^{N} \exp[-\beta V_N(m)]/W(m)} \quad . \tag{2.16}$$

Here, the Boltzmann distribution itself,

$$W(m) \propto \exp[-\beta V_N(m)] \quad , \tag{2.17}$$

is of particular interest, because in this case equation (2.15) reduces to

$$\langle F \rangle \approx \frac{1}{\mathcal{N}} \sum_{m=1}^{\mathcal{N}} F(m) \quad . \tag{2.18}$$

The canonical average is therefore obtained as an *unweigthed* average over configurations in the sample [31].

The principal difficulty is to find a procedure which generates configurations with the desired distribution. The Metropolis algorithm is a technique employed in standard MC simulations to generate a sequence of random states, i. e., a trajectory in the configuration space, according to the Boltzmann distribution: Starting from a system in a state m, a new *trial* configuration n is generated which only slightly differs from m (by displacing one of the N particles by a small random vector $\delta\mathbf{r}$). Let $\Delta V_N = V_N(n) - V_N(m)$ be the difference in the total potential energy of the old and the new trial state. If the new configuration is energetically more favourable, i. e., $\Delta V_N < 0$, the new configuration is accepted. In the other case ($\Delta V_N > 0$), the trial move is accepted only with the probability $\exp(-\beta\,\Delta V_N)$. In this case, whether a trial move is accepted or rejected is decided by generating a random number $\xi \in [0, 1]$: if $\xi \leq \exp(-\beta\,\Delta V_N)$, it is accepted, otherwise, the displaced particle is set back to its old position.

In case of short range interactions (short compared to the size of the simulation box), most particles do not contribute to the energy of a particle i. As the energy calculation is time consuming, it is desirable only to take into account the particles in the vicinity of the particle under consideration and to exclude the non-interacting particles from this calculation. This can be achieved by using Verlet lists, cell lists, or a combination of both methods [27, 38, 39].

In Monte Carlo simulations of the bead-thread model, it is not necessary to calculate the potential energy or the forces; one only needs to check for overlaps of particles, and whether the maximum bond length condition is fulfilled. If one of these conditions is violated, the trial move is rejected in any case, so the search for further overlaps can be aborted. Furthermore, due to the very short range of the hard sphere interaction, neighbour lists are very efficient. Therefore, Monte Carlo simulations of this model are very fast, which is important due to the exponential growth of the number of monomers with the generation number.

Chapter 3

Isolated Dendrimers

In this chapter, we examine the sizes and conformations of flexible dendrimers of generation numbers $G = 4$ *to* $G = 9$ *by means of Monte Carlo simulations on a coarse-grained level. To this end, we introduce a simple, 'bead-thread' model with variable thread-to-bead size ratio* δ*. In addition, we compare the results from this model to previously calculated ones, based on a soft-sphere–spring model, in order to test the dependence of the results on the microscopic details. We find a clear insensitivity of the resulting conformational properties on those, both models leading to dense-core density profiles and to increasingly compact structures upon increase of the terminal generation. Moreover, we calculate the distribution of the end-monomers, which turns out to be broad and extending throughout the volume occupied by the dendrimer. The dependence of the radius of gyration* R_g *on the monomer number* N *does not follow the scaling law* $R_g \sim N^{1/3}$ *that has been often put forward in the literature, but rather it obeys, for high generation numbers, a dependence of the form* $R_g \sim N^{0.24}$*. (Published in Ref. [75].)*

3.1 Introduction

Research on dendrimers is a part of modern nano-science with the aim of tailoring material properties at the molecular level. The motivation for the current investigations rests on the enormous flexibility in modifying the architecture of the dendrimers, in line with the general scheme sketched above, and which leads to the possibility of adapting dendrimers to meet various needs in applications [2]. The two-dimensional rendition of the dendrimer's shape shown in Figure 1.1 suggests a structure with internal voids and with a dense shell, and has thus led to the concept of the hollow 'dendritic box' that can be employed as carrier for smaller molecules encapsulated in its interior [11]. This *dense-shell* or *hollow-core* model of dendrimers was also put forward in the early theoretical analysis of de Gennes and Hervet [12] that was based on self-consistent field (SCF) calculations. Following the pioneering work of Lescanec and Muthukumar [14], however, it has been demonstrated in various simulational studies during the last 10 years that the dense-shell model does not describe the conformations of self-avoiding, neutral dendrimers, as we discuss in more detail below. The pitfall in the SCF-calculations of de Gennes and Hervet has been their implicit assumption that the end-groups of the dendrimers are localised on their periphery. When this restriction is relaxed, then the improved SCF calculations lead to the opposite, *dense-core* picture of the dendrimers, in which the monomer density monotonically decays with the distance from their centre and the end-monomers are distributed throughout the molecule. The pioneering theoretical study that led to the dense-core model has been carried out by Boris and Rubinstein [15]. Zook and Pickett [16] have recently revisited the arguments of de Gennes and Hervet and pointed out to the weakness that led to the erroneous, dense-shell prediction. The problem lies in the assumption that there is a unique, typical trajectory of a chain that dominates all others, equivalently, a unique 'ground state' of the system. However, it turns out that there are infinitely many, degenerate trajectories for the self-consistent potential, in analogy to the well-known case of the parabolic, planar polymer brush [40]. When the degeneracy is taken into account, a parabolic density profile with a maximum at the core as well as a distribution of the chain tips throughout the dendrimer [16].

Various different models for dendrimers have been proposed in simulation studies of the same, ranging from atomistic ones [21–24], in which detailed force-fields are employed, to coarse-grained ones [28, 35–37, 44–49], in which the steric and bonding interactions are modeled by means of simple, radially symmetric pair potentials. Often the simulations of coarse-grained models require specially designed algorithms, such as pivot moves [45, 46]. Also, some of the simulations are performed on lattice models and there special care has to be taken in order to employ moving algorithms that satisfy detailed balance [41, 42, 44, 51]. It is desirable, thus, to develop an off-lattice model, so that an artificial discretization of space can be avoided, which at the same time is simple enough to be simulated by standard techniques and also sufficiently realistic to capture the salient features of the dendrimers' behavior at the mesoscopic length scale.

In this chapter, we introduce a model for dendrimers that is particularly well-suited for performing Monte-Carlo (MC) simulations. Due to its simplicity, it allows for a systematic investigation of the dendrimers' properties for a a wide range of generations G. Moreover, its implementation can be carried out by employing the standard, Metropolis Monte Carlo algorithm: no resorting to specially designed moves is necessary. In our approach, we envision every monomer as a hard sphere of diameter σ whereas the bonding between monomers is modeled by flexible threads of maximum extension $\Delta = \sigma(1 + \delta)$. The extension of the thread can be varied and offers one tunable parameter for the model. On the other hand, in order to test the sensitivity of the conformational properties of the dendrimers on the details of the microscopic interactions employed, we compare the results of the bead-thread model to those of the standard model of Murat and Grest [28]. We examine exclusively dendrimers with spacer length $P = 1$ and we adopt the notation G for the terminal generation and $g \leq G$ to denote internal generations within the dendrimer. The main results of our work read as follows: we find clear evidence of *universality* of the static conformational properties of the dendrimers at the mesoscopic level. When scaled with the radius of gyration, density profiles and form factors arising from different models practically collapse on one another for a wide parameter range. Moreover, we calculate the evolution of the scattering form factor with generation, finding a tendency of the molecules towards sphericity and compactness with growing G, in accordance with recent experimental results [52]. The distribution of end-monomers is also broad, once again in agreement with recent SANS measurements [43]. Finally, the radius of gyration R_g does not scale with the number of monomers N as a simple power law for the whole range of N considered.

3.2 Simulation Details

We simulated dendrimers of terminal generations $G = 4$ to $G = 9$ having the architecture sketched in Figure 1.1. To generate an initial configuration, a dendrimer of generation G is built of a dendrimer of generation $G - 1$ by trying to attach the additional end groups during a separate Monte Carlo simulation. To achieve this, for all monomers of the generation $G - 1$ that do not have end-groups yet, we generate randomly two test monomers at a distance σ. These two test monomers are checked for overlap with each other and all other existing monomers. If no overlap occurs, the test monomers are accepted as end monomers and subsequently they are allowed to move up to a maximum distance $(1 + \delta)\sigma$ from their parent monomer, according to Eq. (2.14). Otherwise, new positions for the test monomers are generated up to 100 times. This procedure is repeated during each MC step.

As an alternative way to produce the initial configuration, we also generate one of the two arms of the dendrimer randomly, which is subsequently duplicated and mirrored. These two arms are then pulled together in a separate MC simulation. In order to create the random arm, we use a recursive function that creates two new randomly oriented unit-vectors to a given vector, i.e., the direction of the connection between the considered monomer and its origin monomer in the generation below. For these two new positions, overlaps are checked and, if they are accepted, the function calls itself for these two vectors until the requested generation number is reached. If after 10 000 test positions no two new vectors could be found, the recursion is aborted and started anew at the central monomer. This second method, though, yielded accepted configurations within feasible time scales only up to terminal generations $G = 7$; for higher G's the required time turns out to be prohibitively long. We have tested that the two methods of generating the initial configuration lead to identical conformational averages after the equilibration time, guaranteeing that the dendrimers have relaxed and we are indeed sampling equilibrium configurations. We were not able to find any acceptable initial states for dendrimers larger than G9 employing thread lengths $\delta = 0.05$ and 0.10. However, growth of a G10-dendrimer has been achieved with thread lengths $\delta = 0.30$ and 0.40. Typically, after a phase of equilibration of 10^7 Monte Carlo steps, 10^8 (for G4) to 10^9 (for G9) MC steps were simulated, of which 4×10^5 to 4×10^6 configurations were used to calculate the statistical averages. In order to provide an additional check of the equilibration procedure, we increased the equilibration time by a factor 10, especially for the G8 and G9 dendrimers, finding no change in the resulting density profiles and sizes beyond the level of statistical noise. Moreover, since there is no energy to be monitored during equilibration in our model (pure hard sphere interactions), we have monitored instead the growth of the radius of gyration during the process of adding end-groups to generate dendrimer GN from an equilibrated dendrimer G$(N - 1)$. Throughout the process of adding the endgroups, R_g grows monotonically. After all the endgroups have been attached, R_g shows small variations well within the equilibration time but after no more that 50 000 MC steps it saturates to its final value and only shows statistical-noise variance around its average thereafter.

3.3 Density Distributions

In this section we present the results regarding the density distributions from MC simulations of the bead-thread model with varying thread length δ and their comparisons with those from MC simulations of the FENE-LJ model described above [35].

The results for the density distribution of a G4 dendrimer are shown in Figure 3.1. The local minimum at $r = 0$ arises from the fact that the centre of mass is located in the neighbourhood of the midpoint between the two monomers making up the zeroth generation and in this region few monomers can be found. Otherwise, we obtain typical dense-core profiles, with a narrow minimum after the first peak that comes about from the coordination between the $g = 0$- and $g = 1$-monomers. As can also be seen in Figure 2.1, end-monomers are distributed throughout the dendrimer. A striking feature that emerges from the comparison between the density profiles of the bead-thread model with two different thread lengths ($\Delta \equiv \delta\sigma = 0.05\,\sigma$ and $0.10\,\sigma$), as well as with the density profile from the FENE-LJ model, is their strong insensitivity on the details of the microscopic interactions employed. When plotted by using σ or σ_{LJ} as units of length, the density profiles from the different models do differ. In particular, with increasing δ, the density spreads out to larger distances and at the same time its height becomes smaller (so that its integral remains fixed to the number of monomers N). However, when the unit of length is rescaled to the gyration radius R_g, all curves practically collapse on one another. The effect of changing the thread's contour length can still be discerned in the slightly weaker correlations present for larger δ but it is rather small (see also Figure 3.2). When the constraint $\delta < \sqrt{2} - 1$ is lifted, so that crossing of bonds is also allowed, the correlation peaks disappear with growing thread length and the dense core character becomes even more pronounced (Figure 3.3).

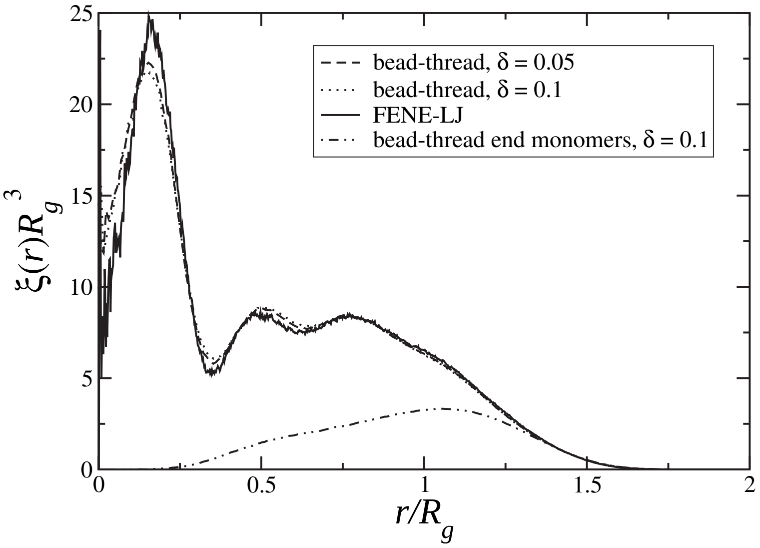

Figure 3.1: Radial density distribution of a G4 dendrimer with respect to the centre of mass, normalised by the radius of gyration R_g. The solid line shows the result for the FENE-LJ model (Ref. [35], courtesy of Holger Harreis), the dashed and dotted lines are the results for the bead-thread model with the values $\delta = 0.05$ and 0.10. The density distribution of the end-monomers for the bead-thread model is shown as dashed-dotted line.

The procedure of using the radius of gyration as the length scale is not only the natural one for the coarse-grained description of the dendrimers but it provides contact with experiments as well. Indeed, the microscopic parameter σ has no direct physical meaning, apart from the obvious requirement that it must be of the order of the length of a Kuhn segment. In adopting a certain model to describe experimental data, the radius of gyration R_g which is measurable in small-angle scattering experiments provides the missing link between theory and experiment and allows for the assignment of a certain value to the parameter σ, see also Ref. [35]. What we find here (and will be further confirmed in what follows) is that a broad one-parameter family of models, generated by a varying the absolute value of a

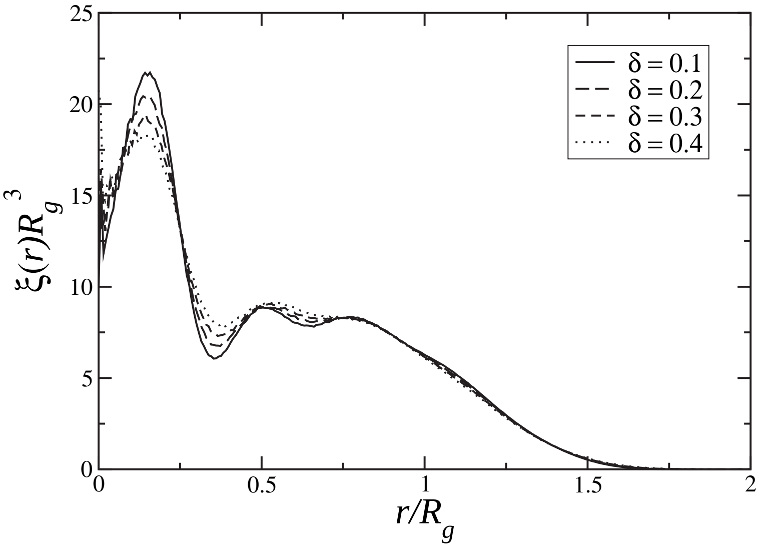

Figure 3.2: The radial density distribution of a G4 dendrimer for different values of δ. The dendrimer becomes larger for increasing δ, but R_g also increases, so that the extension of the density in terms of r/R_g remains constant. The peaks of the different shells are smeared out as δ increases, because the connections become more loose.

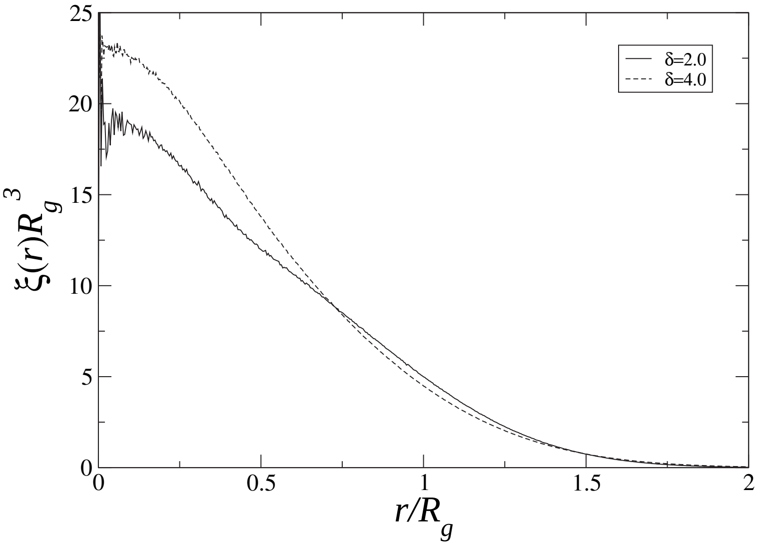

Figure 3.3: Same as Fig. 3.2, but for $\delta = 2.0, 4.0$.

single microscopic scale, lead to practically identical results for the description of the dendrimers at the nano-scale.

This universality picture is further confirmed by the results for the G5-dendrimers, shown in Figure 3.4. Comparing with the density profile of the G4-dendrimers, three features show up: first, the correlation effects manifested in the peaks and troughs of the density profile become more pronounced. Second, a plateau of roughly constant density starts developing in the region $0.5 \lesssim r/R_g \lesssim 1.0$ but it should be emphasised that the height of this plateau is *not* constant but growing with G. Finally, the end-monomer distribution leaks more towards the central region of the molecule. We will return to the first two points shortly.

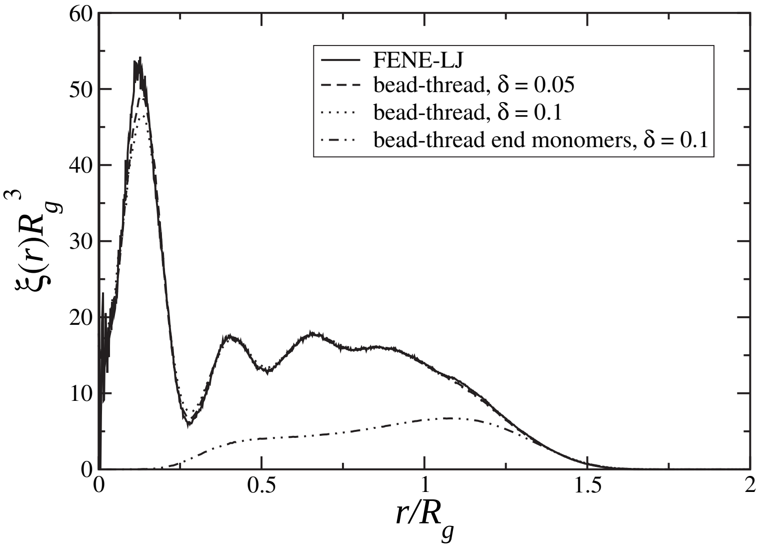

Figure 3.4: Same as Figure 3.1 but for a G5 dendrimer. The results for the LJ-FENE potential (solid line) are courtesy of Holger Harreis.

At this stage, it is interesting to monitor the development of the end-monomer distribution as a function of G for high generation numbers, G6 to G9. The result is shown in Figure 3.5. The outermost part of the dendrimer is populated by end-monomers but the converse is not true. With increasing G, the end-monomers tend to distribute themselves within the molecule. There is a depression following the maximum at the edge of the molecule, caused by the fact that there the density profile of the $G-1$-generation monomers displays its own local maximum. Some substructure is visible for $G = 8$ and $G = 9$ dendrimers. Strong back-folding of the dendra is taking place, a necessary mechanism for accommodating the increasingly large number of monomers, in agreement with findings in previous on- and off-lattice simulation studies involving a variety of model interparticle forces [14, 24, 28, 37, 44–

49]. Preceding studies were limited to generation numbers $G \leq 7$, however. In this work, we demonstrate that the backfolding mechanism is also present for higher-generation dendrimers but it can only be efficient if substantial stretching of the inner generations takes place. This stretching can be observed in Figure 3.6, where the monomer density distribution of the inner generations ($g = 0 - 8$) of a G9 dendrimer is shown together with the complete density distribution (i. e., $g = 0 - 8$ too) of a G8 dendrimer: compared to the G8 dendrimer, the density profile of inner monomers of the G9 dendrimer increases at the periphery; in other words, the inner monomers take a larger volume, and as a consequence, the average monomer density decreases in the centre of the molecule, leaving space for the additional g=9 monomers. Simultaneously, the coordination peaks slightly shift to higher radii. In order to visualise the very high degree of back-folding, we show in Figure 3.7 a simulation snapshot from a G6-dendrimer in which one selected, back-folded branch has been explicitly marked and in Figure 3.8 a snapshot of a G9-dendrimer and a view of the same configuration cut through the middle of the molecule.

By comparing Figures 2.1, 3.7, and 3.8, we first note that an increase in the terminal generation has the effect of turning the dendrimer more compact and its boundary sharper. Indeed, the loose outermost ‘blobs’ that are visible for the G4 and G6-dendrimers have disappeared in the case of the G9-molecule. The distribution of end-monomers in the whole of the molecule is evident. In the case of the G9-dendrimer, a very interesting feature emerges, namely the following: since the number of terminal monomers to be accommodated is becoming exceedingly high, the corresponding voids have to be created at some other place in the molecule, in particular in its interior. Thereby, the chains building the lower generations (up to $g = 4$) stretch and open up. The end-monomers are now folding back into precisely the voids created by this stretching, as can be seen also by comparing the terminal-generation and total density profiles in Figures 3.5 and 3.9. There is strong localization of the low-generation monomers and the dendritic structure up to $g = 4$ becomes clearly visible. This should be compared with the snapshot of a dendrimer of *terminal* generation 4 in Figure 2.1. If the bonds were omitted there, it would be hard to say that the spheres belong to a dendrimer, whereas in Figure 3.8 the dendritic architecture of the lowest generations is immediately recognizable and has a clear similarity with the ‘flattened out’, rigid chemical structure shown in Figure 1.1.

These features can be quantified by looking now at the total density profiles of the dendrimers, shown in Figure 3.9. With increasing G, strong peaks develop for the first few generations, indicating the strong localization of the monomers belonging to those and the stretching of the inner parts of the arms. This finding is in agreement with the recent theoretical results of Timoshenko *et al.* [50] who considered a model of beads connected by harmonic springs. They found that the innermost springs connecting monomers are the most extended, with the degree of

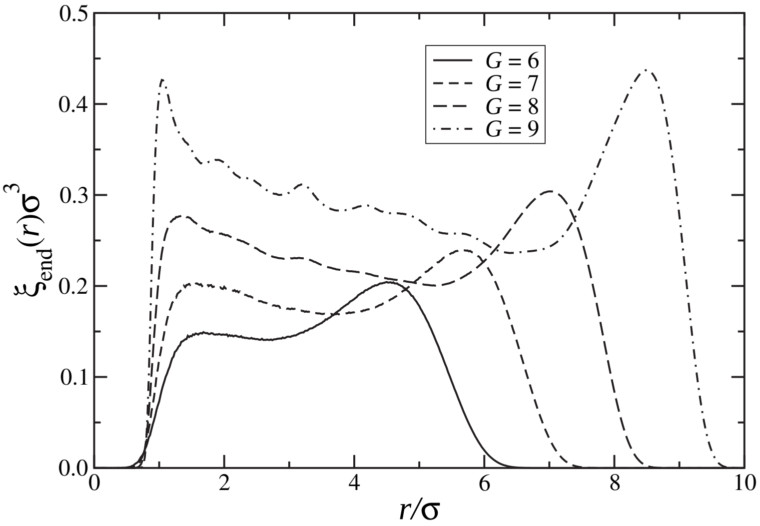

Figure 3.5: End-monomer density distributions for G6-G9 dendrimers, as obtained by the MC-simulation of the bead-thread model with $\delta = 0.10$.

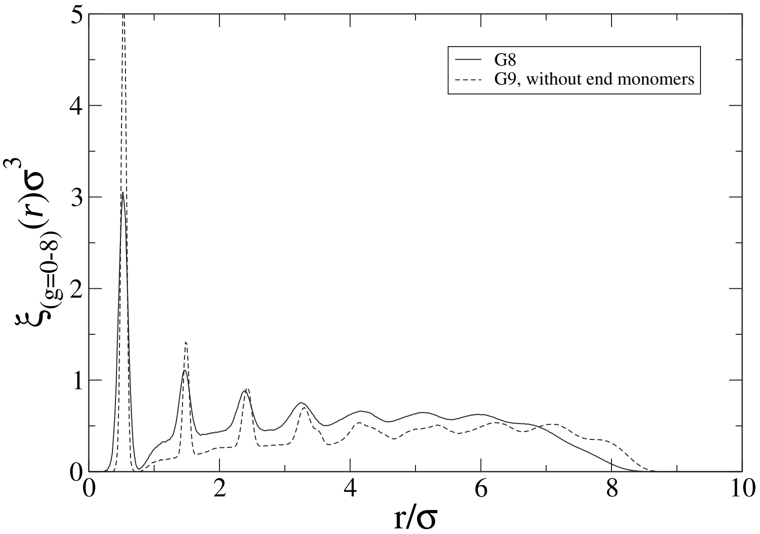

Figure 3.6: The solid line shows the overall monomer density distribution for a G8 dendrimer, and the dashed line shows monomer density distribution of the inner generations, $g <$ G, of a G9 dendrimer ($\xi(r) - \xi_{\text{end}}(r)$).

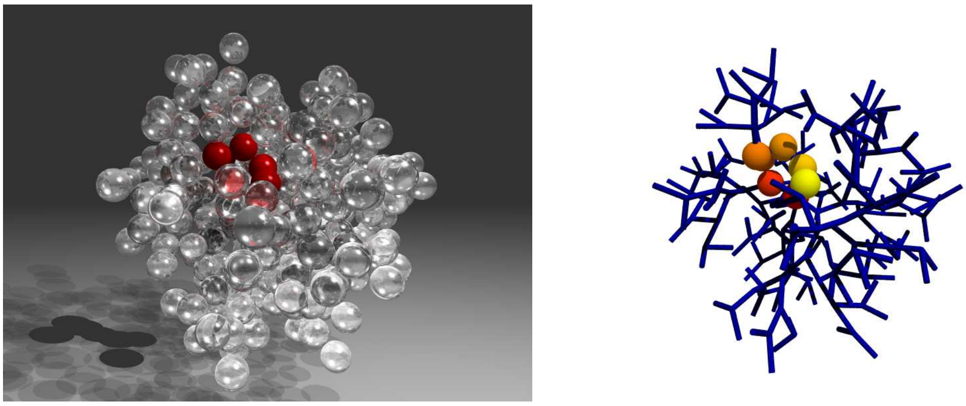

Figure 3.7: Simulation snapshot of a G6-dendrimer obtained by employing the bead-thread model with $\delta = 0.10$. The left panel shows all monomers rendered as spheres of diameter σ. A single, back-folded branch has been selected and colored red, whereas all other monomers are rendered as glass spheres. The shadowing assists in demonstrating the back-folding of the branch within the body of the dendrimer. Right panel: here only the monomers of the back-folded branch are shown as spheres and they are color-coded as follows: the end monomer is colored yellow and it is situated within the dendrimer. Starting from this, a path leads to one of the two innermost monomers, colored red. Increasing intensity of red denotes approaching of the aforementioned central monomer. All other monomers are omitted for clarity, but the bonds are rendered as cylinders.

stretching decreasing as one moves along the terminal bead along a dendrimer's branch. In comparing the locations of the weak local maxima of the end-monomer distribution for G9, shown in Figure 3.5 with the total density profile in Figure 3.9, we see that the end-monomers that fold back into the inner part of the molecule are to be found in the void regions created by the strongly stretched first few generations. These form a rigid structure, witnessed by the strong coordination peaks of the total density profiles in Figure 3.9. Additionally, we remark that the density profiles at $r = 0$ decrease to zero value upon increasing G. This implies that the centre of mass becomes more and more sharply localised at the midpoint between the two beads of the zeroth generation as G increases, where no monomers are ever found. For lower values of G, the fluctuations of the molecule can displace the centre of mass considerably and bring it occasionally in coincidence with the position of one of the central monomers, giving rise to the nonzero value of $\xi(r = 0)$. We draw the conclusion that dendrimers with $G \geq 6$ possess a rigid, non-fluctuating core consisting of the stretched first few generations and in those all (weak) fluctuations take place at the outermost part of the molecule.

Another question that has caused quite some controversy in the literature is that of the scaling of the gyration radius R_g with the number of monomers N. Lescanec

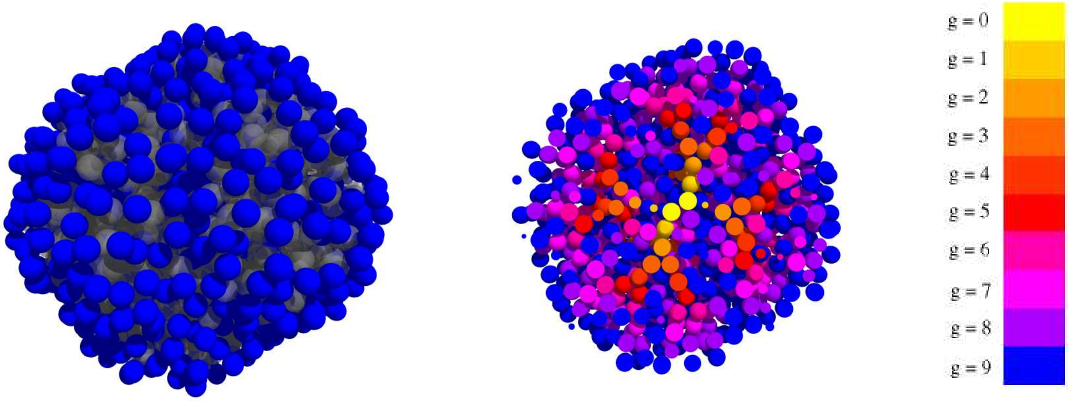

Figure 3.8: Simulation snapshot of a G9-dendrimer obtained by employing the bead-thread model with $\delta = 0.10$. The left panel shows all monomers rendered as spheres of diameter σ, with those belonging to the end-generation colored blue and all other rendered as semi-transparent spheres of diameter σ. The outer surface is covered exclusively by $g = 9$-monomers but there are also many end-monomers within the dendrimer that are somewhat obscured by the high concentration of semi-transparent spheres. Right panel: a cut through the middle of the configuration on the left, showing the coordination of the monomers belonging to various generations within the dendrimer. The generations are color-coded as indicated in the color bar on the right.

and Muthukumar [14] found in their pioneering simulation work $R_g \sim N^{0.22\pm0.02}$ but some doubts regarding the equilibrated character of their configurations remained [28]. Murat and Grest [28] on the other hand, report a scaling relation of the form $R_g \sim N^{1/3}$, indicating that dendrimers are compact structures with a constant average density within their volume. Since then, there have been various claims both in favor of the $\sim N^{1/3}$-law [22, 24, 49, 51] and in favor of a $\sim N^{1/5}$-dependence [36, 46]. Sheng *et al.* [36], who employed the same model as we do for the special case $\delta = 0.40$, offered an explanation for these discrepancies. They found that when R_g is considered as a function of N for *fixed thread length* P (the monomer number N changing through a change of the final generation G), then a scaling $R_g \sim N^{1/3}$ obtains. If one now keeps the *generation number* G *fixed* and varies N through a change of the thread length, a different scaling, $R_g \sim N^{3/5}$, identical to the behavior of linear polymers obtains. But if one wants to describe all dependencies of R_g in a single scaling law, then the correct dependence is indeed $R_g \sim (PG)^{2/5}N^{1/5}$, as conjectured by Chen and Cui [46]. In all preceding studies, typical generations range from G3 to G7 and monomer numbers lie in the domain $10 \lesssim N \lesssim 1000$.

We have also examined the N-dependence of R_g in our study, in which however we have a fixed spacer number $P = 1$ and thus we can vary N only through a vari-

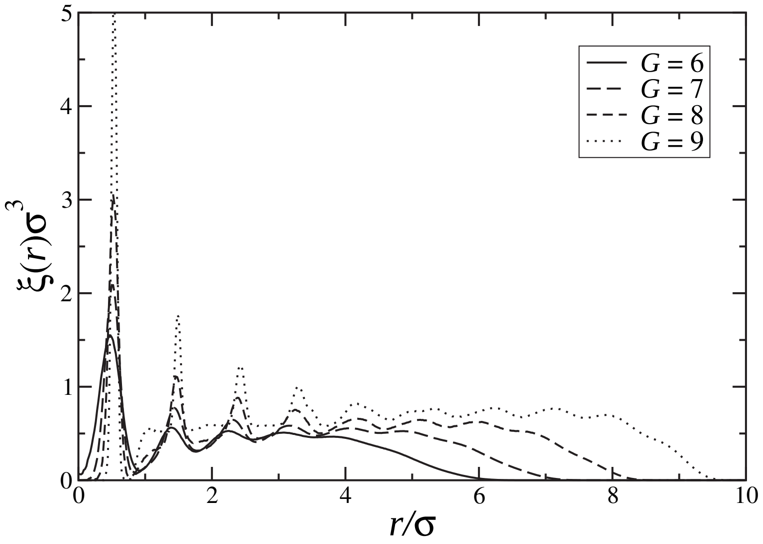

Figure 3.9: The density profiles for G6 to G9 dendrimers, obtained from the bead-thread model with $\delta = 0.10$. Here, the bead diameter σ is used as the unit of length.

ation of the generation number G. The results are shown in Figure 3.10. It is clear that a single power-law of the type $R_g \sim N^{1/3}$ does not describe the R_g-dependence in the whole range of N considered. Even at small generation dendrimers, G4 to G7, there are slight deviations from this law, which become strong for the higher generations, G7 to G9. For the latter case, a dependence of the form $R_g \sim N^{0.24}$ appears to hold. Taking into account the finding of Sheng *et al.* [36] that the correct scaling has the form $R_g \sim (PG)^{2/5}N^{1/5}$ and that in our model $P = 1$ and $G \sim \ln N$, we see that rather a dependence of the type $R_g \sim (\ln N)^{0.4}N^{0.2}$ obtains. In the N-domain corresponding to G7-G9 dendrimers, this dependence *strongly resembles* a $\sim N^{0.24}$-law. Thus, our finding should not be interpreted as a universal law but rather as a local fit of the results in the region $400 \lesssim N \lesssim 2000$. Our results are in agreement with the original prediction of an exponent $x = 0.22 \pm 0.02$ of Lescanec and Muthukumar [14] within error bars and close to the exponent 1/5 of Chen and Cui [46] and Sheng *et al.* [36]. Giupponi and Buzza [51] also reported deviations from the 1/3-exponent in their lattice model, however these were much weaker than the ones we find here. The explanation for the deviation from the 'compact sphere'-exponent 1/3 can be found in Figure 3.9 showing the density profiles of the dendrimers. It can be seen that there exists a large plateau in the monomer profiles, in which the density is roughly constant. Were this constant value to be also independent from G, this would lead to the conclusion of a $R_G \sim N^{1/3}$-dependence. We notice, however, that by increasing G the height of the plateau itself increases. Thus, if we envision the dendrimers as homogeneous spheres to a first approximation, we

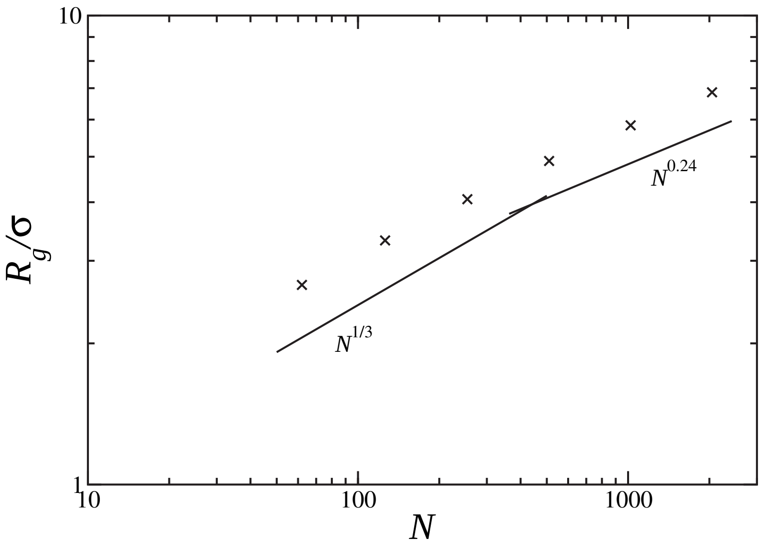

Figure 3.10: Double-logarithmic plot of the radius of gyration R_g against the number of monomers N of the dendrimers. The change in N is caused by an increase of G and the results shown are for G = 4, 5, 6, 7, 8 and 9. It can be seen that the results for large N can be fitted by a power-law $R_g \sim N^x$ with $x = 0.24$ and not by $R_g \sim N^{1/3}$. The error bars on the data are of the order of $10^{-3}\,\sigma$.

see that the density of these spheres grows with G and thus the $N(G)$ monomers are packed more and more densely. This causes the exponent to be significantly smaller than 1/3 and having the apparent value 0.24. It should also be noted that the deviation from the $R_G \sim N^{1/3}$-dependence is connected with the stretching of the innermost generations for the G7, G8 and G9-dendrimers, in conjunction with the short-spacer condition, $P = 1$, employed in our study. The innermost generations for these dendrimers cannot be described as flexible chains any more and hence a universal scaling law cannot be valid.

The existence of the density plateau is in agreement with the result of Murat and Grest [28] but our findings are at odds with their claim that the value of the density at this plateau is independent of the generation number. On the other hand, our simulation is in agreement with two recent scattering studies. A clear deviation from the $N^{1/3}$-law for dendrimers with $4 \leq G \leq 8$ has been seen in the SAXS-experiments of Rathgeber *et al.* [52] An analysis of the results reported there on the basis of a Guinier fit of the scattering intensities (Table 1 and Figure 6 of Ref. [52]) yields the law $R_g \sim N^{0.24}$, in precise agreement with our results. The authors of Ref. [52] also argued on the grounds for this slower increase of R_g along the same lines as we do.[1] Moreover, Mallamace *et al.* [53] report for high-generation dendrimers a scaling

---

[1] The dendrimers of Ref. [52] had again a slightly different architecture than ours, for which the

exponent $R_g \sim N^{0.21}$ from a Guinier fit of SAXS-measurements, again close the value 0.24 we obtained in our simulations but very different from the oft-proposed value 0.33.

3.4 Form Factors

An important test for a coarse grained model lies in examining whether its form factor, equation (2.5), reproduces the experimental scattering data. Very good agreement between the experimentally determined form factor for G4-dendrimers and the one obtained from simulations of the FENE-LJ model has been found in Ref. [35].

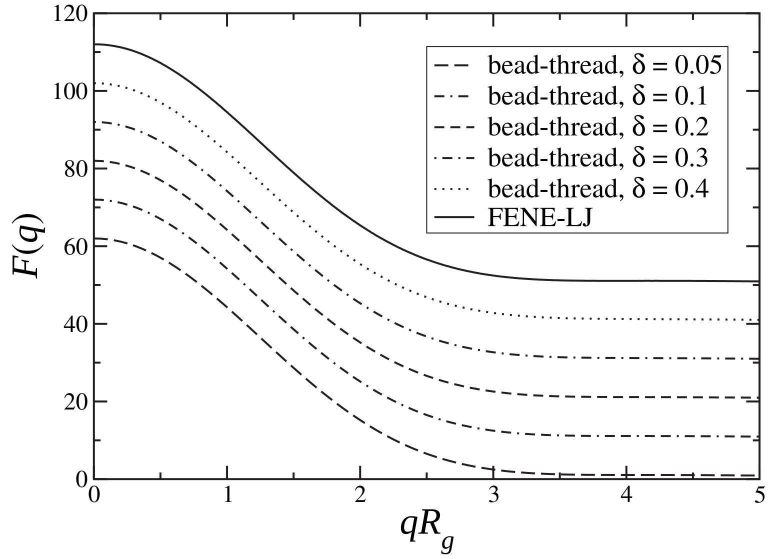

Figure 3.11: Form factors of G4 dendrimers (solid line: FENE-LJ model, Ref. [35]; dashed lines: bead-thread model with $\delta/\sigma = 0.05, 0.10, 0.20, 0.30, 0.40$). For clarity, the curves have been shifted upwards in amounts of 10 (from bottom to top), otherwise they all collapse and they become indistinguishable.

It can be seen from Figure 3.11, that the simulated form factor is nearly independent of microscopic details like the thread length δ within a wide parameter range, or even the model type itself (FENE-LJ, bead-thread), when q is scaled with the

---

number of monomers $M(g)$ up to generation g is given by $M(g) = (f-1)^{g+3} - f$. Comparing this relation with Eq. (2.1), we find $N(g) = M(g-1) + 1 \cong M(g-1)$ since $M(g-1) \gg 1$. Thus our simulation results for dendrimers of generation G correspond, in the notation of Ref. [52], to experimental ones for dendrimers of generation $G-1$.

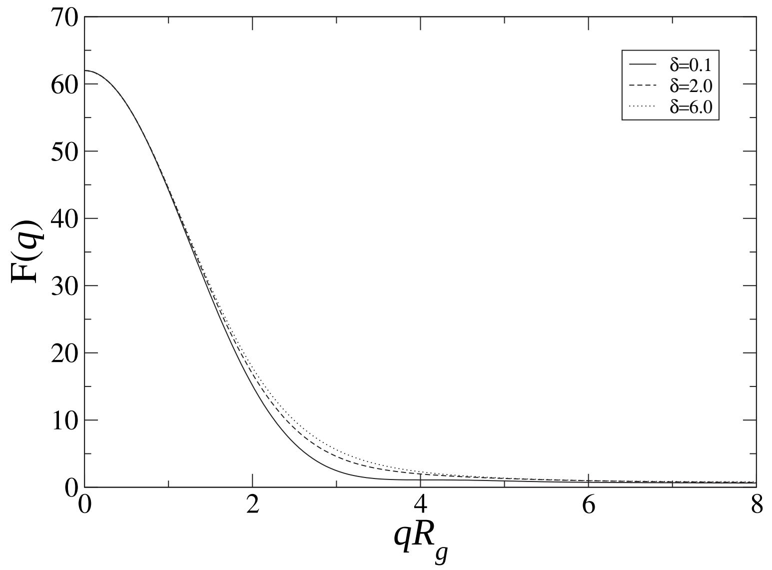

Figure 3.12: Form factors of G4 dendrimers obtained by simulation of the bead-thread model for $\delta = 0.1, 2.0, 6.0$.

radius of gyration R_g. This feature is similar to the one already discussed regarding the density-profiles but it is even stronger for the form factor because the various $F(q)$-curves indeed collapse on one another for $\delta \leq 0.4$. For very long thread lengths in the bead-thread model, as shown in Figure 3.12 for $\delta = 2.0$ and $\delta = 6.0$ deviations in $F(q)$ arise. When the form factor is rescaled with the experimental value of the radius of gyration, $R_g = 1.489$ [30], the simulation data can be compared to the scattering data obtained by SANS [29,30] as shown in Figure 3.13. The differences of the form factors belonging to the various simulated cases are small compared to the error bars in the experimental data. Therefore, the form factor alone, and its comparison to scattering data, is not sufficient to decide which model is most suitable to describe the given dendrimers. As it will be shown in the next chapter, the structure factor of solutions can provide a test criterion for this purpose.

Finally, in Figure 3.14 we show the form factors of G4 - G9 dendrimers on a double logarithmic scale. With increasing generation number, an oscillatory structure in the domain $qR_g \gtrsim 3$ shows up, signaling the fact that the dendrimers develop sharper boundaries. The oscillations first appear for generation numbers exceeding $G = 5$, in agreement with other simulation studies [49, 51, 54]. The form factor for $G = 9$ has an envelope that scales as $\sim q^{-4}$ at high values of the wavenumber, which represents Porod's law for scattering from a compact sphere [53]. The shapes of the curves, their evolution with G as well as the locations of the minima are additionally in very good agreement with experimental scattering curves from dendrimers of

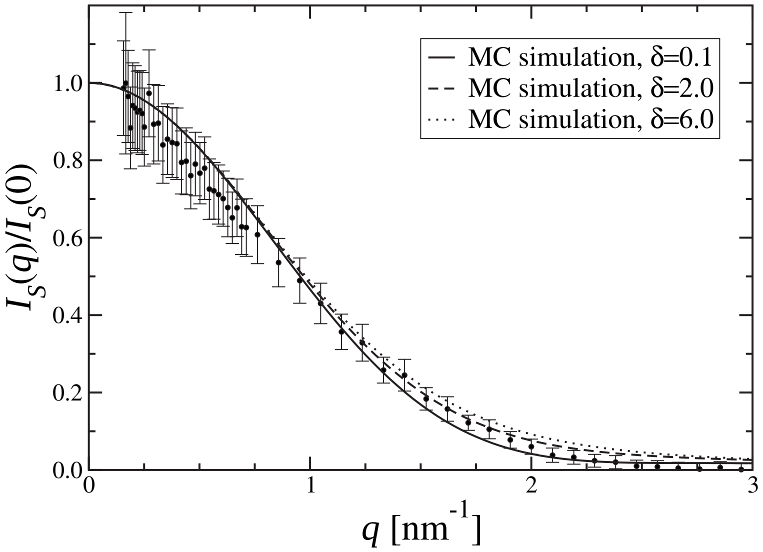

Figure 3.13: Total scattering intensity $I_S(q)$ from a dilute solution of G4 dendrimers. The circles are SANS-data from Ref. [30]. The lines are obtained from the simulation form factor of the bead-thread model with $\delta = 0.10, 2.0, 6.0$. The simulation yields $F(q)$ as a function of $q\sigma$. The value of σ is determined so as to obtain the experimentally measured radius of gyration, $R_g = 1.489\,\mathrm{nm}$ in this case, and the horizontal axis is appropriately rescaled. Experimentally, the forward scattering intensity $I_S(0)$ is not directly measurable, but can be calculated via the experimentally measured volume of the molecule [58].

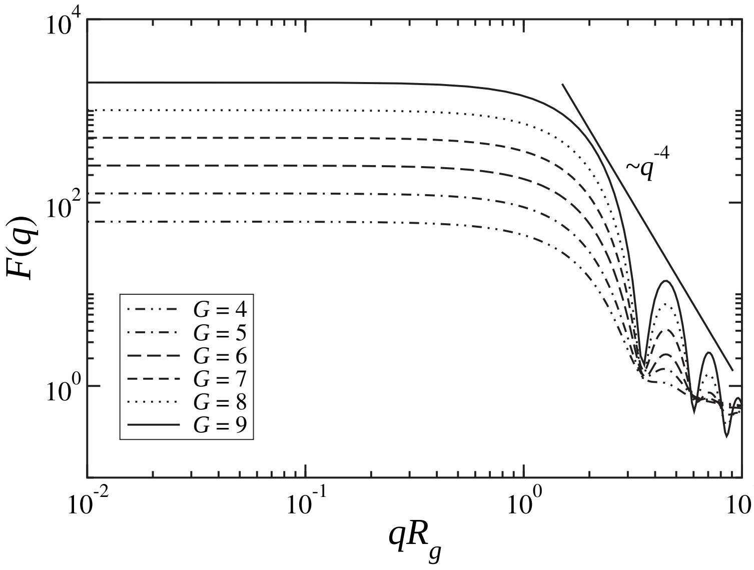

Figure 3.14: Double-logarithmic plot of the form factors for dendrimers G4 to G9 obtained by the simulation of the bead-thread model with $\delta = 0.10$. The straight solid line represents Porod's law, $F(q) \sim q^{-4}$.

varying generation numbers [52, 53, 55, 56]. This amply demonstrates the ability of the present model to describe real dendrimers.

Chapter 4

Effective Interactions

We employ extensive Monte Carlo and Molecular Dynamics simulations to investigate the effective interactions between the centres of mass of dendritic macromolecules of variable flexibility and generation number. Two different models for the connectivity and steric interactions between the monomers are employed, the first one being purely entropic in nature and the second explicitly involving energetic interactions. We find that the effective potentials have a generic Gaussian shape, whose range and strength can be tuned via modifications in the generation number and flexibility of the spacers. We supplement our simulation analysis by a density-functional approach in which the connectivity between the monomers is approximated by an external confining potential that holds the monomer beads together. Using a simple density functional for the interactions between the monomers, we find semi-quantitative agreement between theory and simulation. The implications of our findings for the interpretation of scattering data from concentrated dendrimer solutions are also discussed. (Published in Ref. [94].)

4.1 Introduction

Most of the theoretical investigations on the properties of dissolved dendrimers have focused on the questions of their internal conformations and sizes [17]. Much less is known about the effective interaction (to be defined in Sec. 4.2) between two dendrimers, which is important in many respects: provided the particles interact through pairwise-additive forces, the thermodynamic properties of the system may be calculated theoretically [31], and the reduction of complexity allows efficient simulations of large systems. Finally, it enables calculation of the structure factor and thus comparison to scttering experiments.

Lue and Prausnitz [37] as well as Lue [47] have carried out simulations based on a tangent-sphere model for the dendrimers, whereas Likos *et al.* [57,58] have presented a Flory-type theory yielding a Gaussian interaction potential. Nevertheless, the detailed form of the effective interaction as well as its dependence on generation number and spacer length between the branching points has not been investigated to date. The purpose of this chapter is to examine in detail this question.

Having established the validity of the bead-thread model in chapter 3 by comparing its properties for isolated dendrimers to another coarse-grained model and to experiments, we may now proceed to use it to derive the effective pair interaction between dendrimers. This is achieved in two different ways: first, we directly measure the effective potential by means of simulations for varying parameters. Here, again, we compare the results to those for the FENE-LJ model. Secondly, we employ a density functional theory based on the simulational radial monomer density of isolated dendrimers.

4.2 Theoretical Concepts

A very useful concept for understanding at least the *equilibrium* behavior of complex fluids is that of the *effective interaction* between suitably chosen degrees of freedom [19]. Since we are not interested in keeping track of all the fluctuating, microscopic degrees of freedom, it is pertinent to choose one effective coordinate that represents somehow the whole macromolecule, integrate out the rest, and envision thereafter the dendrimers as 'point particles' interacting by means of an effective potential. The latter includes all the effects of the integrated-out degrees of freedom and the thermodynamics of the system is preserved.

The choice of the effective degrees of freedom is largely a matter of convenience. For star-branched macromolecules, such as star polymers [59] or polyelectrolyte stars, [60] the common anchoring point is the natural choice. For linear polymer chains, both the central monomer [61] and the centre of mass [62–67] have been used as effective coordinates. For dendrimers, the centre of mass is a natural choice for two reasons: first, many experimental dendrimers lack a central particle and second because it is precisely the correlations between the centres of mass that are probed in scattering experiments [30]. Since the centres of mass are not real particles of the system, the definition of the effective interaction between those requires some explanation. We present a mathematical definition of this concept below.

Consider two macromolecules consisting of N monomers each. Let $\alpha = 1, 2$ denote the composite molecule and $i = 1, 2, \ldots, N$ be the index characterizing the individual monomer, so that $\mathbf{p}_{i\alpha}$ uniquely denotes the canonical momentum of a particular monomer of mass m and $\mathbf{r}_{i\alpha}$ its position vector. Our starting point is the Hamiltonian of the whole system, $\mathcal{H}$, which can be decomposed as follows:

$$\mathcal{H} = \mathcal{H}_{11} + \mathcal{H}_{12} + \mathcal{H}_{22}. \tag{4.1}$$

Here, $\mathcal{H}_{\alpha\beta}$ includes terms pertaining to interactions between monomers of macromolecules α and β only, i.e., $\mathcal{H}_{11}$ and $\mathcal{H}_{22}$ include the interactions between monomers of the same dendrimer (as well as the trivial, kinetic energy terms), whereas in $\mathcal{H}_{12}$ all cross-interactions between monomers belonging to different dendrimers are incorporated. Introducing the pair potential functions V_{c} and V_{s} that model the connectivity and the steric interactions between the beads, respectively, we can therefore write:

$$\begin{aligned} \mathcal{H}_{\alpha\beta} &= \delta_{\alpha\beta}\sum_{i=1}^{N}\frac{\mathbf{p}_{i\alpha}^{2}}{2m} + \delta_{\alpha\beta}\sum_{i<j}\left[V_{\mathrm{c}}(\{\mathbf{r}_{i\alpha}\}) + V_{\mathrm{s}}(\{\mathbf{r}_{i\alpha}\})\right] \\ &\quad + (1-\delta_{\alpha\beta})\sum_{i=1}^{N}\sum_{j=1}^{N} V_{\mathrm{s}}(\{\mathbf{r}_{i\alpha}, \mathbf{r}_{j\beta}\}) \\ &= K + V_{\alpha\beta}, \end{aligned} \tag{4.2}$$

where $\{\mathbf{r}_{i\alpha}\}$ is a shorthand for $(\mathbf{r}_{1\alpha}, \mathbf{r}_{2\alpha}, \ldots, \mathbf{r}_{N\alpha})$, K stands for the kinetic energy and $V_{\alpha\beta}$ for the potential energy. The canonical partition function of the system, Q, is defined as

$$Q = \left\{\prod_{\alpha=1}^{2} h^{-3N_\alpha}\int \mathrm{d}\mathbf{p}_{\alpha}^{N}\int \mathrm{d}\mathbf{r}_{\alpha}^{N}\right\}\exp(-\beta\mathcal{H}), \tag{4.3}$$

where $\int \mathrm{d}\mathbf{p}_{\alpha}^{N}$ is a shorthand for the multiple integral $\int\int\cdots\int \mathrm{d}^3p_{1\alpha}\mathrm{d}^3p_{1\alpha}\ldots\mathrm{d}^3p_{N\alpha}$, similarly for $\mathrm{d}\mathbf{r}_{\alpha}^{N}$, h denotes Planck's constant, and $\beta = (k_BT)^{-1}$, with Boltzmann's constant k_B and the absolute temperature T. Note the absence of the combinatorial factors $N!$ in the definition of the partition function, since the particles are in this case distinguishable due to their connectivity constraints.

In order to define the effective interaction between the centres of mass of the dendrimers, we proceed in a way analogous to that employed for linear polymer chains [64] and introduce the centres-of-mass density operators

$$\hat{\rho}_{\mathrm{cm}}^{(\alpha)}(\mathbf{R}_\alpha) = \delta\left(\mathbf{R}_\alpha - \frac{1}{N}\sum_{i=1}^{N}\mathbf{r}_{i\alpha}\right), \tag{4.4}$$

where $\mathbf{R}_\alpha$ denotes the position vector of the centre of mass of the dendrimer α and $\delta(\cdot)$ is Dirac's delta function. We keep the centres of mass fixed at the positions $\mathbf{R}_1$ and $\mathbf{R}_2$ and, following Ref. [64], we define the effective interaction $V_{\mathrm{eff}}(\mathbf{R}_1, \mathbf{R}_2)$ as

$$\begin{aligned} V_{\mathrm{eff}}(\mathbf{R}_1, \mathbf{R}_2) = -k_BT\ln\Bigg\{\frac{\Omega^2}{Q_1^2}h^{-6N}\int \mathrm{d}\mathbf{p}_1^N\mathrm{d}\mathbf{p}_2^N\int \mathrm{d}\mathbf{r}_1^N\mathrm{d}\mathbf{r}_2^N\hat{\rho}_{\mathrm{cm}}^{(1)}(\mathbf{R}_1)\hat{\rho}_{\mathrm{cm}}^{(2)}(\mathbf{R}_2) \\ \times\exp[-\beta(\mathcal{H}_{11}+\mathcal{H}_{12}+\mathcal{H}_{22})]\Bigg\}, \end{aligned} \tag{4.5}$$

where Ω is the volume of the system and Q_1 is the partition function of an isolated dendrimer:

$$Q_1 = h^{-3N} \int \mathrm{d}\mathbf{p}_1^N \int \mathrm{d}\mathbf{r}_1^N \exp(-\beta\mathcal{H}_{11}). \tag{4.6}$$

The connection of V_{eff} to the thermodynamics of the system is provided by Eqs. (4.1), (4.3), and (4.5), from which it follows

$$Q = \frac{Q_1^2}{\Omega^2} \int\int \mathrm{d}\mathbf{R}_1 \mathrm{d}\mathbf{R}_2 \exp[-\beta V_{\text{eff}}(\mathbf{R}_1, \mathbf{R}_2)]. \tag{4.7}$$

The effective potential depends only on the magnitude R of the separation vector $\mathbf{R} = \mathbf{R}_1 - \mathbf{R}_2$ between the centres of mass, $V_{\text{eff}} = V_{\text{eff}}(R)$. Its definition in Eq. (4.5) makes manifest the property $V_{\text{eff}}(R) \to 0$ as $R \to \infty$. Since the effective potential has the form of a restricted partition function, its direct calculation through Eq. (4.5) in a simulation cannot be achieved through standard simulation techniques [27]. However, it is easy to show from Eq. (4.5) that the $V_{\text{eff}}(R)$ is related to the correlation function $G(R)$ between the positions of the centres of mass through

$$\begin{aligned} G(R) &\equiv \langle \hat{\rho}^{(1)}(\mathbf{R}_1)\hat{\rho}^{(2)}(\mathbf{R}_2)\rangle \\ &= \frac{\exp[-\beta V_{\text{eff}}(R)]}{\Omega \int \mathrm{d}\mathbf{R} \exp[-\beta V_{\text{eff}}(R)]}, \end{aligned} \tag{4.8}$$

where $\langle \cdots \rangle$ denotes a canonical average. Since the calculation of expectation values is straightforward in a computer simulation, the last result provides a possibility to measure $V_{\text{eff}}(R)$ by using standard techniques.

An alternative possibility is offered by considering the force $\mathbf{F}_\alpha = -\nabla_{\mathbf{R}_\alpha} V_{\text{eff}}(\mathbf{R}_1, \mathbf{R}_2)$ acting on the centre of mass of dendrimer α. It can be shown that this force can be calculated as the expectation value of the sum of the forces exerted on the individual monomers, i.e.,

$$\mathbf{F}_\alpha(R) = \left\langle \sum_{i=1}^{N} \mathbf{F}_{i\alpha} \right\rangle_R \tag{4.9}$$

where the subscript on the right-hand side implies that the average has to be evaluated at fixed separation R between the centres of mass. Since the proof of Eq. (4.9) above is somewhat technical, we relegate it to the Appendix.

4.3 Simulation

We have applied two different simulation models, the bead-thread and the FENE-LJ model, so as to obtain independent results and provide a comparison between them. In addition, the application of different simulation models helps to shed light into the question of the sensitivity of the effective interaction on the microscopic details of the system. As will be demonstrated below, the results do depend quantitatively on the numerical values of the microscopic parameters, it is nevertheless possible to make a broad correspondence between different models, so that they yield very similar results for the effective interaction.

4.3.1 Simulation Details

Simulations of the bead-thread model

Within the bead-thread model, the most efficient way of measuring the effective interaction is offered by Eq. (4.8), a technique also applied by Dautenhahn and Hall to measure the potential between two polymer chains [65]. Indeed, since all forces between monomers identically vanish, Eq. (4.9) is of no use. The function $G(R)$ in this case can be obtained by letting two dendrimers freely move within the simulation box (accepting the moves according to the Metropolis criterion), and then making a histogram of the centre-of-mass distance R. In order to fulfill the condition $V_{\text{eff}}(R) \to 0$ for large separations R, the histogram has to be normalised in such a way that $G(R) \to 1$ in the same limit. Then, we can simply set

$$\beta V_{\text{eff}}(R) = -\ln[G(R)]. \tag{4.10}$$

Since the range of the interaction is anticipated to be finite (of the order of the gyration radius R_g of the dendrimers), we do not need statistics for large distances where the interaction potential vanishes, as this would cost unnecessarily simulation time. In order to prevent this, we accept only moves where the centre-of-mass distance is smaller than a cutoff distance $R_{\text{cut}} \cong 4R_g$. Furthermore, the repulsion between dendrimers at close separations can be very strong, therefore configurations with small R are extremely unlikely and would not occur in reasonable simulation times. In order to deal with this problem and sample all relevant separations equally, we apply an additional *attractive* external potential $\Phi(R)$ acting on the centres of mass. The total interaction potential is then $\bar{V}(R) = V_{\text{eff}}(R) + \Phi(R)$, giving rise to the correlation function $\bar{G}(R)$. Then, Eq. (4.10) becomes

$$\begin{aligned} \bar{G}(R) &= \exp[-\beta\bar{V}(R)] \\ &= \exp[-\beta(V_{\text{eff}}(R) + \Phi(R))], \end{aligned} \tag{4.11}$$

where $V_{\text{eff}}(R)$, the real effective interaction potential, is then obtained by

$$\beta V_{\text{eff}}(R) = -\ln[\bar{G}(R)] - \beta\Phi(R). \tag{4.12}$$

The MC simulation is carried out as follows: we try to move a monomer, and for the new position we check for overlaps and if the maximum bond length condition is fulfilled. If the new position is not allowed, the particle is set back to its old position. This procedure is repeated with all $2N$ particles. In order to apply the external potential acting on the centres of mass, we use the Metropolis algorithm: Consider a configuration with a centre-of-mass distance R_{old}. After all $2N$ particles have been moved (or have been tried to move), we calculate the new centre-of-mass distance R_{new}. If $R_{\text{new}} < R_{\text{old}}$, the new configuration is accepted, as the external potential is attractive. Otherwise, the new configuration is only accepted with the probability $\exp\{-\beta[\Phi(R_{\text{new}}) - \Phi(R_{\text{old}})]\}$. If it is rejected, all $2N$ particles are set back to their old positions.

Good statistics can only be achieved if the total potential $V_{\text{total}}(R) = V_{\text{eff}}(R) + \Phi(R)$ is smaller than $\sim k_BT$ for all distances R; optimally, $V_{\text{total}}(R)$ should be independent of R, so that histograms are flat and all R-regions are sampled equally frequently. As $\Phi(R)$ has to be chosen in that way that the real potential and the external potential nearly cancel each other, and $V_{\text{eff}}(R)$ is not known a priori, $\Phi(R)$ can only be determined within a trial-and-error procedure, where the external potential is improved after each cycle. In contrast to the simulation of the Lennard-Jones–FENE model (see the following subsection), where separate simulations are used for discrete values of R, this method yields the potential for the whole range $0 < R < R_{\text{cut}}$ in one simulation. Therefore, very long runs are necessary to obtain good statistics. Here we use 10^{10} MC steps.

In Fig. 4.1, simulation snapshots of two G4 dendrimers are shown for a centre of mass distance $R \approx 0$ and $R \approx 4\sigma$, respectively. When the dendrimers approach each other, they are deformed due to the repulsive interaction. As can be discerned from Fig. 4.1(b), the dendrimers become almost flat at the midplane between their centres of mass for intermediate separations R, whereas they recover their spherical shape for full overlaps, Fig. 4.1(a). Results for the effective interaction $V_{\text{eff}}(R)$ obtained within this model will be presented in Sec. 4.3.2.

Simulations of the FENE-LJ model[1]

To supplement our study, we furthermore carry out Molecular-Dynamics (MD) simulations[2] of two dendrimers employing the FENE-LJ model. The location of divergence in the FENE potential, R_0 in equation (2.12), determines the maximum bond length between two monomers. The average bond-length is additionally influenced by the prefactor U_0. Both can be varied to account for different experimentally realised dendrimers exhibiting different effective Kuhn lengths. Finally let us note that the temperature of the system is fixed at $T = 1.2\epsilon/k_B$.

---

[1] Carried out by Holger M. Harreis and published jointly in [94].

[2] In MD simulations, the trajectories of the particles are determined by the classical equations of motion.

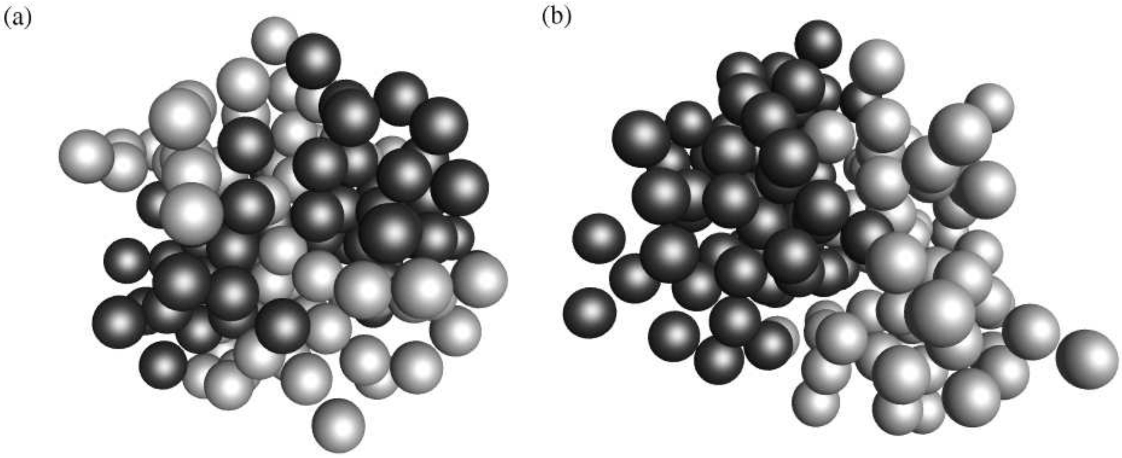

Figure 4.1: Simulation snapshots of two G4 dendrimers. The monomers of one dendrimer are rendered as dark spheres, the monomers of the other as light spheres of diameter σ. The centre of mass distance is (a) $R \approx 0$ and (b) $R \approx 4\sigma$.

To determine the effective interaction between two dendrimers at a given centre-of-mass separation R we proceed as follows: Two dendrimers are placed at the distance R and standard Molecular-Dynamics simulation techniques are employed to generate sample configurations. In order to effect the sampling at the given center-of-mass separation, we introduce an external force acting on the two centres of masses after each MD time step in the form of a rigid translational move bringing the two dendrimers back to a center-of-mass separation of R. Typically 6×10^7 MD steps were simulated, with a time-step of $10^{-3}\tau$, yielding a total MD simulation time of $6 \times 10^4\tau$, whereby τ is the MD time unit, $\tau = \sqrt{m\sigma_{\mathrm{LJ}}^2/\epsilon}$. Here, m is the mass of one bead. Of the 6×10^7 MD steps, 10^7 were used for equilibration. In the remaining simulation time, 5×10^3 configurations were used to calculate statistical averages of the effective force acting between the two dendrimers centres of masses. Concurrently, statistical averages of the radial density distribution $\xi(r)$ of the dendrimer around its centre of mass, the monomer pair distribution function $g(r)$, the form factor $F(q)$, as well as its radius of gyration R_g were measured, yielding results similar to the ones presented in Ref. [35].

4.3.2 Results

We start with the MC-simulation of the bead-thread model. In Figs. 4.2 and 4.3 we show the simulation results for G4 and G5 dendrimers with different spacer lengths. Although the repulsion is very strong, the dendrimers are interpenetrable.

Generation	δ	ϵ_1	ϵ_2	α	γ
G4	0.1	55	5.5	6.25	0.950
G4	0.2	49	5.5	6.50	0.925
G4	0.3	44	5.0	6.75	0.925
G4	0.4	39	4.5	5.00	0.900
G4	2.0	12	0.6	7.00	0.700
G5	0.1	120	11.0	6.25	0.900
G5	0.2	104	11.0	6.50	0.875
G5	0.3	89	10.0	6.75	0.850
G5	0.4	78	9.5	7.00	0.850

Table 4.1: The values of the fit parameters of Eq. (4.13) that describe the effective interaction between dendrimers, for different values of the thread length δ.

Increasing the thread length leads to a softer interaction whose range is also longer. The effective interaction for all thread lengths considered can be fitted by a sum of two Gaussian functions having the form:

$$\beta V_{\text{eff}}(R) = \epsilon_1 \exp\left(-\frac{3R^2}{4R_g^2}\right) + \epsilon_2 \exp\left[-\alpha(R/R_g - \gamma)^2\right], \tag{4.13}$$

where R_g is the radius of gyration of the dendrimers, as obtained by simulation using the same model. The first term in Eq. (4.13) above is identical in form to the one used previously to describe the interaction in the framework of a Flory-type theory, [57, 58] whereas the second provides a small correction. The quantities ϵ_1, ϵ_2, α and γ are fit parameters, whose values are summarised in Table 4.1.

As can be read off from Table 4.1, the effective interaction between dendritic macromolecules has, to an excellent approximation, a Gaussian form centred at the origin, the second term in Eq. (4.13) providing simply a small correction. Moreover, the strength of the interaction is governed by the thread length, providing thus a mechanism for *tuning* the potential experimentally by employing dendrimers of varying flexibility. In particular, in order to achieve an interaction strength of roughly $10\,k_{\mathrm{B}}T$, which is the value used to provide an excellent agreement with experimental data for G4-dendrimers, [58] a rather long thread length, $\delta = 2.0$ must be employed. An additional parameter that allows the tuning of the effective potential is the terminal generation number, with G5-dendrimers displaying a stronger interaction than G4 ones for the same thread length. The effect of the stiffening of the effective interaction with decreasing δ for fixed G and/or increasing G for fixed δ can be understood by means of the increased crowding of the hard spheres in the interior of the dendritic macromolecule.

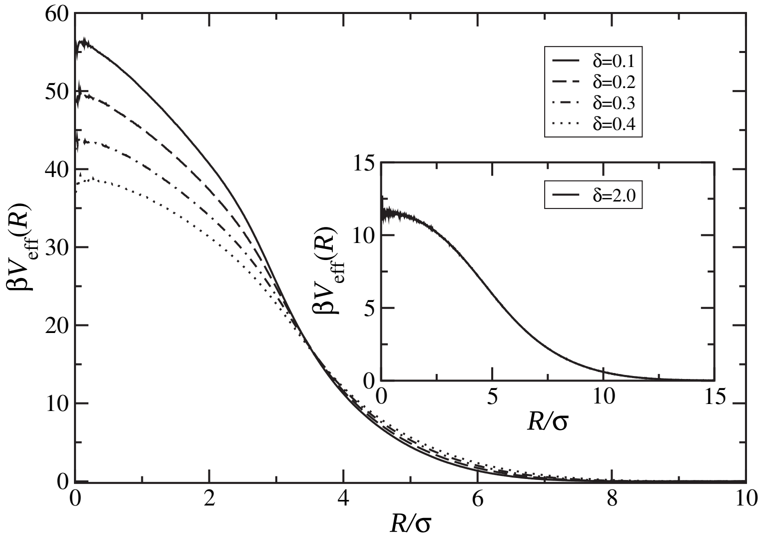

Figure 4.2: Simulation results for the effective interaction of G4 dendrimers obtained by employing the bead-thread model for different values of the thread length δ.

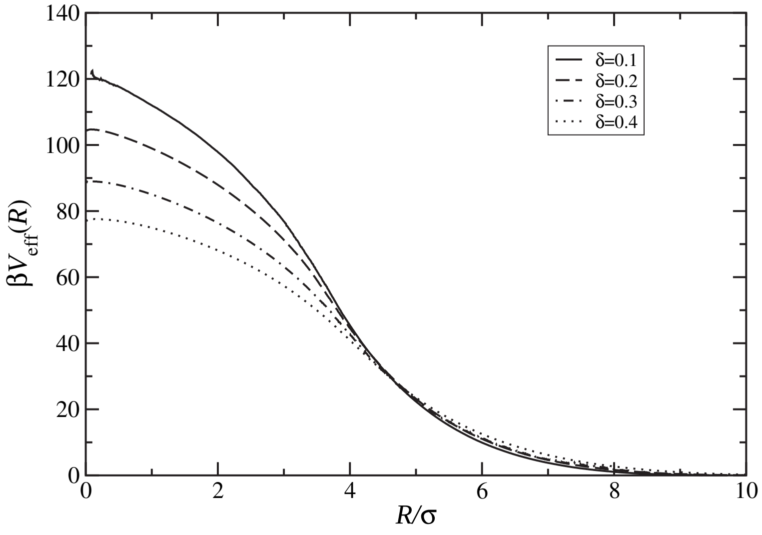

Figure 4.3: Same as Fig. 4.2, but for G5-dendrimers.

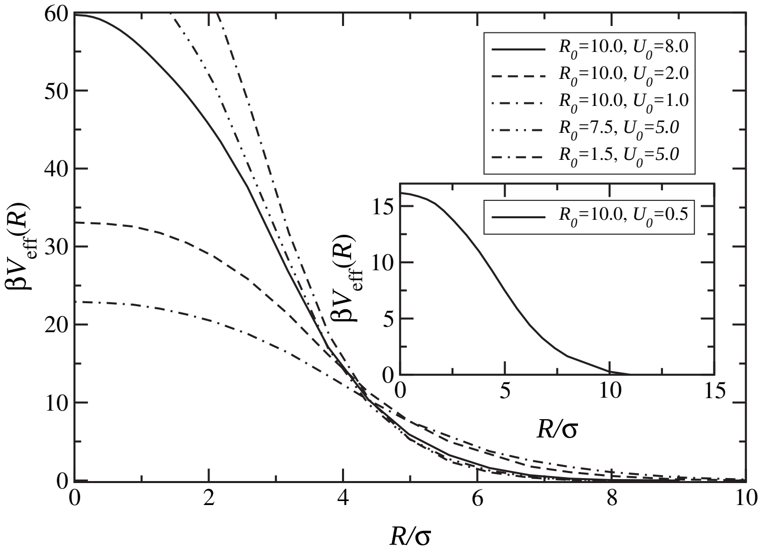

Figure 4.4: Simulation results for the effective interaction of G4 dendrimers obtained by employing the Lennard-Jones–FENE model for different values of the divergence length R_0 and the prefactor U_0.

In Fig. 4.4 we show the results obtained by performing MD-simulations employing the Lennard-Jones–FENE model of Eqs. (2.10), (2.11) and (2.12). It can be seen that the specific microscopic model employed does not affect the generic form of the interaction. Once more, the shape of the effective potential is Gaussian and the quantitative details of $V_{\rm eff}(R)$ can be now tuned by changing the microscopic energy parameter U_0 and the maximum length R_0 of the inelastic springs. In order to attain a value comparable to experiment, $\sim 10\, k_BT$, the microscopic energy parameter and the maximum bond length must be tuned to $U_0 = 0.5$ and $R_0 = 10.0$, as can be read off from the inset of Fig. 4.4. It is worthwhile noting that a simple increase in the value of R_0 is not sufficient to bring down the strength of the interaction to $\sim 10\, k_BT$, as can be seen from the main plot of Fig. 4.4. In contrast to the bead-spring model, the maximum extent of the spring is associated with an energetic cost set by the parameter U_0. Thus, only a decrease in the value of U_0 can bring about the desired strength of the effective interaction and an increase of R_0 alone is not sufficient. Otherwise, the understanding the influence of these two parameters on the stiffening of the pair potential is quite intuitive: the repulsion that every monomer feels from any monomer of the other dendrimer gets lower the smaller U_0 is and, in addition, the larger R_0 the more space it has to avoid it.

4.4 Density Functional Theory

In this section we put forward a first attempt to estimate the effective interaction between dendrimers by using techniques from classical density functional theory (DFT). DFT is a powerful theoretical tool that allows for the calculation of equilibrium density profiles of inhomogeneous fluids and at the same time provides a way for calculating the free energy of the same under the influence of arbitrary external potentials [68]. For simple classical fluids composed of nonbonded molecules, various approximate functionals have been developed in the last two decades. The situation for polymeric fluids, where the bonding between the monomers plays a crucial role, is much less developed. Approximate functionals for polymer chains have been proposed recently, [69–71] however the complicated, branched connectivity of dendrimers renders their application to the problem at hand untenable. Hence, we put forward the idea of removing all the bonds from the molecules and formally replacing them with an appropriate external potential $V_{\mathrm{ext}}(r)$, which is chosen in such a way that the equilibrium profile of an isolated dendrimer coincides with the one that has been obtained from simulation.

Let us consider, therefore, an isolated dendrimer whose one-particle density profile is $\xi(r)$, where r measures the distance from its centre of mass. The inhomogeneity of this profile is caused by the bonding between the molecules, which, in the spirit of the bead-thread model, we consider as hard spheres of diameter σ. In order to achieve *the same* inhomogeneous profile $\xi(r)$ in a fluid of hard spheres composed of exactly the same number of particles as those in the dendrimer, one needs to act on the system with an external potential $V_{\mathrm{ext}}(r)$. For this system, we thus write down a classical density functional $\mathcal{F}[\xi]$ of the form

$$\begin{aligned} \mathcal{F}[\xi] &= k_B T \int \mathrm{d}^3 r \xi(r) \left[\ln(\xi(r)\sigma^3) - 1\right] \\ &+ \mathcal{F}_{\mathrm{ex}}[\xi] + \int \mathrm{d}^3 r V_{\mathrm{ext}}(r) \xi(r), \end{aligned} \tag{4.14}$$

where $\mathcal{F}_{\mathrm{ex}}[\xi]$ is the excess contribution arising from the excluded volume interactions between the monomers. For this term we use the simplest weighted density approximation that was introduced first by Nordholm [72] and later refined by Tarazona, [73] namely

$$\mathcal{F}_{\mathrm{ex}}[\xi] = \int \mathrm{d}^3 r \xi(r) \psi_{\mathrm{ex}}(\bar{\xi}(r)), \tag{4.15}$$

with the weighted density $\bar{\xi}(r)$

$$\bar{\xi}(r) = \frac{3}{4\pi\sigma^3} \int \mathrm{d}^3 r \Theta(\sigma - r) \xi(r) \tag{4.16}$$

and the excess free energy of the homogeneous hard sphere fluid [74]

$$\beta\psi_{\mathrm{ex}}(\xi) = \eta(4-3\eta)(1-\eta)^{-2}, \qquad \eta = \frac{\pi\xi\sigma^3}{6}. \tag{4.17}$$

In Eq. (4.16) above, $\Theta(\sigma - r)$ is the Heaviside step function.

In order to determine the fictitious external potential $V_{\mathrm{ext}}(r)$, we took the equilibrium density profile $\xi(r)$ from the MC-simulation of an isolated dendrimer of the bead-thread model. Requiring that the functional of Eq. (4.14) is minimised for this profile, we obtain the equation

$$\ln\left[\xi(r)\sigma^3\right] + \frac{\delta\beta\mathcal{F}[\xi]}{\delta\xi(r)} + \beta V_{\mathrm{ext}}(r) = \beta\mu, \tag{4.18}$$

where the second term on the left-hand side denotes the functional derivative with respect to the density and μ is a Lagrange multiplier introduced to guarantee that the number of particles is kept fixed at the number of beads of the dendrimer. Eq. (4.18) can be immediately solved for $V_{\mathrm{ext}}(r)$.

Due to the approximate character of the excess functional, Eqs. (4.15)-(4.17), a technical problem occurs. The high values of $\xi(r)$ close to the origin, see Fig. 4.5, cause the external potential $V_{\mathrm{ext}}(r)$ to develop a deep minimum at $r = 0$. The density profile and the external potential are denoted in Fig. 4.5 and in the inset with the dashed lines. When this potential is reintroduced in Eq. (4.18) and used to calculate the equilibrium profile, it yields as stable solution *not* the original one but a new profile, which is similar to the old one away from the origin but has a much higher peak close to $r = 0$. This is a combined artifact of the approximate nature of the excess functional and the assumption that all bonds can be removed. In order to remedy this deficiency, we remove the large peak from the simulation density profile, which arises from the two monomers of the zeroth generation, and work with a modified profile that includes the effects of the subsequent generations *only*. This modified profile is denoted with the solid line in Fig. 4.5. With this modification, a new fictitious external potential is obtained, denoted with the solid line in the inset of Fig. 4.5, which is now self-consistent: introducing anew $V_{\mathrm{ext}}(r)$ in Eq. (4.18) and calculating $\xi(r)$ yields as equilibrium profile the input density, denoted with the solid line in Fig. 4.5. Though this procedure may seem arbitrary at first sight, it carries two additional physical motivations. First, the fact that the bonding between the two innermost monomers cannot be completely removed, hence we replace both of them with a potential barrier into which the monomers of the subsequent generations cannot penetrate. And secondly, since we are eventually interested in the calculation of the effective interaction, which is caused mainly by the overlap and deformation of the outermost generations, the details in the treatment of the innermost monomers should be not crucial.

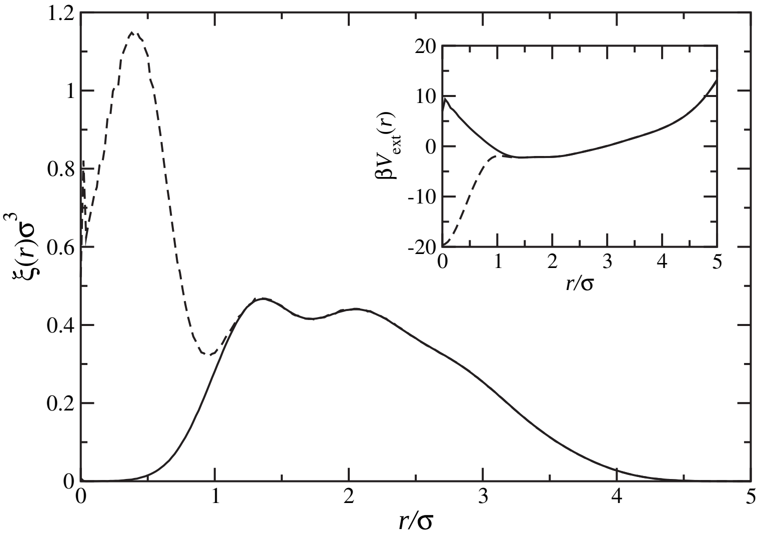

Figure 4.5: The simulation density profile of a G4-dendrimer with thread length $\delta = 0.1$ (dashed line) and the modified profile that results after removing the high peak arising from the two monomers of the zeroth generation (solid line). The inset shows the external potentials $V_{\rm ext}(r)$ that give rise to these profiles in the framework of our density-functional approach. The lines in the inset are coded in the same way as those in the main panel. For an explanation of the meaning of the modified profile, see the text.

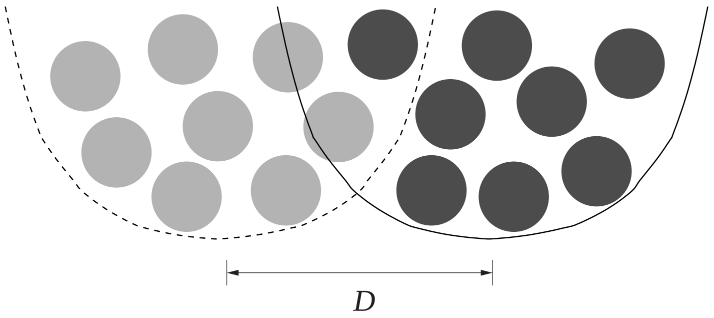

Figure 4.6: A sketch showing two confined hard-sphere fluids whose confining potentials are kept a distance D apart. All particles interact with one another but the light (dark) spheres only feel the effect of the light (dark) external potential. Due to the deformation of the density profiles, the distance D does not coincide with the separation R between the centres of mass of the confined fluids.

In order to calculate the effective interaction $V_{\text{eff}}(R)$, we now extend the treatment to *two* dendrimers. Consistently with the picture of a single dendrimer, these are modeled as two confined hard-sphere fluids, whose respective external potentials are separated by a distance D. All hard spheres interact with each other but the molecules of species i only feel the external potential $V_{\text{ext}}^{(i)}(\mathbf{r})$ that represents the bonding within the macromolecule labelled by i $(i = 1, 2)$. Since the profiles will be distorted, D is not identical to the centre-of-mass separation R in general and only in the trivial cases $D = 0$ and $D = \infty$ it holds $D = R$. Positioning the first dendrimer at the origin and the second at a distance D, it clearly holds $V_{\text{ext}}^{(2)}(\mathbf{r}) = V_{\text{ext}}^{(1)}(\mathbf{D} - \mathbf{r})$. The physical setup is schematically depicted in Fig. 4.6. The density functional of Eqs. (4.14)-(4.17) is now generalised to two interacting dendrimers and reads as

$$\begin{aligned} \mathcal{F}[\xi_1, \xi_2; D] &= k_B T \sum_{i=1}^{2} \int \mathrm{d}^3 x \xi_i(\mathbf{r}) \left[\ln(\xi_i(\mathbf{r})\sigma^3) - 1\right] \\ &+ \mathcal{F}_{\text{ex}}[\xi_1 + \xi_2; D] + \sum_{i=1}^{2} \int \mathrm{d}^3 r V_{\text{ext}}^{(i)}(\mathbf{r})\xi_i(\mathbf{r}), \end{aligned} \tag{4.19}$$

where the D-dependence arises from the separation between the two fictitious external potentials. Since the term $\mathcal{F}_{\text{ex}}$ describes the effect of the interactions between *all* beads, irrespective of the dendrimer to which they belong, it depends on the *total* density profile $\xi_1(\mathbf{r}) + \xi_2(\mathbf{r})$.

For every separation D, this functional has been minimised with respect to $\xi_1(\mathbf{r})$ and $\xi_2(\mathbf{r})$. The equilibrium density profiles serve then to determine also the centre-of-mass separation R that corresponds to every D and a relation $D = D(R)$ is established. Clearly, due to the symmetry of the problem, it holds $\xi_2(\mathbf{r}) = \xi_1(\mathbf{D} - \mathbf{r})$, as for the external potentials.

The advantage of this approach compared to the simple Flory-type theory presented in Refs. [57] and [58] is that the resulting density profiles are now *deformed* with respect to their shape at $R \to \infty$, since the presence of the hard spheres belonging to one dendrimer takes away allowable configurations from those of the other.

The next issue is to identify the effective interaction $V_{\text{eff}}(R)$ between the two dendrimers. At first sight, it would appear that one should state $V_{\text{eff}}(R) = \mathcal{F}[\xi_1, \xi_2; D(R)] - \mathcal{F}[\xi_1, \xi_2; \infty]$ but this is physically unrealistic. First of all, the true dendrimers are not under the influence of an external potential; the latter has been introduced only as an intermediate step in order to estimate the deformed density profiles. Moreover, the first term in the right-hand side of Eqs. (4.14) and (4.19) does not accurately describe the ideal free energy of bonded molecules, which has a much more complicated form that can be read off in Ref. [69]. We make here instead the physical assumption that, due to the very high connectivity between the beads, the true ideal term is much smaller in magnitude than the one introduced here. The only term that is realistically reproduced by our hybrid DFT is the excess contribution, $\mathcal{F}_{\rm ex}$, which is also mainly responsible for the reduction of available states for one dendrimer in the presence of the other. Our approach is similar to the Flory idea of removing all connections between monomers and estimating the effective interaction from the overlap of the two undisturbed density profiles. We maintain this spirit but use now the *deformed* density profiles that arise from the DFT to write

$$V_{\rm eff}(R) \approx \mathcal{F}_{\rm ex}[\xi_1 + \xi_2; D(R)] - \mathcal{F}_{\rm ex}[\xi_1 + \xi_2; \infty]. \tag{4.20}$$

Clearly, the last term is just twice the excess free energy of an isolated dendrimer.

The results from the DFT-approach are presented in Figs. 4.7 and 4.8 and compared there to simulation. It can be seen that, although the agreement is not spectacular, the approximate DFT introduced here captures the features of the effective interaction semi-quantitatively. The evolution of the strength of $V_{\rm eff}(R)$ with spacer length and the general shape of the effective potential are reproduced. A general deficiency of the DFT is the systematic overestimation of the width of the effective interaction. This may arise both from the approximate form of the excess density functional and from the fact that we did not allow, in this approach, the fictitious external potentials to vary with R. Indeed, in the true dendrimers the bonds bend and yield as R varies, whereas here $V_{\rm ext}(r)$ maintains its shape for isolated dendrimers for all values of R. This constraint causes an overestimation of the effective interaction, however it is not clear at present how it could be lifted in a self-consistent way.

As a quantitative measure of the deformation of the dendrimers with respect to their undisturbed shape, we introduce the overlap parameter $O(R)$, defined as follows: consider the midplane between the line connecting the centres of mass of the dendrimers and count the average number of monomers $N(R)$ belonging to the dendrimer whose centre of mass lies *to the right* of this plane, and which lie *to the left* of the plane (the words ‘right’ and ‘left’ can be interchanged here.) With N being the total number of monomers in the dendrimer, we define

$$O(R) = \frac{2N(R)}{N}. \tag{4.21}$$

The definition above guarantees that in the limit $R = 0$ the overlap parameter attains the value unity. In Fig. 4.9 we show a representative result, obtained for two G4-dendrimers of thread length $\delta = 0.1$. Though the DFT still overestimates the overlap between the dendrimers, it provides an improvement upon the result of the undistorted density profiles, which is denoted by the dotted line in Fig. 4.9.

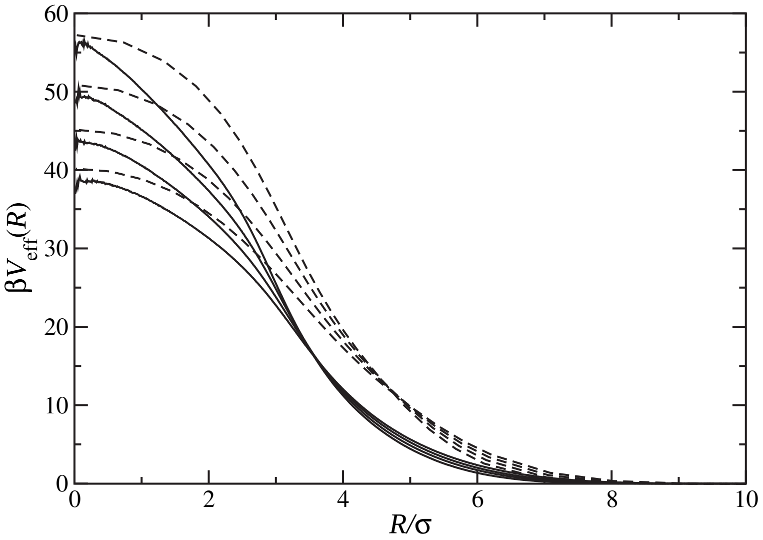

Figure 4.7: Simulation results (solid line) and DFT results (dashed line) for G4 dendrimers with $\delta = 0.1, 0.2, 0.3, 0.4$ (top to bottom).

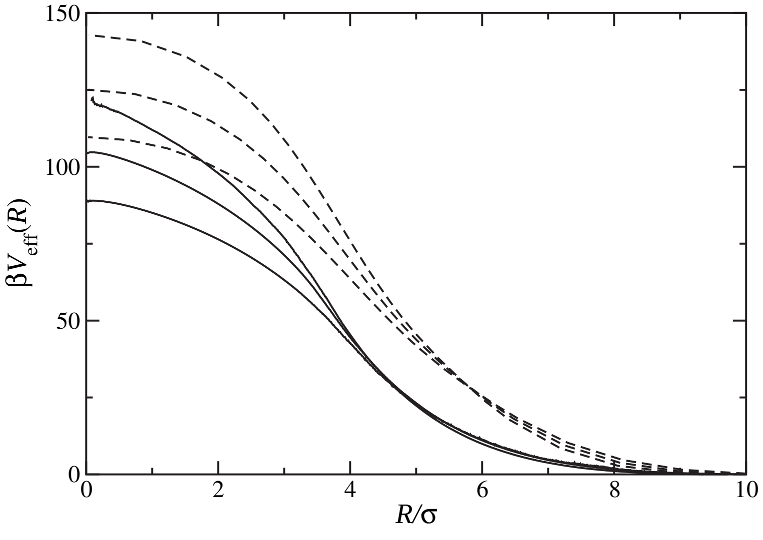

Figure 4.8: Simulation results (solid line) and DFT results (dashed line) for G5 dendrimers with $\delta = 0.1, 0.2, 0.3$ (top to bottom).

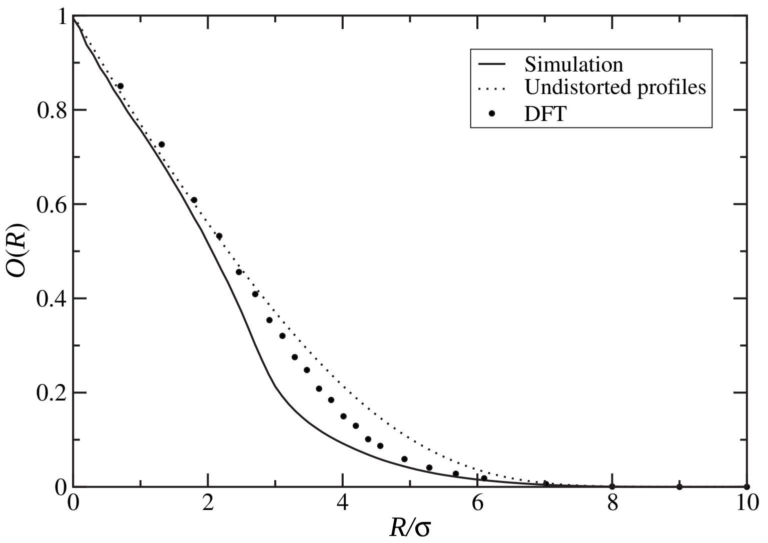

Figure 4.9: The overlap parameter defined in Eq. (4.21) for two G4-dendrimers with thread length $\delta = 0.1$, as a function of the centre-of-mass separation R.

4.5 Connection to experiments

In scattering experiments at vanishing concentration of dendrimers, the form factor $F(q)$ of the macromolecules is measured as a function of the scattering wavevector q. The form factor provides information about the size and typical conformation of dendrimers. In chapter 3 and two recent publications, [35, 75] it has been demonstrated that both the bead-thread model and the Lennard-Jones–FENE model yield results that can bring about excellent agreement with experimental data on the form factor of G4-dendrimers. Moreover, the bead-thread model correctly predicts the evolution of dendrimers toward compact hard spheres with growing terminal generation number. [52, 75] As it has been argued before, chapter 3 the broad family of the bead-thread model, parametrised by the value of the spacer length δ, possesses a degree of universality as far as the form factors are concerned: when plotted against the dimensionless parameter qR_g, the form factors arising from different values of δ show only minor differences to each other and, when compared to SANS-experiments, all lie within experimental uncertainties. Since in the bead-thread model it holds $R_g = \alpha_\delta \sigma$, where α_δ is a δ-dependent numerical coefficient of order unity, for every value of δ a corresponding length scale σ (say, in nm) can be chosen, so that the simulation results and the given experimentally measured $F(q)$ agree quantitatively. In other words, on the basis of experimental information on $F(q)$ alone, it cannot be determined which member of the δ-parametrised family is the best model to describe the real system.

The situation is different when experimental results from concentrated dendrimer solutions are available. In this case, the total scattering intensity contains information about the correlations between the different dendrimers, which is encoded in the static structure factor $S(q)$. The latter quantity is sensitive to the strength of the effective interaction between the centres of mass. As demonstrated in Fig. 4.10, a soft interaction, such as the one that arises from the bead-thread model for high values of δ, gives rise to structure factors that are deprived of any significant peaks. [57, 58] On the other hand, stiff dendrimers with short spacer lengths (small δ) are expected to give rise to scattering profiles exhibiting a strong degree of liquid-like ordering in the system, as can be seen in Fig. 4.10. The structure factor $S(q)$ does not display the universality of the form factor $F(q)$, even when plotted as a function of qR_g. Thus, it provides a suitable tool to determine which member of the bead-thread family best describes a given solution of flexible dendrimers.

Finally, we note that in view of the fact that the Gaussian interaction between dendrimers can attain values exceeding $100\,k_BT$ at full overlap (see Figs. 4.2 and 4.3), the interesting possibility opens up, that one might be able to form crystalline phases in a many-body system of dendrimers. Indeed, as it has been shown recently, [76] the above-mentioned value is the threshold above which particles interacting by means of Gaussian potentials can form stable crystals.

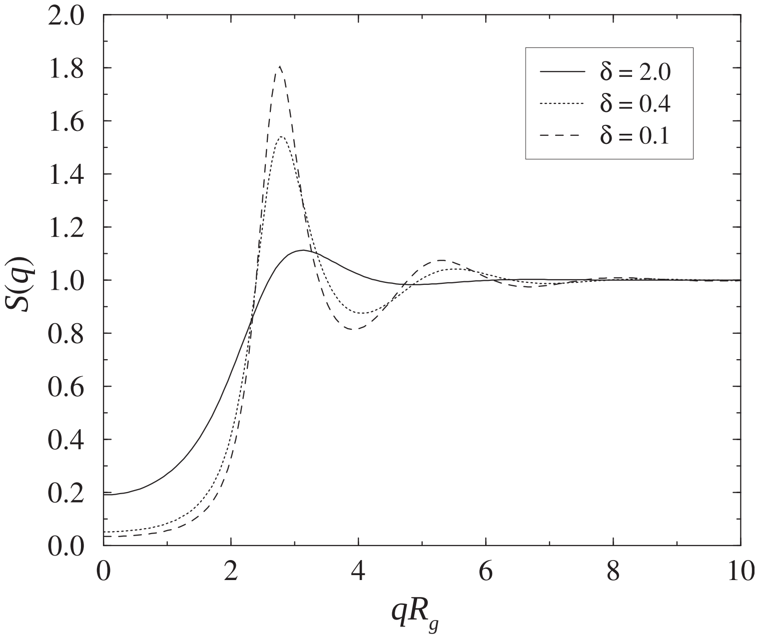

Figure 4.10: Theoretical structure factors for a concentrated solution of G4-dendrimers at a density $\rho R_g^3 = 0.06$. These structure factors have been obtained by solving the hypernetted-chain closure for the effective interactions of Eq. (4.13), reading off the parameter values from Table 4.1. Depending on the value of δ in the bead-thread model, $S(q)$ may show pronounced peaks that signal a strong liquid-like ordering or may be deprived of any significant structure.

Chapter 5

Concentrated Dendrimer Solutions

We employ monomer-resolved computer simulations of model dendrimer molecules, to examine the significance of many-body effects in concentrated solutions of the same. In particular, we measure the radial distribution functions and the scattering functions between the centres of mass of the dissolved dendrimers at various concentrations, reaching values that slightly exceed the overlap density of the macromolecules. We analyse the role played by many-body effective interactions by comparing the structural data to those obtained by applying exclusively the previously obtained two-body effective interactions between the dendrimers (chapter 4 and Ref. [94]). We find that the effects of the many-body forces are small in general and they become weaker as the dendrimer flexibility increases. Moreover, we test the validity of the oft-used factorisation approximation to the total scattering intensity into a product of the form- and the scattering factors, finding a breakdown of this factorisation at high concentrations. (Published in Ref. [95].)

5.1 Introduction

The use of effective potentials greatly facilitates the investigation of large systems. However, only the *pair* interaction potentials can easily computed, as shown in chapter 4. The simplicity of the bead-thread model also allows explicit monomer-resolved simulation of systems containing many dendrimers. Comparison to simulations employing the effective pair potentials from chapter 4 enables to test the validity of the pair potential approximation, where the many-body terms are neglected.

There is a number of subtleties associated with the effective potential energy function that have to be taken into account when a coarse-grained statistical mechanical treatment of a soft matter system is employed. Two of them are particularly relevant in the context of calculating thermodynamic quantities and tracing out phase diagrams. First, the potential energy cannot, in general, be written as a sum of pair interactions:[1] the process of eliminating the microscopic degrees of freedom inadvertently generates higher-order, many-body potentials [77–79]. Truncating the effective potential energy function at the pair-level constitutes the *pair potential approximation*, whose validity is not *a priori* guaranteed and has to be explicitly checked. And secondly, that the contributions to the potential energy are in general state-dependent, the most prominent example of the latter being the Debye-Hückel effective pair potential that has been extensively employed to model charge-stabilised colloidal suspensions under certain physical conditions [80]. Sometimes the state-dependence of an effective pair potential hides precisely the effect of many-body forces and then particular care has to be taken in the ways in which the pair potential is employed, so as to avoid blatant thermodynamic inconsistencies [81–84].

Many-body potentials are already encountered in the realm of atomic systems, the Axilrod-Teller interaction [85] being a characteristic example that has been shown to be relevant for the description of high-precision measurements of the structure factor of rare gases [86]. A formal decomposition of the effective potential energy function between the particles of one kind in a binary mixture in which the particles of the other kind are traced out has been given in Refs. [78] and [79]. Unfortunately, the treatment there applies only to mixtures for which the number densities of the two components can be varied at will, e.g., colloid-polymer or hard-sphere mixtures. It is not applicable to two broad categories of soft matter systems, namely charged mixtures and solutions of polymers of arbitrary architecture. In the former case, the number densities of the two components are constrained by the electroneutrality condition. In the latter, where one specific monomer [59,61] or the centre of mass of the molecule [66, 67, 87–89] are chosen as effective, mesoscopic coordinates, the total number of monomers and the number of effective particles are coupled to each other through the constraint of keeping the number of monomers per macromolecule fixed.

In charge-stabilised colloidal suspensions, three-body forces are generated by nonlinear counterion screening. Their effects have been examined by density functional theory and simulations [90] as well as by numerical solution of the nonlinear-Poisson Boltzmann equation [91,92]. It has been found that the three-body forces in this case are *attractive* [90–92], a result confirmed by direct experimental measurements using optical tweezers [91,92]. As far as polymeric systems are concerned, the triplet forces in star polymer solutions have been analysed by theory and simulations

---

[1] An important exception, however, is the depletion attraction in colloid-polymer mixtures described by the idealised Asakura-Oosawa model. In this case, all n-th order polymer-mediated effective interactions between colloids vanish identically for $n \geq 3$ if the polymer-to-colloid size ratio does not exceed $2\sqrt{3}/3 - 1$. See Ref. [77] for details.

in Ref. [93], where it was found that they play a minor role for concentrations vastly exceeding the overlap density. For linear chains, on the other hand, the many-body forces appear to have a more pronounced effect, as witnessed by the considerable state-dependence of the effective pair potential that reproduces the correlation functions of concentrated polymer solutions [67, 89]. The general functional form of the centre-of-mass effective interaction between polymer chains was found to preserve its Gaussian form, its strength and range being nevertheless modified within a range of $\sim 10\%$ of their original values, due to many-body effects [67, 89].

Another polymeric system that serves as a prototype for a tunable colloidal system that displays a Gaussian, soft effective pair interaction is that of a solution of dendritic macromolecules, or dendrimers for simplicity [17]. It has been recently shown that a Gaussian effective pair potential can describe extremely well the scattering intensities obtained experimentally from concentrated dendrimer solutions [57, 58]. The Gaussian pair interaction has also been explicitly measured in recent computer simulations that employed two different coarse-grained models for the microscopic, monomer-monomer interactions (chapter 4 and [94]). Nevertheless, in the approach of chapter 4 only *two* dendritic molecules were simulated, hence no information about many-body forces was gained. In the present work, we address the issue of the magnitude and importance of many-body effective interaction potentials in concentrated dendrimer solutions. We do not attempt to derive an explicit decomposition of the potential energy function into n-body terms, $n = 2, 3, 4, \ldots$; this would require separate simulations of just n dendrimers. Instead, we explicitly simulate a large number of interacting dendrimers at the microscopic level simultaneously. We measure thereby the pair correlation functions in the concentrated system directly and we compare the result with the one obtained by simulating the *same* number of dendrimers as effective entities interacting exclusively by means of pair potentials. The discrepancies in the results from the two approaches for the correlation functions yield then information regarding the importance of the many-body forces *of all orders*. We find that the many-body effects are of minor importance, especially for flexible dendrimers.

5.2 Simulation Details

In this chapter, we focus exclusively on dendrimers of the fourth generation (G4). For the monomer resolved simulations the bead thread model is employed.

The effective *pair* interaction potential between the centres of mass of two G4-dendrimers has been determined with the help of configuration-biased Monte Carlo simulations of this model in chapter 4. The strength of the interaction between dendrimers can be tuned by varying the number of generations or the parameter δ. Denoting by R the centre of mass separation, the δ-dependent effective pair potential $V_{\text{eff}}^{(2)}(R;\delta)$ has been found to have a Gaussian form with small, additional corrections. In particular, it can be fitted by the function:

$$\beta V_{\text{eff}}^{(2)}(R;\delta) = \epsilon_0 \exp\left(-\frac{R^2}{\gamma_0}\right) + \epsilon_1 \exp\left[-\frac{(R-R_1)^2}{\gamma_1}\right] - \epsilon_2 \exp\left[-\frac{(R-R_2)^2}{\gamma_2}\right], \quad (5.1)$$

where $\beta = (k_{\text{B}}T)^{-1}$ with Boltzmann's constant k_{B} and the absolute temperature T; the numerical values of the various fit parameters, depending on the choice of δ, are given in Table 5.1. Note that the precise values of the fit parameters are slightly different than those given in chapter 4, since there we employed a more constrained fit by setting $\gamma_0 = 4R_{g,\infty}^2/3$, with the radius of gyration $R_{g,\infty}$ of the dendrimers at infinite dilution, and $\epsilon_2 = 0$. The gyration radius is also shown at the last column of Table 5.1. Here, we consider G4-dendrimers with two different values, $\delta = 0.1$ and $\delta = 2.0$, representing the two extreme cases studied in chapter 4.

Let $\rho = M/\Omega$ be the number density of a sample containing M dendrimers enclosed in the volume Ω. The definition of the overlap density ρ_* of a dendrimer solution requires some care, as it is not a sharply defined quantity. Previous simulation studies with this system in chapter 3 have revealed that the monomer density profiles around the dendrimer's centre of mass decay to zero at a distance $r_{\text{c}} \cong 1.5\, R_{g,\infty}$. Motivated by this fact, we envision every dendrimer as a 'soft sphere' of radius r_c and define the overlap density through the relation:[2]

$$\frac{4\pi}{3}\rho_* r_{\text{c}}^3 = 1. \quad (5.2)$$

Moreover, we introduce the diameter of gyration at infinite dilution, $\tau \equiv 2R_{g,\infty}$, as the characteristic mesoscopic length scale to be used to introduce a dimensionless expression for the number density, $\rho\tau^3$. In these terms, the overlap density of Eq. (5.2) above is given by $\rho_*\tau^3 = 0.566$. The highest density in the simulation was $\rho_{\text{max}}\tau^3 = 0.605$, slightly exceeding the overlap value, since $\rho_{\text{max}} = 1.07\rho_*$.

δ	ϵ_0	γ_0/σ^2	ϵ_1	γ_1/σ^2	R_1/σ	ϵ_2	γ_2/σ^2	R_2/σ	$R_{g,\infty}/\sigma$
0.1	55.75	9.75	5.0	0.9	2.5	0.1	1.5	7.2	2.665
2.0	11.35	33.0	0.8	10.0	3.7	0.0	—	—	4.939

Table 5.1: The numerical values of the fit parameters of the effective pair potential between the centres of mass of two G4-dendrimers appearing in Eq. (5.1) for two different values of δ. At the last column the gyration radius $R_{g,\infty}$ at infinite dilution is also shown.

---

[2] In the literature, there are alternative definitions. For polymer chains, for instance, the definition $\frac{4\pi}{3}\rho_* R_g^3 = 1$ was used in Ref. [89].

For both values of δ, ten different concentrations were simulated, in particular at the densities $\rho/\rho_{\max} = 0.1, 0.2, \ldots, 1.0$. Periodic boundary conditions were employed throughout. At all densities, systems of 500 dendrimers were simulated, whereby each dendrimer consists of $N = 62$ monomers, and the size of the simulation box was changed in order to modify the dendrimer number density. The minimum box length was $L_{\min} = 9.384\,\tau$, yielding a system with the density $\rho_{\max}$. The equilibration criterion for the system at hand requires some care, as there are is no internal energy in the microscopic model, since all interactions are either zero or infinity. We therefore took advantage of the fact that the *effective*, pair interaction $V_{\text{eff}}^{(2)}(R;\delta)$ between the centres of mass is known and given by Eq. (5.1) with the parameters given in Table 5.1. Hence, we chose to monitor the total effective pair potential energy $U^{(2)}(M;\delta)$ given by

$$U^{(2)}(M;\delta) = \frac{1}{2}\sum_{i=1}^{M}\sum_{j\neq i}^{M} V_{\text{eff}}^{(2)}(|\mathbf{R}_i - \mathbf{R}_j|;\delta), \tag{5.3}$$

where $\mathbf{r}_{i,j}$ denotes the position of the i,j-th centre of mass.

Two different starting configurations were tried. In the first one, the centres of mass dendrimers possessing identical microscopic conformations were placed at the vertices of a fcc-lattice, which was achieved without violation of the excluded volume conditions. This procedure is particularly useful especially at the highest density, $\rho_{\max}$, where a random distribution of the centres of mass will result with high probability into a forbidden state with monomer overlaps. The system was then equilibrated, monitoring $U^{(2)}(M;\delta)$ described above. In the second one, the dendrimers' centres of mass were placed in a random arrangement. Although this procedure requires a large number of failed attempts before an allowed configuration is found, especially at high densities, such configurations are possible. Once again, we monitored the total effective pair potential energy during the equilibration period, finding that it converges to the same value as the one obtained from the fcc-initial state. In this way, sufficient equilibration of the system was guaranteed. Finite-size effects were checked by selectively simulating some systems with 256 of dendrimers, in a box having a correspondigly smaller volume, so that the same density is achieved, and finding agreement between the two attempts.

For $\delta = 0.1$, $N_{\text{equil}} = 10^7$ MC steps were used to equilibrate the system, and about $N_{\text{run}} = 2 \times 10^8$ steps to gather statistics. Statistical averages were calculated every $N_{\text{meas}} = 10\,000$ MC steps. For $\delta = 2.0$, where a much larger random displacement for the monomers can be used, the equilibration phase consisted of $N_{\text{equil}} = 10^6$ steps and statistical averages were calculated every $N_{\text{meas}} = 1000$ steps over a period of $N_{\text{run}} = 2 \times 10^8$ steps. The quantities measured were monomer profiles around the centres of mass, the radial distributions functions of the latter, radii of gyration, form factors, structure factors from the centres of mass and total scattering intensities;

all these quantities will be precisely defined in the sections that follow.

In Figs. 5.1 and 5.2, we show simulation snapshots of the monomer-resolved simulations for the lowest and the highest density for the thread length $\delta = 0.1$. (For clarity, in Fig. 5.1 we show only a section of the simulation box of the same size as in Fig. 5.2.) Although at Fig. 5.1 individual dendrimer molecules can still be resolved, since the density is much smaller than ρ_*, in Fig. 5.2 this is not any more possible. Here, $\rho = 1.07\rho_*$ and the whole system appears as a dense solution of monomers, in which the individual character of each macromolecule is lost. We will return to the implications of this fact in section 5.4.

In addition, a different kind of Monte Carlo simulations was also carried out, in which the monomers were not explicitly resolved. Instead, the dendrimers were replaced entirely by their centres of mass, which were then treated as effective, soft particles interacting exclusively by means of the pair potential of Eq. (5.1). Accordingly, we call this approach an *effective* simulation. As all monomers have dropped out of sight in the effective approach, it is only possible to measure quantities pertaining to the centres of mass, i.e., their radial distribution functions and structure factors. Comparison of the results regarding these quantities that are obtained through the two different types of simulations yields important information by way of testing whether the pair-potential approximation is meaningful.

5.3 Monomer Resolved vs. Effective Simulations

Each dendrimer of the fourth generation consists of $N = 62$ monomers. Let i, j be monomer indices within a given dendrimer whereas α, β are integers describing the dendrimer molecules as whole entities. In particular, let $\mathbf{R}_\alpha$ stand for the position of the centre of mass of the α-th dendrimer, $\mathbf{r}_\alpha^i$ denote the position vector of the i-th monomer in the α-th dendrimer, and $\mathbf{u}_\alpha^i$ stand for the same quantity but now measured in a coordinate system centred at $\mathbf{R}_\alpha$. Obviously, it holds

$$\mathbf{r}_\alpha^i = \mathbf{R}_\alpha + \mathbf{u}_\alpha^i. \tag{5.4}$$

In the monomer-resolved simulation, the following quantities were measured: The radial distribution $G(R)$, its Fourier transform $S(q)$, the form factor $F(q)$, the radial monomer distribution within the dendrimers $\xi(r)$ and the radius of gyration R_g. Here, we recapitulate their defintions from section 2.2 and generalise the quantities defined there for a single dendrimer to the case of M dendrimers.

The radial distribution function $G(R)$ between the centres of mass, defined as

$$G(R) = \frac{1}{M}\left\langle \sum_{\alpha=1}^{M}\sum_{\beta\neq\alpha}^{M} \delta\left(\mathbf{R} - \mathbf{R}_{\alpha\beta}\right)\right\rangle, \tag{5.5}$$

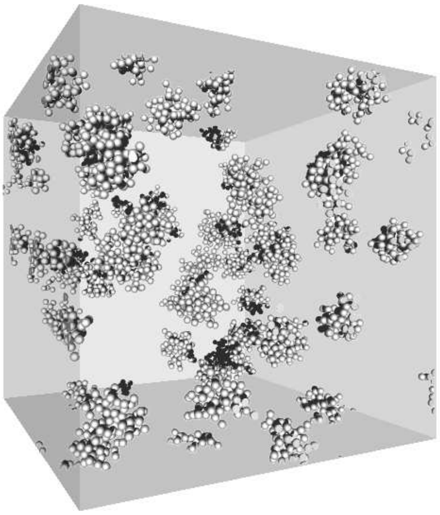

Figure 5.1: A snapshot from the monomer resolved-simulation of dendrimers. The monomers are rendered as spheres of diameter σ. Here, dendrimers with threads characterised through $\delta = 0.1$ at a density $\rho\tau^3 = 0.0605$ are shown. Note that only a part of the simulation box is shown, which has the same size as the full box depicted in Fig. 5.2.

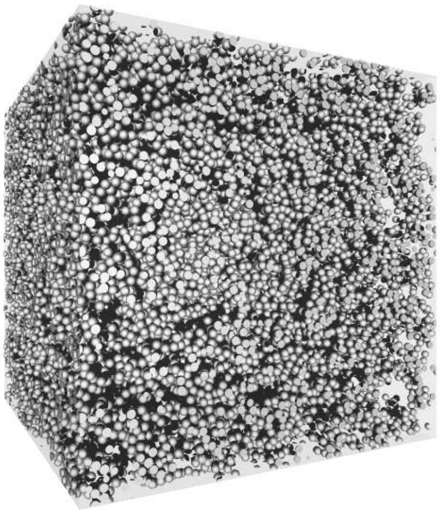

Figure 5.2: Same as Fig. 5.1 but at density $\rho\tau^3 = 0.605$. Here the complete simulation box is shown.

where $\langle \cdots \rangle$ denotes a statistical average and $\mathbf{R}_{\alpha\beta} = \mathbf{R}_\alpha - \mathbf{R}_\beta$. Related to this quantity by a Fourier transformation is the structure factor $S(q)$ that describes the correlations between the centres of mass in reciprocal space and it is given by

$$S(q) = \frac{1}{M} \left\langle \sum_{\alpha=1}^{M} \sum_{\beta=1}^{M} \exp\left[-\mathrm{i}\mathbf{q} \cdot (\mathbf{R}_\alpha - \mathbf{R}_\beta)\right] \right\rangle . \tag{5.6}$$

Moreover, we took advantage of the microscopic nature of the simulation to measure the dendrimers' form factor $F(q)$ at every simulated density ρ. This quantity is expressed by the relation:

$$F(q) = \frac{1}{M} \sum_{\alpha=1}^{M} \frac{1}{N} \left\langle \sum_{i=1}^{N} \sum_{j=1}^{N} \exp\left[-\mathrm{i}\mathbf{q} \cdot \left(\mathbf{u}_\alpha^i - \mathbf{u}_\alpha^j\right)\right] \right\rangle , \tag{5.7}$$

Another quantity of interest is the monomer distribution around the centre of mass, $\xi(r)$, which can again be measured at any desired overall density and is given by the expression:

$$\xi(r) = \frac{1}{M} \sum_{\alpha=1}^{M} \left\langle \sum_{i=1}^{N} \delta\left(\mathbf{r} - \mathbf{u}_\alpha^i\right) \right\rangle , \tag{5.8}$$

The overall size of the dendrimer is characterised by its radius of gyration R_g, which was measured in the simulation by calculating the quantity:

$$R_g = \frac{1}{M} \sum_{\alpha=1}^{M} \sqrt{\frac{1}{N} \left\langle \sum_{i=1}^{N} \mathbf{u}_\alpha^i \cdot \mathbf{u}_\alpha^i \right\rangle} , \tag{5.9}$$

In Eqs. (5.7) - (5.9) above, the summand in the sum over α is the corresponding quantity (form factor, density profile, and radius of gyration, respectively) of the α-th dendrimer. The additional summation over α and the division by the total number of dendrimers corresponds to an additional average over *all* dendrimers. Since all macromolecules are equivalent, the expectation values are identical for every summand. Finally, we also measured the scattering function $I(q)$ of the concentrated solution, which corresponds to the coherent contribution of the total scattering intensity in a SANS experiment, under the assumption that all monomers possess the same scattering length density [29, 30, 96, 97]. This is given by the equation:

$$I(q) = \frac{1}{MN} \left\langle \sum_{\alpha=1}^{M} \sum_{\beta=1}^{M} \sum_{i=1}^{N} \sum_{j=1}^{N} \exp\left[-\mathrm{i}\mathbf{q} \cdot \left(\mathbf{r}_\alpha^i - \mathbf{r}_\beta^j\right)\right] \right\rangle , \tag{5.10}$$

i.e., it is the total coherent scattering intensity from all monomers of the system.

In the effective picture, all information regarding the monomers' degrees of freedom is lost, hence in the effective simulation we can only measure the corresponding radial distribution function $G_{\text{eff}}(R)$ and its Fourier transform, the structure factor $S_{\text{eff}}(q)$ of the centres of mass. These are given by Eqs. (5.5) and (5.6) above but with the averages now performed with the effective Hamiltonian, i.e.,

$$G_{\text{eff}}(R) = \frac{1}{M}\left\langle \sum_{\alpha=1}^{M}\sum_{\beta\neq\alpha}^{M} \delta\left(\mathbf{R}-\mathbf{R}_{\alpha\beta}\right)\right\rangle_{\mathcal{H}_{\text{eff}}}, \tag{5.11}$$

and

$$S_{\text{eff}}(q) = \frac{1}{M}\left\langle \sum_{\alpha=1}^{M}\sum_{\beta=1}^{M} \exp\left[-\mathrm{i}\mathbf{q}\cdot\left(\mathbf{R}_{\alpha}-\mathbf{R}_{\beta}\right)\right]\right\rangle_{\mathcal{H}_{\text{eff}}}. \tag{5.12}$$

The effective Hamiltonian $\mathcal{H}_{\text{eff}}$ involves the momenta $\mathbf{p}_{\alpha}$ and positions $\mathbf{R}_{\alpha}$ of the centres of mass only and contains exclusively pair interactions, i.e.,

$$\mathcal{H}_{\text{eff}} = \sum_{\alpha=1}^{M}\frac{\mathbf{p}_{\alpha}^{2}}{2m} + \frac{1}{2}\sum_{\alpha=1}^{M}\sum_{\beta\neq\alpha}^{M} V_{\text{eff}}^{(2)}(|\mathbf{R}_{\alpha}-\mathbf{R}_{\beta}|;\delta), \tag{5.13}$$

where m is the dendrimers' mass, which is irrelevant as far as static quantities of the system are concerned. In the simulations, $G(R)$ and $G_{\text{eff}}(R)$ can be simply calculated by counting the number of pairs separated at a distance within an interval around R and normalising the histograms appropriately [26]. A particular property of the effective description of a complex system is that it leaves all correlation functions between the coarse-grained degrees of freedom invariant *provided* that the mapping into the effective system is *exact* [19]. In other words, if the effective Hamiltonian contains the contributions to the effective potential at *all orders*, it makes no difference whether one calculates quantities such as $G(R)$ or $S(q)$ in the original, microscopic description or in the coarse-grained one. As our effective Hamiltonian $\mathcal{H}_{\text{eff}}$ is truncated at the pair level, the deviations between $G(R)$ and $G_{\text{eff}}(R)$ or, equivalently, between $S(q)$ and $S_{\text{eff}}(q)$ will be a measure of the importance of the neglected many-body terms in Eq. (5.13).

Representative results comparing between the two approaches are shown in Fig. 5.3, pertaining to the dendrimers with $\delta = 0.1$ and in Fig. 5.4, which refers to dendrimers with $\delta = 2.0$. The length scale used in this plot is the zero-density gyration radius of the dendrimers, $R_{g,\infty}$. For clarity, only the results only for three different densities obtained from the monomer resolved simulations are compared to those from the effective ones. At sufficiently low densities, $\rho = 0.1\rho_{\text{max}}$, the results from the two types of simulations are indistinguishable, hence the pair-potential approximation is an excellent one and many-body forces seem to play no role there; they can be thus safely ignored. Deviations between the two descriptions arise nevertheless

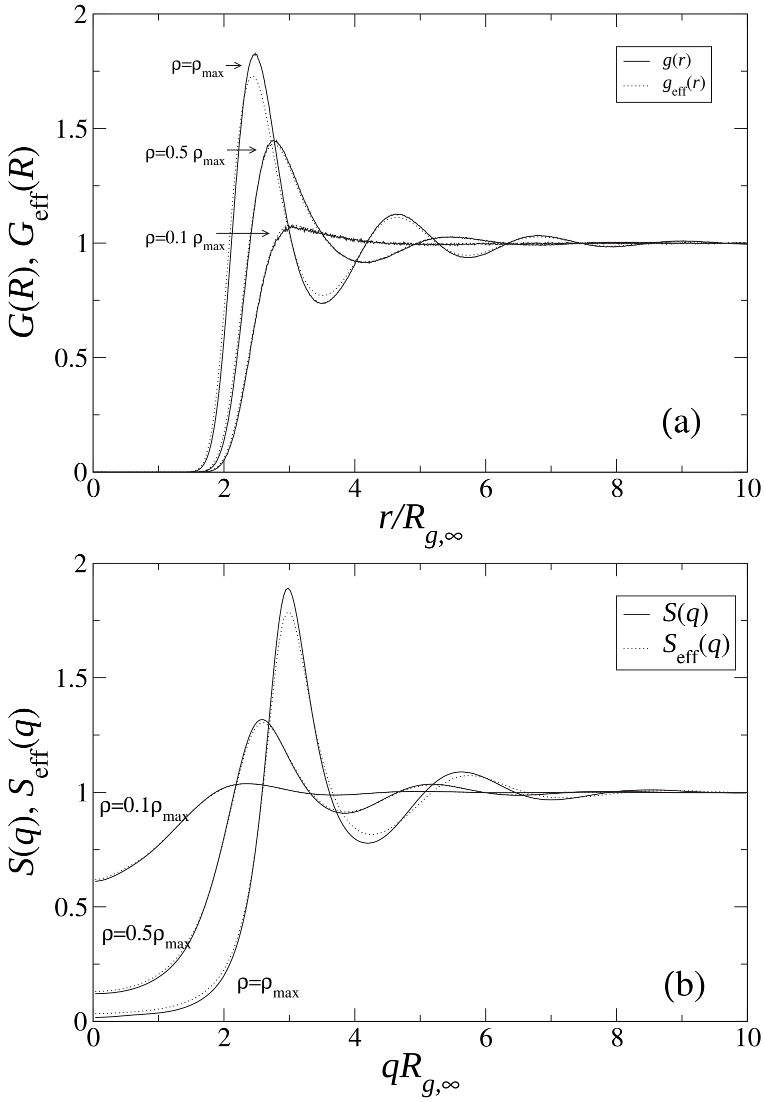

Figure 5.3: Comparison between the results from the monomer-resolved and the effective simulation of concentrated dendrimers with maximal thread length $\delta = 0.1$ of the bonds. The three different densities are $\rho = 0.1\rho_{\max}$, $0.5\rho_{\max}$ and $\rho_{\max}$, as indicated on the plots, with $\rho_{\max}\tau^3 = 0.605$. Results are shown for (a) the radial distribution function $G(R)$ and (b) the structure factor $S(q)$ of the centre of mass coordinates.

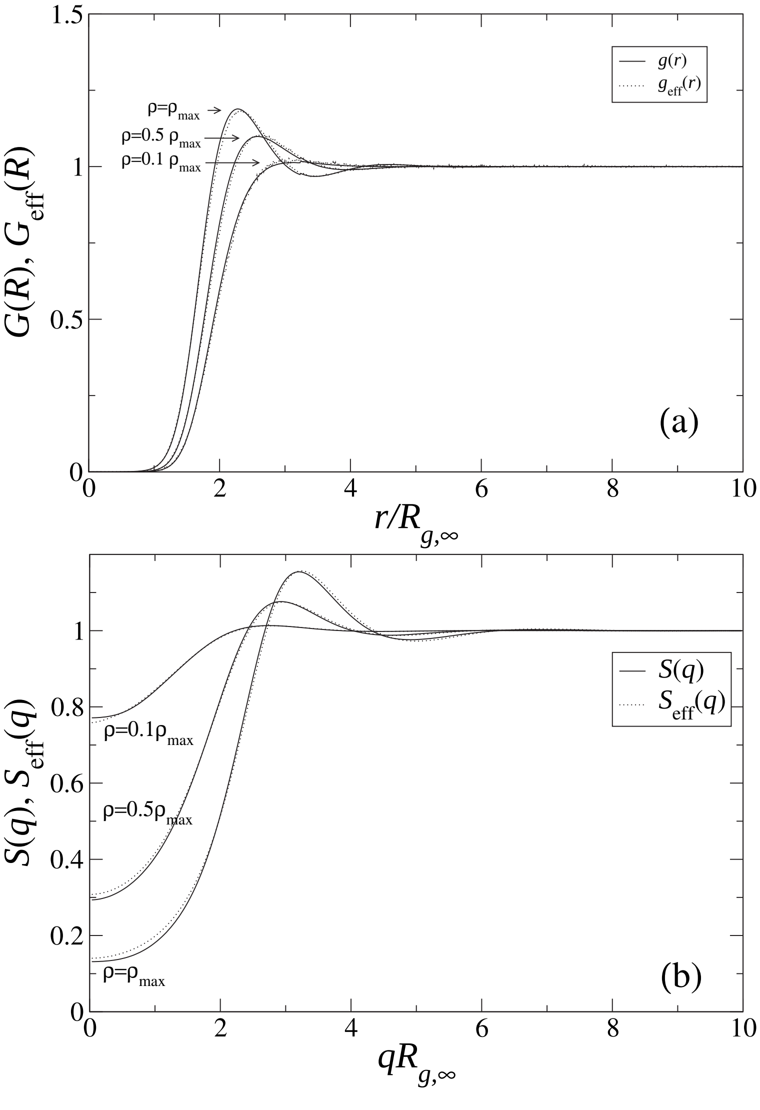

Figure 5.4: Same as Fig. 5.3 but for thread length $\delta = 2.0$.

as the overall concentration of the solution grows. Referring to Fig. 5.3(a), we see that for the $\delta = 0.1$-dendrimers, which have a rather high internal monomer density, the deviations are already visible (but small) at a density $\rho = 0.5\rho_{\mathrm{max}}$ and they become more pronounced at the highest simulated density, $\rho = \rho_{\mathrm{max}}$. The true radial distribution function $G(R)$ between the centres of mass shows a more pronounced coordination than the effective one, $G_{\mathrm{eff}}(R)$, and this effect is also reflected in the corresponding structure factors. The peak height of $S(q)$ is higher than the one of $S_{\mathrm{eff}}(q)$, pointing to the fact that the zero-density pair potential underestimates somehow the strength of the repulsions between the dendrimers' centres of mass. The relative deviation between the two descriptions as far as the peak height is concerned are at the highest density about 6%. Much more drastic is the discrepancy of the $S(q \to 0)$ limit, for which $S(q \to 0) = 0.018$ whereas $S_{\mathrm{eff}}(q \to 0) = 0.033$. Given the fact that the $S(q = 0)$-value is proportional to the osmotic isothermal compressibility of the solution, employing the effective picture can lead here to serious errors in the calculation of the thermodynamics of the system. Two integrations of the inverse compressibility are needed in order to obtain the Helmholtz free energy of the solution, hence errors at all lower densities accumulate in performing such an integration and they can lead to a serious underestimation of the free energy if the effective picture is employed.

The agreement between the microscopic and the coarse-grained approaches is a lot better for the case of the $\delta = 2.0$-dendrimers, which possess a much lower internal monomer density than their $\delta = 0.1$-counterparts. Indeed, as can be seen in Fig. 5.4(a), the radial distribution functions $G(R)$ and $G_{\mathrm{eff}}(R)$ barely show any difference, all the way up to the maximum density ρ_{max}. Similar to the case $\delta = 0.1$, $G(R)$ shows a slightly more pronounced coordination than $G_{\mathrm{eff}}(R)$, the difference between the two is nevertheless extremely small. The same holds for the structure factors $S(q)$ and $S_{\mathrm{eff}}(q)$, shown in Fig. 5.4(b). Here, even the discrepancy in the compressibility is very small, with $S(q \to 0) = 0.132$ and $S_{\mathrm{eff}}(q \to 0) = 0.138$ at $\rho = \rho_{\mathrm{max}}$. For dendrimers with a higher degree of internal freedom, the pair potential approximation holds all the way up to the overlap concentration. In this respect, it is very satisfactory that it is precisely the model with the value $\delta = 2.0$ that has been found to accurately describe scattering data from real dendrimers [94].

Let us now try to to obtain some physical insight into the mechanisms that cause the true correlation functions to show higher ordering than the effective ones. Suppose that the reason lied in the increasing significance of three-body effective forces. Three-body potentials arise through three-dendrimer overlaps: the region of space in which three spherical objects simultaneously overlap is overcounted when one adds over the three pair interactions and it has to be subtracted anew. Given the fact that any overlap between repulsive monomers gives rise to a correspondingly repulsive interaction, together with the fact that the contribution from the triple-overlap region has to be *subtracted*, leads to the conclusion that triple forces

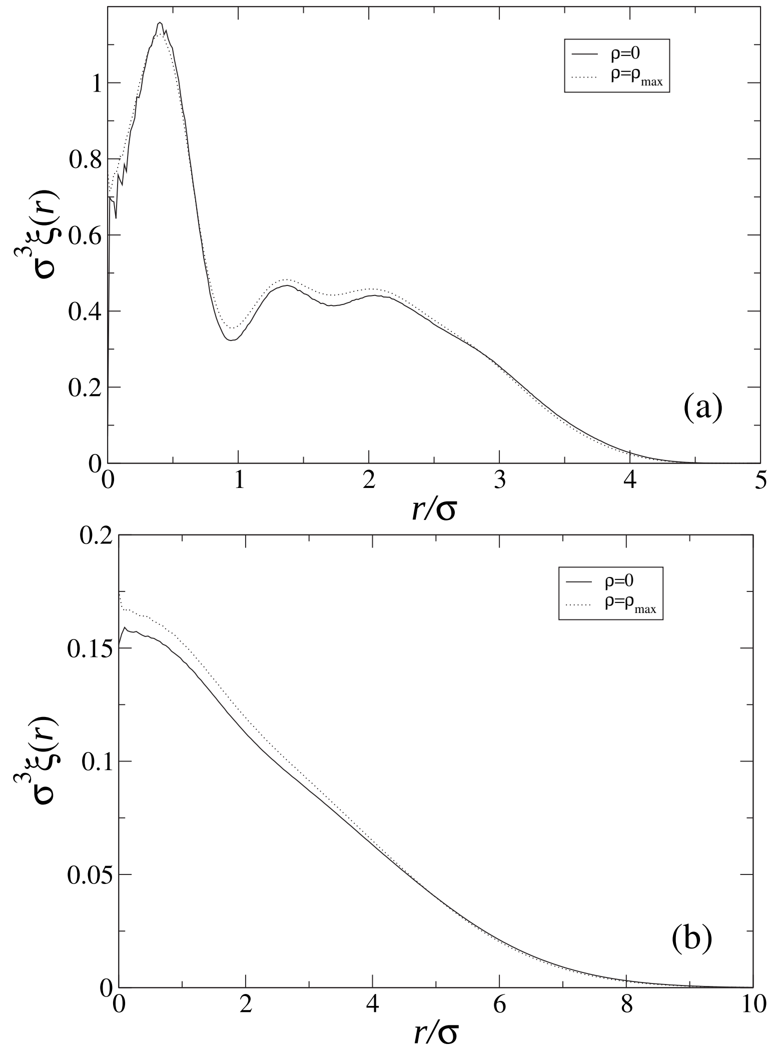

Figure 5.5: The radial monomer density profiles $\xi(r)$ [Eq. (5.8)] of the dendrimers around their centres of mass at infinite dilution ($\rho = 0$) and at the highest density $\rho = \rho_{\max} = 1.07\rho_*$, as indicated on the plots. (a) For model dendrimers with thread length $\delta = 0.1$ and (b) for $\delta = 2.0$. Note the shrinkage and growth of the profiles.

should be *attractive*, as for the case of star polymers [93], as well as self-avoiding polymer chains [89], for which three-body forces have been measured explicitly[3]. Yet, an attractive contribution to the potential energy leads to a *reduced* effective pair repulsion. This is on the one hand intuitively clear and, on the other, it can be put in formal terms by making a density expansion of the density-dependent pair interaction up to linear order in density, see Eq. (10) of Ref. [89]. Thus, we would then obtain a *weakening* of the correlations and an *increase* of the osmotic compressibility, whereas in Figs. 5.3 and 5.4 exactly the opposite is true. In order to obtain the true $G(R)$ at $\rho = \rho_{\max}$ for the $\delta = 0.1$-dendrimers, a renormalised effective pair potential $\tilde{V}_{\text{eff}}^{(2)}(R; \delta, \rho)$ can be employed that is more strongly repulsive than the original one, $V_{\text{eff}}^{(2)}(R; \delta)$; as a matter of fact, we were able to reproduce $G(R)$ at $\rho_{\max}$ by using $\tilde{V}_{\text{eff}}^{(2)}(R; \delta = 0.1, \rho_{\max}) \cong 1.2\, V_{\text{eff}}^{(2)}(R; \delta = 0.1)$. A similar effect has been observed for polymer chains [89], for which the density-dependent, renormalised pair potential necessary to reproduce $G(R)$ at high concentrations was found to be more repulsive than the one that holds at $\rho = 0$, whereas, at the same time, the correction arising from triplet forces alone goes in the opposite direction of weakening the pair repulsions.

The above considerations point to the fact that the deviations between $G(R)$ and $G_{\text{eff}}(R)$ are a genuinely many-body effect that arises from the high concentration of the solution per se and cannot be attributed to three-body forces alone. In particular, the presence of many dendrimers surrounding a given one in the concentrated solution, gives rise to a deformation of the dendrimer itself. To corroborate this statement, we have measured the concentration-dependent monomer density profiles $\xi(r)$ around the dendrimers' centre of mass, given by Eq. (5.8). Results are shown in Fig. 5.5(a) for the case $\delta = 0.1$ and in Fig. 5.5(b) for the case $\delta = 2.0$. It can be seen that as a result of the crowding of the dendrimers at the highest concentration, the monomer profiles become slightly shorter in range and they grow in height; in other words, the dendrimers *shrink* as a result of the increased overall concentration, as can be also witnessed by the reduction of their radius of gyration shown in Fig. 5.6. The molecules that effectively interact are *stiffer* at higher densities than at lower ones; their internal monomer concentration grows with ρ and as a result of this deformation, the interaction between two dendrimers becomes more repulsive than at zero density.

The above claim is supported by the fact that the effect of the concentration on the pair interaction is much more pronounced for the dendrimers with the short thread length than for those with the longer one. Although the monomer profiles for

---

[3] It is intriguing, in this respect, that the three-body forces are also attractive for charged colloids, see Refs. [91] and [92]. However, in the latter case the many-body forces arise through nonlinear counterion screening and the corresponding rearrangements of the counterion clouds, hence a direct analogy with the case at hand cannot be made.

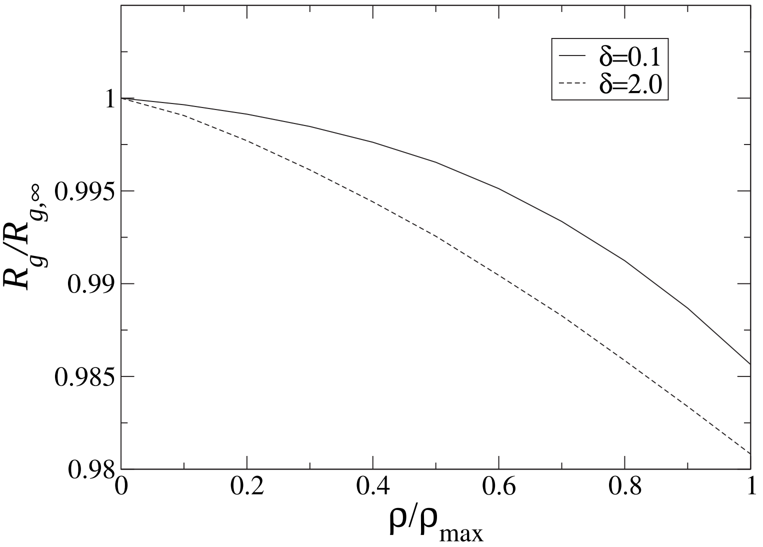

Figure 5.6: The dependence of the dendrimers' radius of gyration on the solution density for the two types of model macromolecules, as indicated in the legend.

both dendrimer kinds grow with ρ, the internal monomer concentration for the stiffer dendrimers is much higher than the one for the softer ones. A concentration-induced increase of $\xi(r)$ has a much stronger effect for the effective interaction of the stiff dendrimers than for the soft ones, since it occurs at a scale of $\sigma^3\xi(r) \sim 0.4$ for the former but at a scale of $\sigma^3\xi(r) \sim 0.1$ for the latter, see Fig. 5.5. The monomer beads are modeled here as hard spheres. The change in the free energy of a hard-sphere fluid upon an increase of the local density is highly nonlinear and grows rapidly with increasing packing fraction, hence the effect is much more pronounced for the case $\delta = 0.1$ than for the case $\delta = 2.0$.

Another way of expressing the vast discrepancy in the monomer crowding of the two systems is to look at the monomer packing fraction η_{m}. As there are N monomers per dendrimer, this quantity is given by the expression

$$\eta_{\mathrm{m}} = \frac{\pi}{6} N\rho\tau^3 \left(\frac{\sigma}{\tau}\right)^3 . \tag{5.14}$$

For both types of dendrimers, $N = 62$ and $\rho_{\max}\tau^3 = 0.605$. Yet, the ratio σ/τ has the value 0.188 for $\delta = 0.1$ and 0.101 for $\delta = 2.0$, see the last column of Table 5.1. Accordingly, at $\rho = \rho_{\max}$ we obtain $\eta_{\mathrm{m}} = 0.13$ for $\delta = 0.1$ but $\eta_{\mathrm{m}} = 0.02$ for $\delta = 2.0$. The soft dendrimers have a much lower monomer packing fraction at ρ_* than the stiffer ones, a result that can be traced to the fact that their radius of gyration is larger.[4] Thus, we conclude that the density-dependence of the pair interaction

---

[4] This is characteristic for non-compact objects: for polymer chains, e.g., one obtains $\eta_{\mathrm{m}} \sim R_g^{-4/3}$

can be traced back to the shrinking of the dendrimers, a phenomenon that leads to increased crowding of the monomers in their interior.

5.4 Total Scattering Intensities and the Factorisation Approximation

In this section we turn our attention to a different question, which is however related to the issues discussed above, namely to the interpretation of scattering data from concentrated dendrimer solutions. As a first step, we consider the form factor $F(q)$, defined by Eq. (5.7). Clearly, $F(q)$ expresses the *intramolecular* correlations between the monomers belonging to a certain dendrimer. When scattering from an infinitely dilute solution, $F(q)$ offers the only contribution to the coherent scattering density. Since all the information about the monomer correlations is encoded in $F(q)$, great experimental effort is devoted to the determination of this quantity. At low values of q, $qR_{g,\infty}$, the form factor delivers information about the overall size of the molecule whereas at higher values of the scattering wavevector, $q \sim 1/a$, where a is the monomer length, information about the monomer correlations and the fractal dimension of the object is hidden [19, 97, 98].

Although $F(q)$ is experimentally measured at the limit $\rho \to 0$, the same quantity can be defined at any density. At arbitrary concentrations, $F(q)$ will in general change with respect to its form at infinite dilution, due to possible deformations of the macromolecules. In Fig. 5.7 we show the form factors for the two model dendrimers at the lowest and at the highest simulate densities. It can be seen there that there is only a small change in both cases, which takes the form of a slight extension of $F(q)$ to higher q-values as the concentration increases. This is consistent with the shrinkage of the dendrimers and the corresponding decrease of the gyration radius. Indeed, in the Guinier regime, $qR_g < 1$, the form factor has a parabolic profile, $F(q) \cong N[1 - (qR_g)^2/3]$, and a reduction of R_g manifests itself as a swelling in q-space and vice versa [99].

Let us now turn our attention to the total coherent scattering intensity from all monomers, $I(q)$, given by Eq. (5.10). It is clear from its definition that $I(q)$ can also be measured in the monomer-resolved simulation and this has been done for both dendrimer species, characterised by the maximum thread extensions $\delta = 0.1$ and $\delta = 2.0$. In attempting to model complex polymeric entities as soft colloids, it is a common procedure to separate the intramolecular from the intermolecular correlations and to write down approximations for the quantity $I(q)$ in which the two types of correlations appear in a factorised fashion. Here we are going to put this approach into a test and figure out the limits of its validity as far as dendritic

---

at the overlap concentration [19].

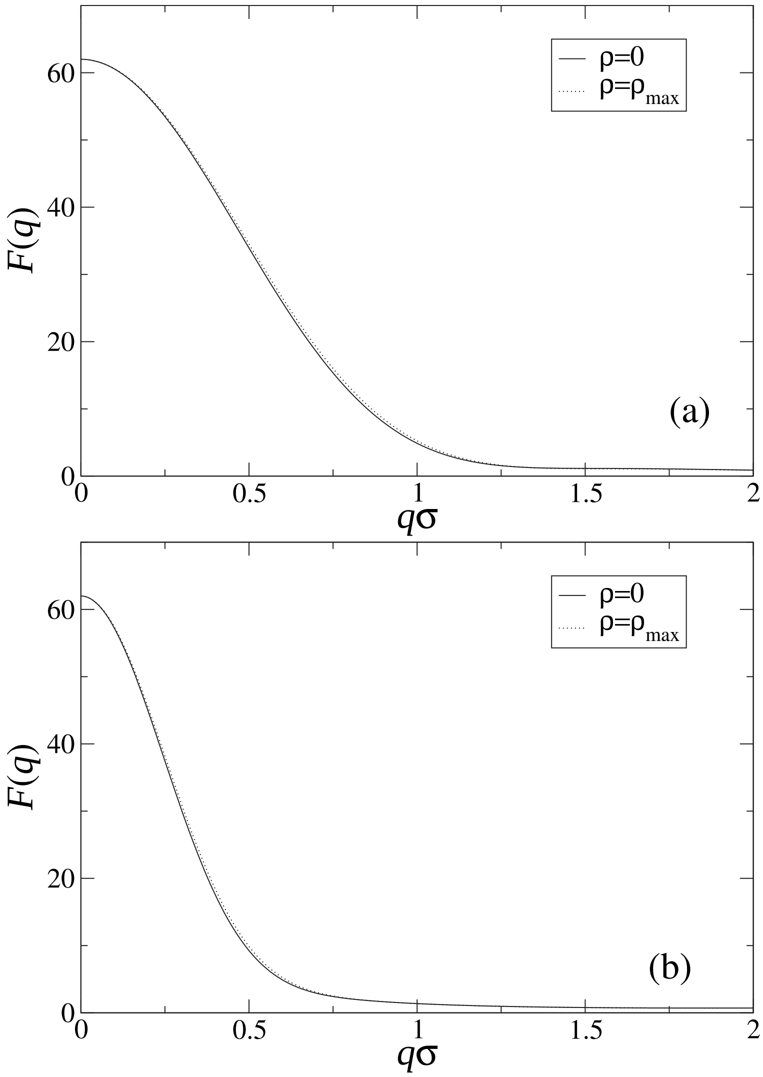

Figure 5.7: The form factors measured in the monomer-resolved simulations for one isolated dendrimer molecule ($\rho = 0$, solid line) and at the highest density ($\rho = \rho_{\max}$, dotted line). The model dendrimers have maximum thread length (a) $\delta = 0.1$ and (b) $\delta = 2.0$.

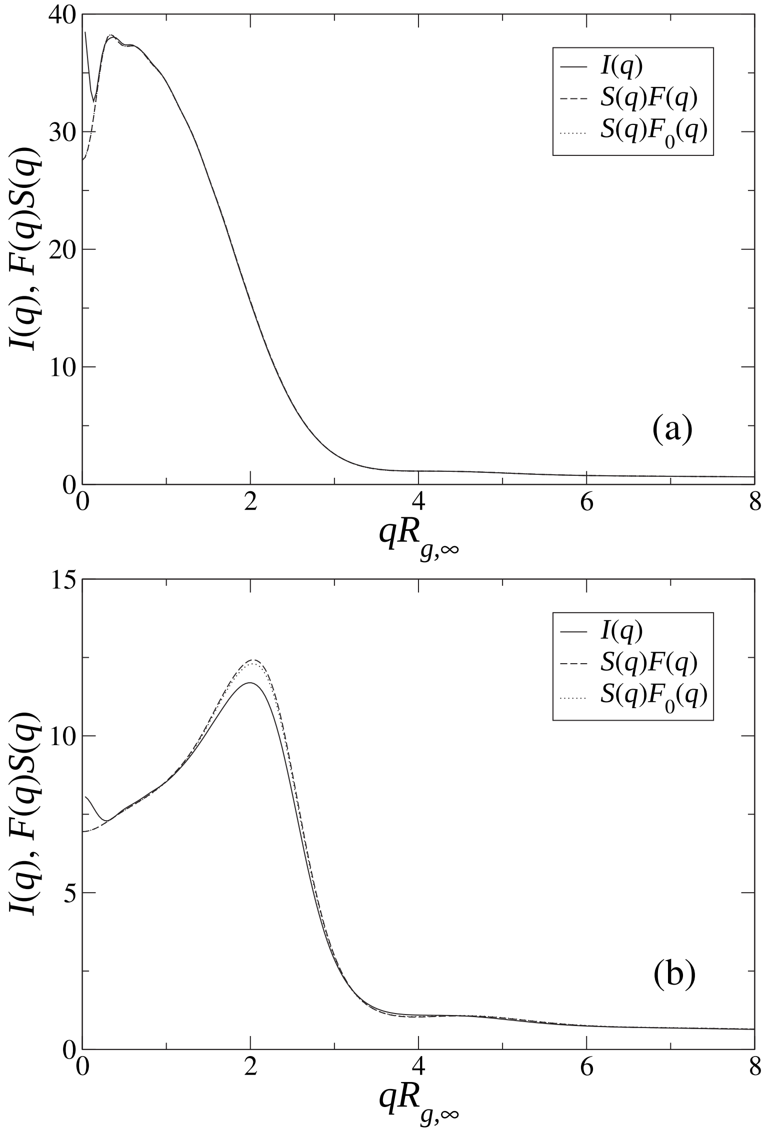

Figure 5.8: The total coherent scattering intensity $I(q)$ [Eq. (5.10)] from concentrated $\delta = 0.1$-dendrimer solutions, compared with the result from the factorisation approximation, Eq. (5.19), at different overall concentrations ρ. (a) $\rho = 0.1\rho_{\max}$ and (b) $\rho = 0.5\rho_{\max}$. Results using both the form factor $F(q)$ at the given density and its counterpart at infinite dilution, $F_0(q)$ are shown for the factorisation approximation.

molecules are concerned. A similar test has been carried out by Krakoviack *et al.* [100] who compared results from the PRISM model for polymers with simulations and with the factorisation ansatz.

As a first approximate step, one assumes that the intramolecular conformations and centre-of-mass correlations decouple from each other. Correspondingly, Eq. (5.10) takes the approximate form:

$$I(q) \cong \frac{1}{MN} \sum_{\alpha=1}^{M} \sum_{\beta=1}^{M} \sum_{i=1}^{N} \sum_{j=1}^{N} \langle \exp\left[-i\mathbf{q} \cdot (\mathbf{R}_\alpha - \mathbf{R}_\beta)\right] \rangle \left\langle \exp\left[-i\mathbf{q} \cdot \left(\mathbf{u}_\alpha^i - \mathbf{u}_\beta^j\right)\right] \right\rangle . \tag{5.15}$$

The approximation inherent in Eq. (5.15) above is a reasonable one for dendrimers. Indeed, as it has been shown in Ref. [35], the monomer degrees of freedom are correlated at length scales $\sim \sigma$, whereas for the overall densities ρ considered here, the centres of mass are correlated at lengths at least $\sim R_g$ and the two are well-separated from each other. Hence, at the wavevector-scale $q_{\mathrm{CM}} \sim 1/R_g$ at which the centre-of-mass $S(q)$ shows structure, the dendrimers still appear as compact objects and the internal fluctuations can be decoupled from the intermolecular ones. The second approximation is now the following. Suppose that we are at sufficiently low densities, so that close approaches between the centres of mass of the dendrimers are very rare and they carry therefore a negligible statistical weight. Then, since monomers belonging to different dendrimers stay far apart, it is reasonable to assume that the deviations from their respective centres of mass are uncorrelated. In this case, one can approximately write:

$$\begin{aligned} \frac{1}{N} \sum_{i=1}^{N} \sum_{j=1}^{N} \left\langle \exp\left[-i\mathbf{q} \cdot \left(\mathbf{u}_\alpha^i - \mathbf{u}_\beta^j\right)\right] \right\rangle &\cong \frac{1}{N} \sum_{i=1}^{N} \sum_{j=1}^{N} \left\langle \exp\left(-i\mathbf{q} \cdot \mathbf{u}_\alpha^i\right) \right\rangle \left\langle \exp\left(i\mathbf{q} \cdot \mathbf{u}_\beta^j\right) \right\rangle \\ &= \frac{1}{N} \left\langle \hat{\xi}_{\mathbf{q}} \right\rangle \left\langle \hat{\xi}_{-\mathbf{q}} \right\rangle , \end{aligned} \tag{5.16}$$

where $\xi_{\mathbf{q}}$ is the Fourier transform of the monomer density operator $\hat{\xi}(\mathbf{r})$ around the centre of mass of an arbitrary dendrimer:[5]

$$\hat{\xi}(\mathbf{r}) = \sum_{i=1}^{N} \delta\left(\mathbf{r} - \mathbf{u}_\alpha^i\right) . \tag{5.17}$$

Clearly, the right hand side of Eq. (5.16) has no dependence on the dendrimer index. At the same time, it has been shown in Ref. [35] that the product $N^{-1}\langle\hat{\xi}_{\mathbf{q}}\rangle\langle\hat{\xi}_{-\mathbf{q}}\rangle$ is an excellent approximation for the form factor $F(q)$ of the dendrimers, deviations from the exact expression in Eq. (5.7), $F(q) = N^{-1}\langle\hat{\xi}_{\mathbf{q}}\hat{\xi}_{-\mathbf{q}}\rangle$, appearing only at high

---

[5] The quantity $\xi(\mathbf{r})$ defined in Eq. (5.8) is simply the expectation value of the operator $\hat{\xi}(\mathbf{r})$.

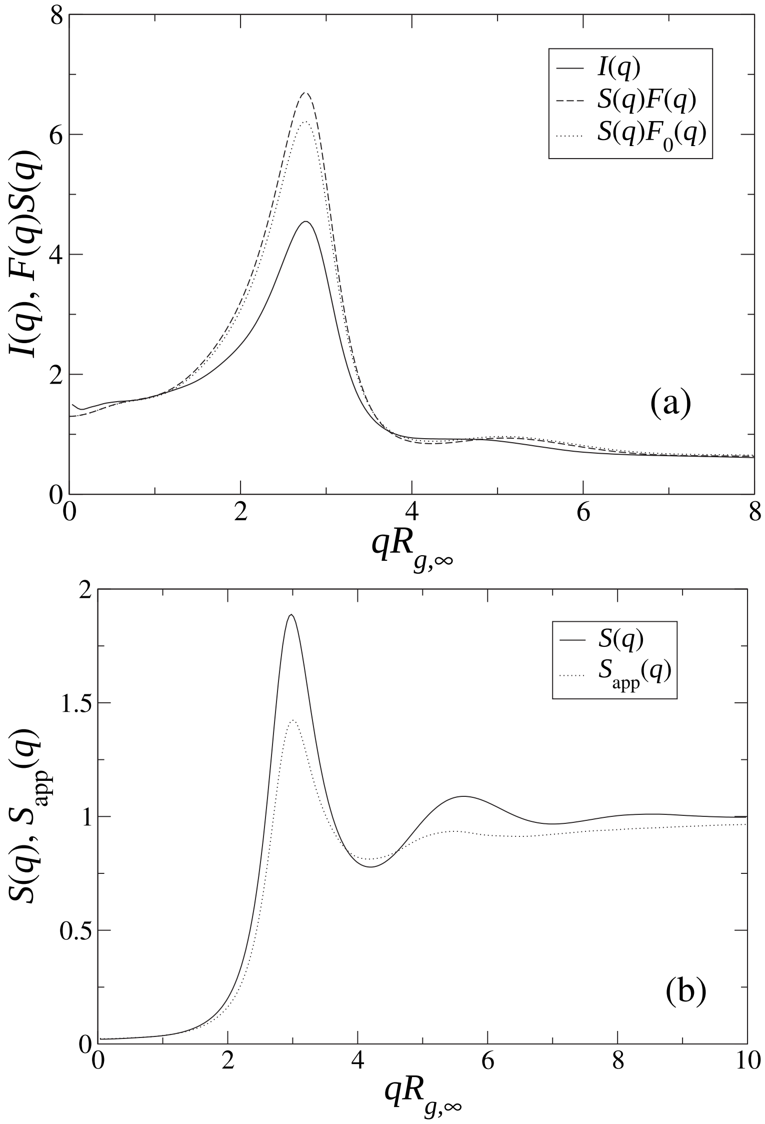

Figure 5.9: (a) Same as Figs. 5.8(a) and (b) but for $\rho = \rho_{\max}$. (b) The true structure factor $S(q)$ between the centres of mass at $\rho = \rho_{\max}$, as obtained from the monomer-resolved simulations, compared with the apparent structure factor $S_{\text{app}}(q) = I(q)/F_0(q)$.

q-values that are unreachable in a typical SANS experiment. The approximation inherent in Eq. (5.16) has been derived for monomers belonging to different dendrimers ($\alpha \neq \beta$) and now, in view of the results of Ref. [35], it can be also applied to the case $\alpha = \beta$. Putting everything together, we obtain

$$\frac{1}{N}\sum_{i=1}^{N}\sum_{j=1}^{N}\left\langle \exp\left[-\mathrm{i}\mathbf{q}\cdot\left(\mathbf{u}_{\alpha}^{i}-\mathbf{u}_{\beta}^{j}\right)\right]\right\rangle \cong F(q). \tag{5.18}$$

Eqs. (5.15) and (5.18) now yield the oft-employed *factorisation approximation*:

$$I(q) \cong S(q)F(q), \tag{5.19}$$

whose validity will be tested in what follows.

The assumptions that went into the derivation of Eq. (5.19) above become exact when the particles from which one scatters are rigid colloids [101], in which case individual scattering centres are devoid of a fluctuating nature. In this context, it is important to note that there is an analog of the factorisation approximation that is applied in the theory of concentrated polymer solutions and carries the name "rigid particle assumption" [100, 102]. Here, one starts from Eq. (5.15) and assumes that monomer-monomer correlations between monomers belonging to different polymers are identical to the intramolecular correlations in any chain [100]. Under this assumption, the second factor on the right-hand-side of Eq. (5.15) above takes the form:

$$\frac{1}{N}\sum_{i=1}^{N}\sum_{j=1}^{N}\left\langle \exp\left[-\mathrm{i}\mathbf{q}\cdot\left(\mathbf{u}_{\alpha}^{i}-\mathbf{u}_{\beta}^{j}\right)\right]\right\rangle \cong \frac{1}{N}\sum_{i=1}^{N}\sum_{j=1}^{N}\left\langle \exp\left[-\mathrm{i}\mathbf{q}\cdot\left(\mathbf{u}_{\alpha}^{i}-\mathbf{u}_{\alpha}^{j}\right)\right]\right\rangle = F(q), \tag{5.20}$$

and, in conjunction with Eq. (5.15), the factorisation approximation of Eq. (5.19) follows once again. Krakoviack *et al.* tested the validity of Eq. (5.19) for polymer solutions, finding that it breaks down for high polymer densities.

We have put the validity of Eq. (5.19) into a strong test by comparing the directly measured total coherent scattering intensity $I(q)$ with the product $F(q)S(q)$, where for the latter quantity both factors are the ones measured in the same simulation. Results are shown in Figs. 5.8 and 5.9(a) for the $\delta = 0.1$-dendrimers as well as in Figs. 5.10 and 5.11(a) for the $\delta = 2.0$-dendrimers. It can be seen that the factorisation approximation is valid at the lowest density shown ($\rho = 0.1\rho_{\mathrm{max}}$) but that its quality becomes poorer as the concentration of the solution increases. A dramatic breakdown can be seen in Fig. 5.9(a) for the more compact dendrimers, whereas the breakdown is also clear (but less spectacular) for the more open dendrimers, Fig. 5.11(a).

We can now trace back to the physical origins of the breakdown of the factorisation approximation, Eq. (5.19). There is first of all a weak breakdown of the

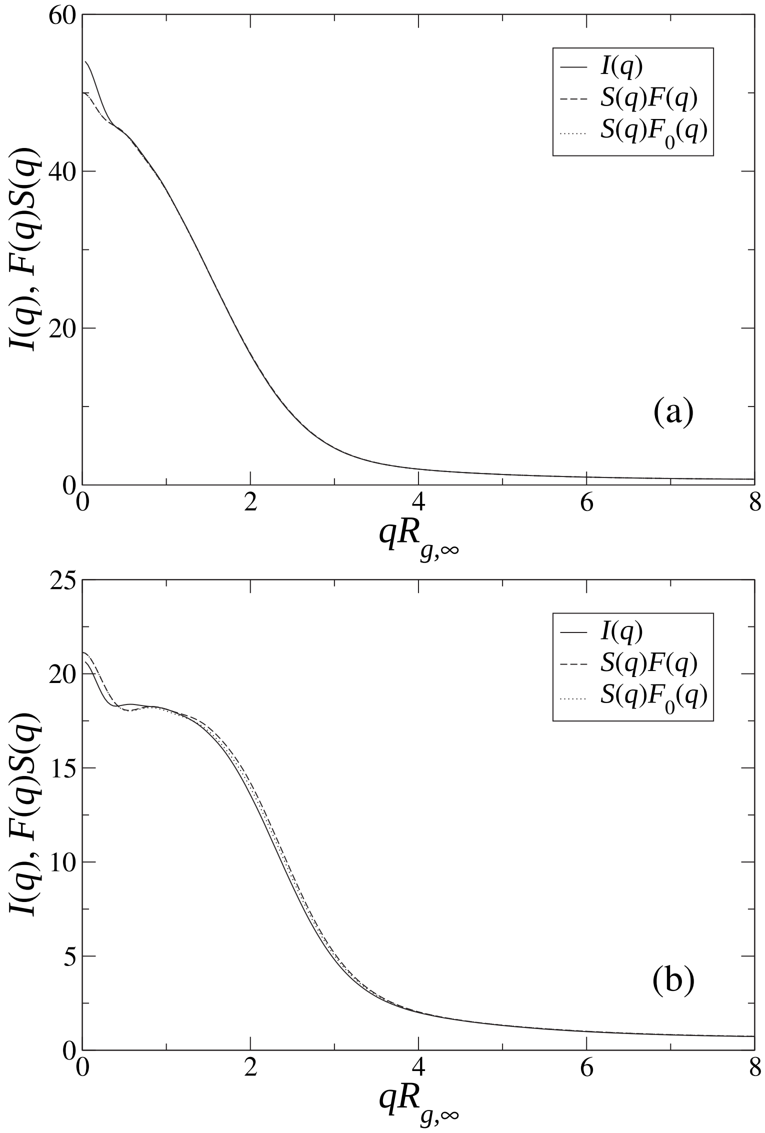

Figure 5.10: Same as Fig. 5.8 but for $\delta = 2.0$-dendrimers.

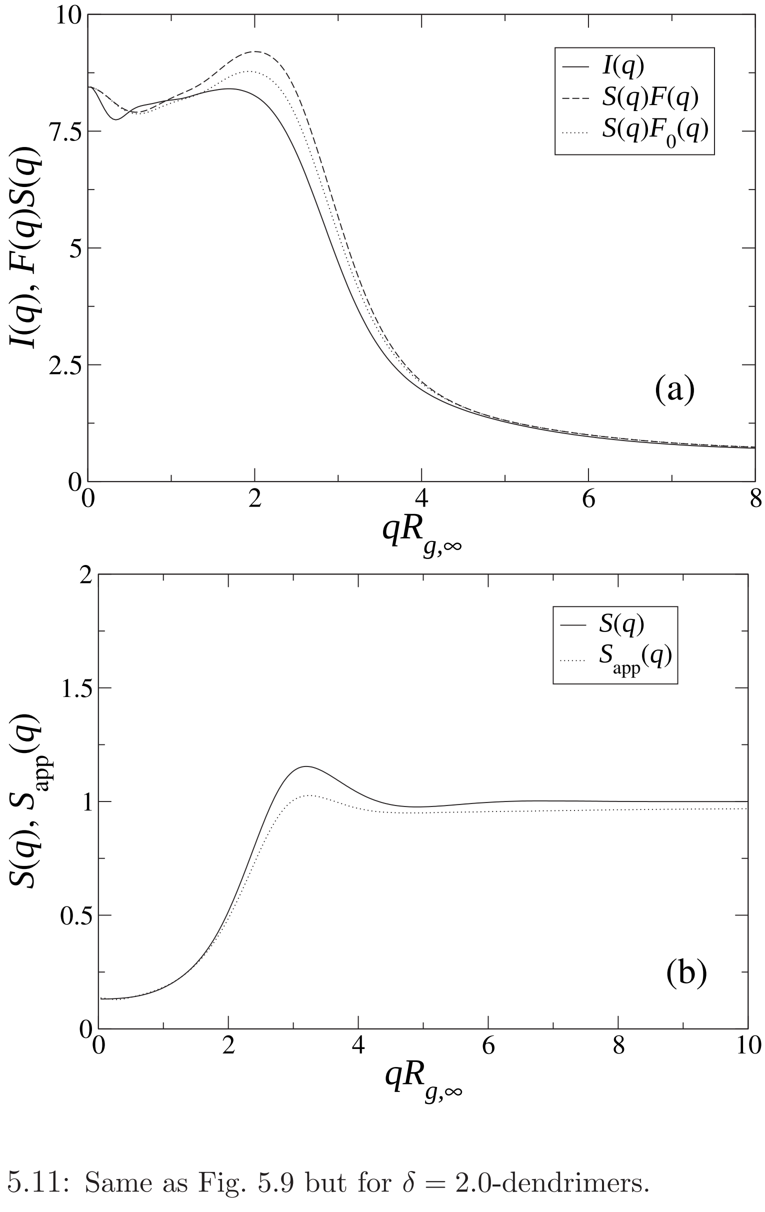

Figure 5.11: Same as Fig. 5.9 but for $\delta = 2.0$-dendrimers.

first assumption, Eq. (5.15), in which the centre-of-mass coordinates were decoupled from the fluctuating monomers. Indeed, were this approximation to be true, then the form factor $F(q)$ would remain unchanged at all concentrations. This is however not the case, as the results in Fig. 5.7 demonstrate: the dendrimers shrink as ρ grows. Yet, the difference between the infinite-dilution form factor, $F_0(q)$ and its counterpart at finite density, $F(q)$, is not sufficient to account for the failure of the factorisation approximation. As can be seen in Figs. 5.8(b), 5.9(a), 5.10(b) and 5.10(a), the product $S(q)F(q)$ is in even *worse* agreement with $I(q)$ than the product $S(q)F_0(q)$. The reason for the breakdown of Eq. (5.19) lies in the assumption inherent in deriving the approximation of Eq. (5.18), namely that fluctuations between monomers belonging to different dendrimers are uncorrelated. At sufficiently low densities ρ, this is a reasonable assumption. However, in approaching the overlap density ρ_*, it does not hold any more. As monomers from different dendrimers begin to crowd with one another, their coordinates with respect to their centres of mass become more and more strongly correlated and Eq. (5.18) loses its validity. In this respect, it is not surprising that the breakdown of Eq. (5.19) is more dramatic for the $\delta = 0.1$-dendrimers than for the $\delta = 2.0$-ones. In the former case, the monomer packing fraction is higher and the corresponding correlations between monomers belonging to different molecules stronger than in the latter. To put it in more pictorial terms: at the overlap concentration it is not any more possible to tell to which dendrimer a monomer belongs, see Fig. 5.2. A clear separation between intra- and inter-dendrimer fluctuations is not any more possible.

We finally discuss the consequences of the above findings for the interpretation of scattering data obtained from concentrated dendrimer solutions. The validity of Eq. (5.19) is often taken for granted: the form factor $F(q)$ is measured in a SANS- or SAXS experiment at low concentrations and extrapolated to infinite dilution to obtain the quantity $F_0(q)$. Thereafter, the measured coherent scattering intensity at any concentration, $I(q)$ is divided through $F_0(q)$, the result being interpreted as the structure factor of the system. In order to differentiate it from $S(q)$, we emphasise here that this is only an *apparent* structure factor $S_{\mathrm{app}}(q)$, given by

$$S_{\mathrm{app}}(q) = \frac{I(q)}{F_0(q)}. \tag{5.21}$$

In Figs. 5.9(b) and 5.11(b) we compare the apparent structure factors for the two dendrimer species at the highest simulated density with the true ones. It can be seen that the process of applying Eq. (5.21) has the effect of producing apparent structure factors that are everywhere lower than the true ones and they even fail to reach the asymptotic value unity at the range considered.

Such structure factors from concentrated dendrimer solutions have been published in Refs. [103] and [104], in which they have been correctly termed 'apparent'. It is important here to point out that apparent structure factors can lead to false conclusions regarding the validity of the pair potential approximation in mesoscopic theories of dendrimer solutions. Indeed, as we have explicitly shown in this work, many-body effective potentials play only a minor role in concentrated dendrimer solutions, therefore, one can obtain accurate structure factors from theory by working with a density-independent pair potential. If, however, these structure factors were to be compared with the apparent experimental quantities $S_{\mathrm{app}}(q)$, discrepancies of the kind shown in Figs. 5.9(b) and 5.11(b) would show up. It would be then possible to argue that these discrepancies are due to the breakdown of the pair potential approximation but, as we have shown here, this conclusion would be unwarranted. The reason for the disagreement between theory and 'experiment' would, in this case, lie in the employment of an *erroneous* approximation, Eq. (5.19), in deriving apparent structure factors from the experimental data. It is worth noting that Krakoviack *et al.* [100] reached similar conclusions for the case of polymer solutions, although they did not formally introduce an apparent structure factor into their considerations.

Chapter 6

Dendrimer Mixtures

We use effective Gaussian interactions to investigate the behaviour of binary dendrimer mixtures. Depending on the choice of the dendrimer architecture, which readily influences the concomitant interaction potentials, we find macroscopic demixing or micro-phase separation, i. e., a state characterised by undamped periodic concentration fluctuations. Furthermore, we observe pattern formation under confinement. (An extended version of this chapter will be published in [111].)

6.1 Introduction

The possibility to realise Gaussian interactions in physical systems opens up a host of possibilities for exploring the occurrence of phenomena that have been predicted recently for Gaussian mixtures. These systems can be materialised, e. g., by using dendrimer mixtures of different generations and/or flexibility, in order to bring about effective Gaussian repulsions in which the non-additivity parameter of the cross-interaction can be tuned. In such cases, one may be able to observe a wealth of interesting phenomena, going from demixing [105] to microphase separation [108, 109] and pattern formation under confinement [108].

The Gaussian interaction potentials employed in [108], the cross-interaction between unlike particles in particular, were chosen reasonably but arbitrarily, in order to obtain micro-phase separation. The possibility to obtain Gaussian interaction potentials from simulations of dendrimers enables us to investigate Gaussian mixtures that correspond to *real* systems. In chapter 4, we only considered the interaction between two dendrimers of the same generation and with the same parameter δ, finding Gaussian potentials. We may now extend this procedure to unlike dendrimers, so that the cross-interaction is consistent within this model. Due to the flexibility in modifying the dendrimers' architecture, the interaction between like particles can be tuned systematically (see chapter 4); the cross-interaction between the two species, however, is hard to pre-estimate.

We investigate two-component dendrimer mixtures by means of theory and MC simulations employing effective interactions. The latter were obtained from monomer resolved MC simulations for dendrimers of different generations and varying thread length δ in the bead-thread model as described in chapter 4. In contrast to chapters 4 and 5, we use here simple Gaussian fits to the effective interaction potentials, which is a good approximation for long thread lengths $\delta \gtrsim \sigma$.

We consider a two-component mixture consisting of M_1 particles of species 1 and M_2 particles of species 2 enclosed in a volume V, with the partial densities $\rho_i = M_i/V, \quad i = 1, 2$ and the total density $\rho = \rho_1 + \rho_2$. Furthermore, we define $x = \rho_2/\rho$ as the concentration parameter for species 2. The pair interaction potential between dendrimers of species i and j obtained from monomer-resolved siulations is given by $V_{ij}(R) = \epsilon_{ij} \exp(-R^2/R_{ij}^2)$.

Under confinement, the concentration fluctuations cannot propagate freely but obey the prescribed geometry leading to patterns in the concentration distribution which can easily be observed in the partial density profiles.

6.2 Theory

The Ornstein-Zernike (OZ) equations for $h_{ij}(R)$ in Fourier space for a two-component liquid can be written as

$$\hat{h}_{ij}(q) = \frac{N_{ij}(q)}{D(q)}, \tag{6.1}$$

where $h_{ij}(R) = G_{ij}(R) - 1$, with the numerators

$$\begin{aligned} N_{11}(q) &= \hat{c}_{11}(q) + \rho_2[\hat{c}_{12}^2(q) - \hat{c}_{11}(q)\hat{c}_{22}(q)]; \\ N_{22}(q) &= \hat{c}_{22}(q) + \rho_1[\hat{c}_{12}^2(q) - \hat{c}_{11}(q)\hat{c}_{22}(q)]; \\ N_{12}(q) &= \hat{c}_{12}(q); \end{aligned} \tag{6.2}$$

and the denominator

$$D(q) = [1 - \rho_1\hat{c}_{11}(q)][1 - \rho_2\hat{c}_{22}(q)] - \rho_1\rho_2\hat{c}_{12}^2(q), \tag{6.3}$$

where $\hat{c}_{ij}(q)$ is the FT of the direct pair correlation function $c_{ij}(r)$ [105]. The partial pair distribution function $G_{ij}(R)$, $(i, j = 1, 2)$, defined as [31]

$$\rho_i\rho_j G_{ij}(R) = \left\langle \sum_{\alpha=1}^{M_i} \sum_{\beta=1}^{M_j} \delta\left(\mathbf{R} + \mathbf{R}_\alpha - \mathbf{R}_\beta\right) \right\rangle \tag{6.4}$$

is proportional to the probability of finding a particle of species i at a distance R from a particle of species j.

When $D(q) = 0$, the partial structure factors $S_{ij}(q) = \delta_{ij} + \sqrt{\rho_i \rho_j}\hat{h}_{ij}(q)$ diverge. If $S(q)$ diverges at $q = 0$, the system becomes unstable to the density modulations of long wavelengths, i. e., the two species demix (macro-phase separation). The condition $1/S(q = 0) \equiv 0$ defines the spinodal line of the phase diagram. A divergence at a wavenumber $q \neq 0$ corresponds to a purely oscillatory behaviour of $Rh_{ij}(R)$ for $R \to \infty$ [108], implying undamped periodic concentration fluctuations, termed micro-phase separation. The λ-line is defined as the locus of of points at which $D(q) = 0$; outside this line $D(q) > 0$ for all q values [108]. On this line, the fluid becomes unstable with respect to periodic concentration fluctuations.

6.3 Random Phase Approximation

We employ the simple random phase approximation (RPA) for the excess Helmholtz free energy functional of the inhomogeneous mixture:

$$\mathcal{F}_{\text{ex}}[\{\rho_i\}] = \frac{1}{2}\sum_{ij}\int \mathrm{d}\mathbf{R}_1 \int \mathrm{d}\mathbf{R}_2\, \rho_i(\mathbf{R}_1)\rho_j(\mathbf{R}_2)V_{ij}(|\mathbf{R}_1 - \mathbf{R}_2|). \tag{6.5}$$

This functional generates the RPA[1] for the pair direct correlation functions,

$$c_{ij}^{(2)}(\mathbf{R}_1, \mathbf{R}_2) = -\frac{\beta\delta^2\mathcal{F}_{\text{ex}}}{\delta\rho_i(\mathbf{R}_1)\delta\rho_j(\mathbf{R}_2)} = -\beta V_{ij}(|\mathbf{R}_1 - \mathbf{R}_2|) \tag{6.6}$$

where $\beta = (k_B T)^{-1}$ [68]. Inserting this simple closure into equation (6.3) yields the spinodal or the λ-line if existing. The validity of the RPA for Gaussian potentials has been established in [76, 88, 105] and generally for bounded or even weakly diverging soft potentials in [106, 107].

The RPA closure to the OZ equations may be used to calculate the pair correlation functions $G_{ij}(R)$ via Fourier transform. Alternatively, they can also be obtained by using DFT via the RPA test-particle route: Within DFT, the profiles $\rho_i(\mathbf{R})$ are calculated by minimising the grand potential functional [68, 108]:

$$\Omega[\{\rho_i\}] = \mathcal{F}[\{\rho_i\}] - \sum_{i=1}^{2}\int \mathrm{d}\mathbf{R}(\mu_i - V_i^{\text{ext}}(\mathbf{R}))\rho_{\mathrm{i}}(\mathbf{R}), \tag{6.7}$$

where $\mathcal{F} = \mathcal{F}_{\text{id}} + \mathcal{F}_{\text{ex}}$, and $\mathcal{F}_{\text{id}}$ is the ideal gas part of the free energy functional, μ_i are the chemical potentials and $V_i^{\text{ext}}(\mathbf{R})$ are the external potentials, in this case those due to the fixed test particle of species j. Then, $G_{ij}(R) = \rho_i(R)/\rho_i^{\text{bulk}}$.

Moreover, the DFT can also be used to calculate density profiles in confined geometries. Here, $V_i^{\text{ext}}(\mathbf{R})$ in equation (6.7) are the wall potentials. The RPA has benn shown to be reliable for the Gaussian core model in [108].

---

[1] Sometimes this approximation is also called mean spherical approximation, or Debye-Hückel approximation in the context of charged systems.

6.4 Bulk Results

In this section, we consider the bulk structure for two different binary mixtures, which exhibit macro-phase and micro-phase separation respectively. Close to the spinodal and the λ-line, bulk simulations become impractical due to the long-range power-law/oscillatory nature of the correlation functions for the case of spinodal/λ-line instabilities, respectively, requiring very large systems. We thus compare theoretical results to simulations well below the spinodal or the λ-line respectively. Here, we can exclude finite size effects by performing simulations at the same density but different total numbers of dendrimers ($M = 20,000$ and $100,000$), that both yield identical results.

6.4.1 Macro-phase Separation

The first system we investigate, hereafter referred to as 'system A', consists of G4 dendrimers with $\delta = 2.0\sigma$, in the following termed species 1, and G3 dendrimers with $\delta = 3.0\sigma$ (species 2). Here, the ranges of the interaction potentials are very similar, but they differ in the prefactor. The parameters of the effective interactions $V_{ij}(R) = \epsilon_{ij} \exp(-R^2/\mathrm{R}_{ij}^2)$ are

$$\begin{aligned} \epsilon_{11} &= 11.6\, k_B T, \quad R_{11} = \sqrt{34}\sigma \\ \epsilon_{22} &= 3.45\, k_B T, \quad R_{22} = \sqrt{31}\sigma \\ \epsilon_{12} &= 6.4\, k_B T, \quad R_{12} = \sqrt{33}\sigma. \end{aligned}$$

Here, we find that $D(q) = 0$ for $q = 0$, i.e., the system demixes and thus has a spinodal. The latter is shown in figure 6.1. The radial distribution functions $G_{ij}(R)$ are shown for a density $\rho \mathrm{R}_{11} = 1.49$ and concentration $x = 0.5$. The results obtained by inserting the RPA closure into the OZ relation fit well to the simulational results for large radii $R > R_{11}$. At small R, deviations and even unphysical negative values of $G(R)$ appear. More accurate results are obtained by using DFT via the RPA test-particle route, where positive values of $G(R)$ are guaranteed.

The spinodal is located at rather high densities: for $x = 0.5$, the corresponding monomer density is $\sigma^3 \rho_m = 0.47$, where σ is the monomer diameter. Here, the validity of pair potential is questionable, but the tendency of macro-phase separation is already observable at lower densities, where the structure factors develop a local maximum at $q = 0$ with increasing density, as shown in figures (6.3)-(6.4) for $x = 0.5$.

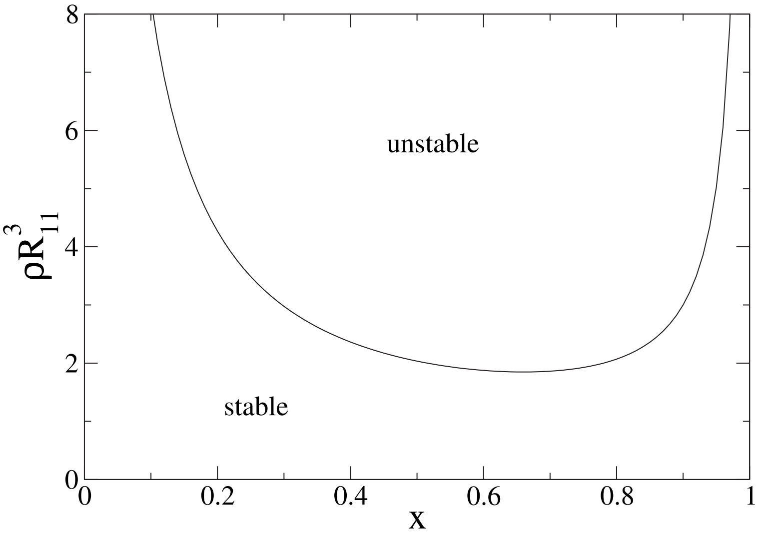

Figure 6.1: Spinodal for system A.

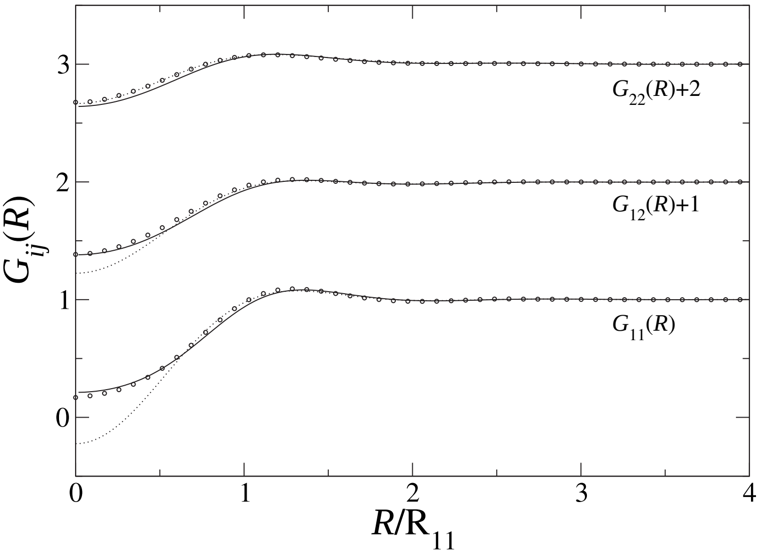

Figure 6.2: Radial distribution function $G_{ij}(R)$ for system A with a total density $\rho R_{11}^3 = 1.49$ and concentration $x = \rho_2/\rho = 0.5$. The circles denote the MC-results, the full lines the DFT test-particle results and the dashed lines are obtained by inserting the RPA closure into the OZ equations. (The DFT results are courtesy of A. J. Archer)

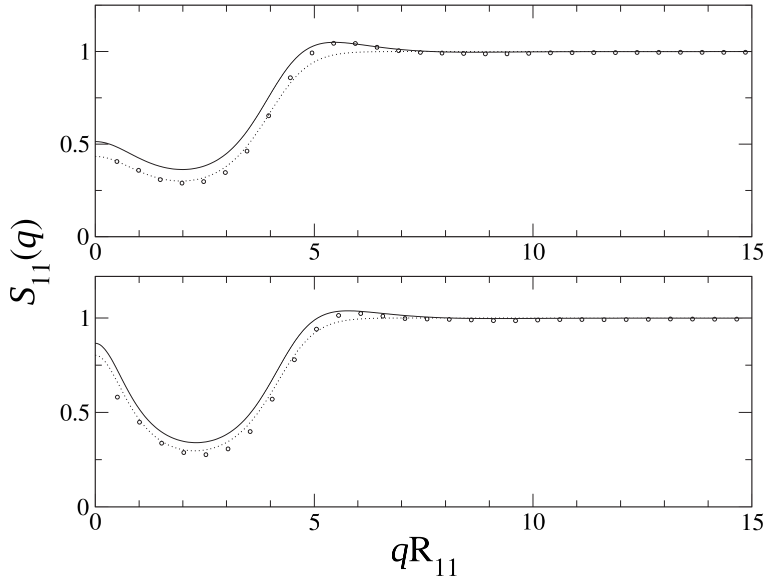

Figure 6.3: The partial structure factor $S_{11}(q)$ for system A at concentration $x = 0.5$ for the densities $\rho\mathrm{R}_{11}^3 = 1.0$ (top) and $\rho\mathrm{R}_{11}^3 = 1.49$ (bottom). The circles denote the MC-results, the full lines the DFT test-particle results and the dashed lines are obtained by inserting the RPA closure into the OZ equations. (The DFT results are courtesy of A. J. Archer)

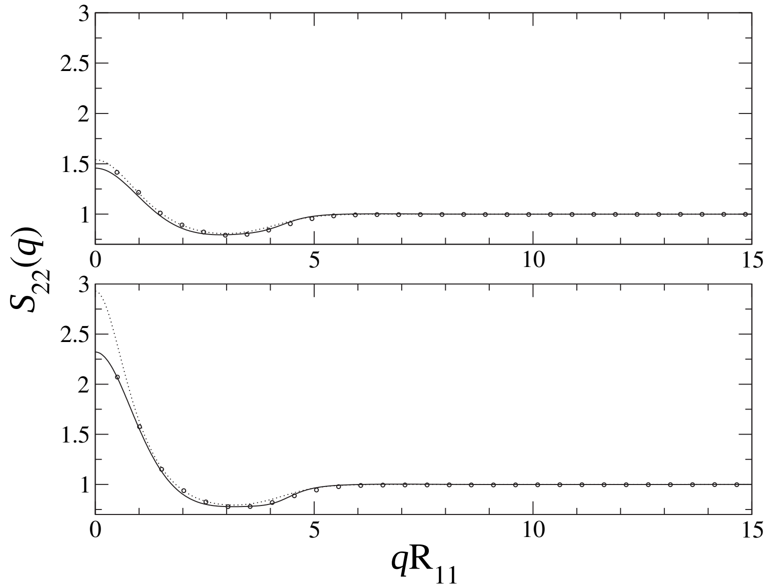

Figure 6.4: Same as figure 6.3 but for S_{22}.

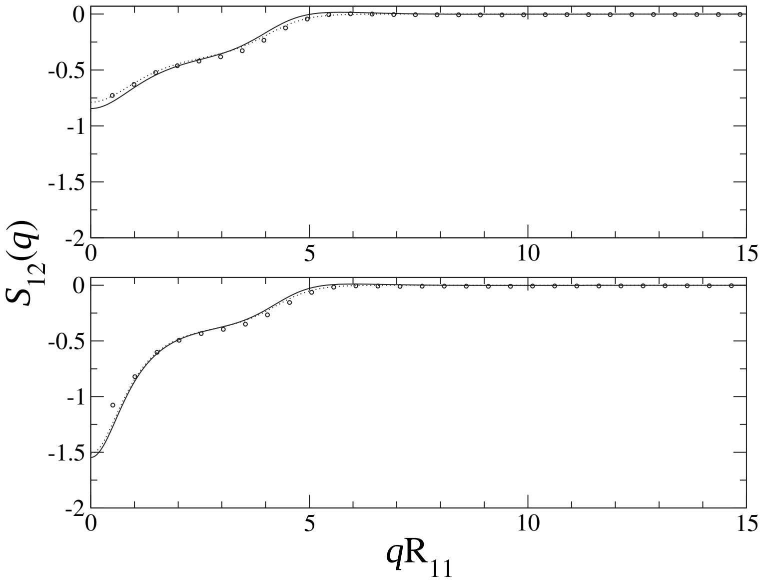

Figure 6.5: Same as figure 6.3 but for S_{12}.

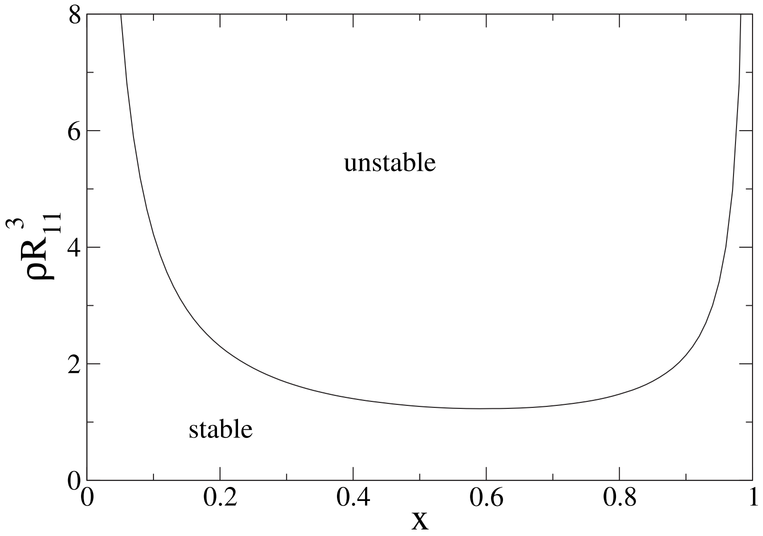

Figure 6.6: The λ-line for system B.

6.4.2 Micro-phase Separation

The second Gaussian mixure we investigate (system ‘B’) represents G3 dendrimers with thread length $\delta = 2.0\sigma$ and G4 dendrimers with $\delta = 4.7\sigma$. Here, the G4-G4 interaction is very soft, and the G3-G3 repulsion is comparatively strong and short ranged. The parameters for the effective interactions $V_{ij}(R) = \epsilon_{ij}\exp(-R^2/\mathrm{R}_{ij}^2)$ obtained from MC simulations are

$$\begin{aligned}\epsilon_{11} &= 6.3\,k_BT, \quad R_{11} = \sqrt{21}\sigma \\ \epsilon_{22} &= 3.1\,k_BT, \quad R_{22} = \sqrt{100}\sigma \\ \epsilon_{12} &= 3.2\,k_BT, \quad R_{12} = \sqrt{52}\sigma.\end{aligned}$$

This system exhibits a divergence of the partial structure factors at a non-zero wavelength. The corresponding λ-line is shown in figure 6.6. It is located at rather high densities: its minimum density $\rho\mathrm{R}_{11}^3 = 1.23$ corresponds to a monomer density of $\sigma^3\rho_m = 0.63$. The radial distribution functions are shown in figure 6.7 for $x = 0.5$ and $\rho\mathrm{R}_{11}^3 = 0.96$ that is 76% of the density at the λ-line for this value of x. Here, long range oscillations with a wavelength $\lambda \sim 1.8\mathrm{R}_{22}$ are already visible. Moreover, the fact that $G_{22}(0) > 1$ shows that the dendrimers of species 2 prefer complete overlap.

Figures (6.8)-(6.10) show the partial structure factors for $x = 0.5$ and the densities $\rho\mathrm{R}_{11}^3 = 0.72$ and $\rho\mathrm{R}_{11}^3 = 0.96$. The peaks arise at a wavenumber $q\mathrm{R}_{11} \sim 1.6$. Again, theory is in good agreement with the simulation results.

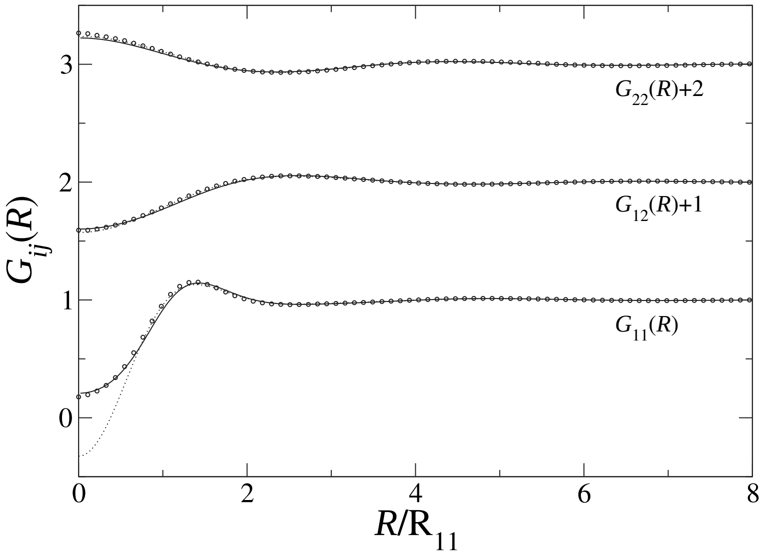

Figure 6.7: Radial distribution function $G_{ij}(R)$ for system B with a total density $\rho \mathrm{R}_{11}^3 = 0.96$ and concentration $x = \rho_2/\rho = 0.5$. The circles denote the MC-results, the full lines the DFT test-particle results and the dashed lines are obtained by inserting the RPA closure into the OZ equations. (The DFT results are courtesy of A. J. Archer)

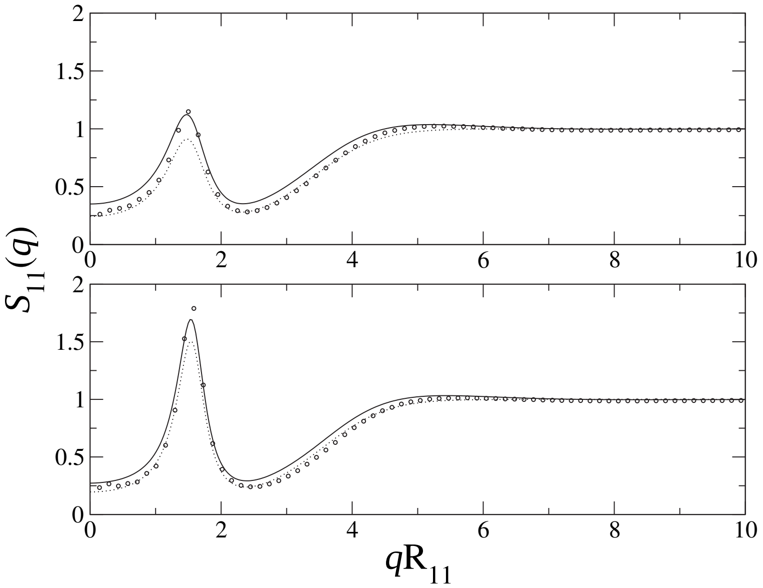

Figure 6.8: The partial structure factor $S_{11}(q)$ for system B at concentration $x = 0.5$ for the densities $\rho\mathrm{R}_{11}^3 = 0.72$ (top) and $\rho\mathrm{R}_{11}^3 = 0.96$ (bottom). The circles denote the MC-results, the full lines the DFT test-particle results and the dashed lines are obtained by inserting the RPA closure into the OZ equations. (The DFT results are courtesy of A. J. Archer)

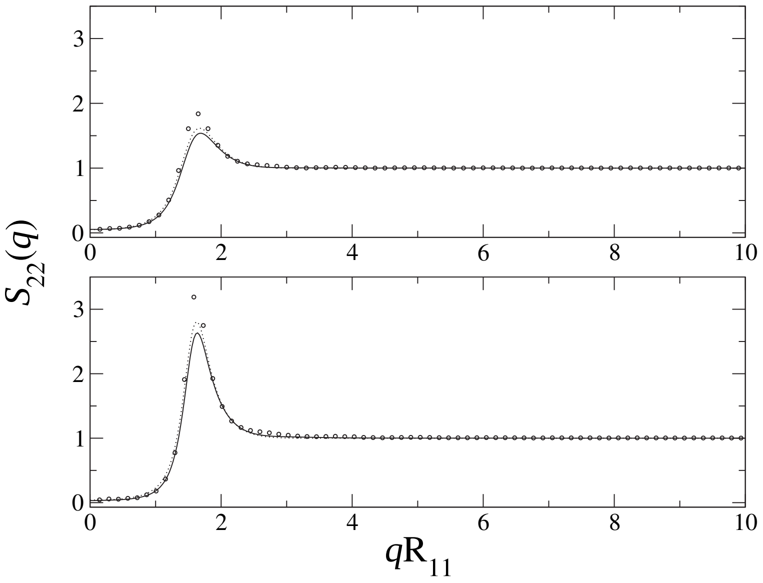

Figure 6.9: Same as figure 6.9 but for S_{22}.

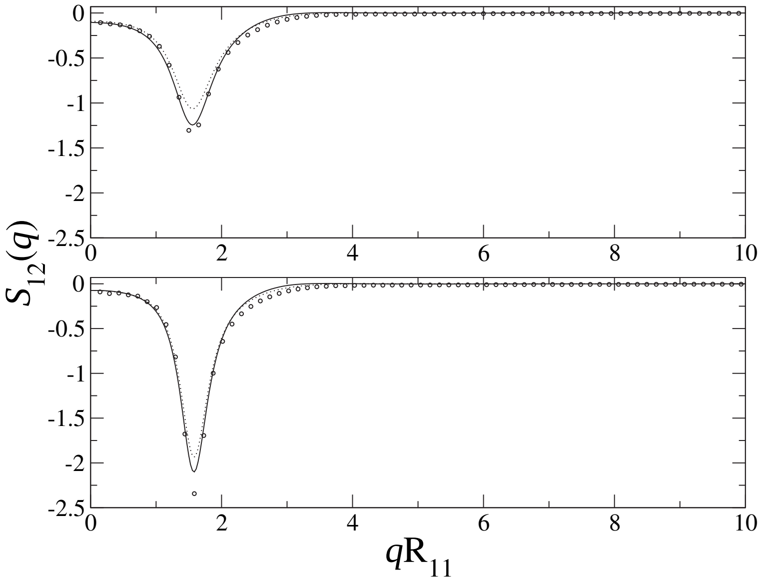

Figure 6.10: Same as figure 6.8 but for S_{12}.

6.5 Confined Geometry

We now expose the systems A and B from the previous section to external potentials. Here, we solely use spherical confinements. First we use the simplest (but somewhat unrealistic) spherical potential, where the centres of the particles interact with a hard wall, i. e.,

$$V_i^{\mathrm{ext}}(R) = \begin{cases} 0 & \text{for} \quad R < \mathrm{R}_{\mathrm{wall}} \\ \infty & \text{otherwise.} \end{cases} \tag{6.8}$$

The radial partial density profiles for systems A and B are shown in figures 6.11 and 6.13 respectively. The DFT results fit very well to the simulational ones and also capture the details of the highly structured profiles. However, a slight phase shift is noticeable in the micro-phase separation case. The bulk behaviour (micro- or macro-phase separation) predicted for the two system is also reflected in the density profiles under confinement. System A separates into two regions as can be seen from figure 6.11: there are almost exclusively particles of species 2 in the center of the cavity for $R \lesssim 8\,\mathrm{R}_{11}$ with constant density, whereas species 1 is located near the wall, showing layer-like ordering due to the presence of the wall. System B, in contrast, shows ‘onion-like’ order of layers alternating from rich in species 1 to rich in species 2.

The above wall potential is unrealistic as the dendrimers do not interact with the wall until their centres of mass have reached it. In order to model the wall interaction more realistic, a soft potential range of the dendrimers’ radius would take into account that the monomers can interact with the wall when its centre of mass approaches to it. Here, we choose Yukawa potentials, given by

$$V_i^{\mathrm{ext}}(R) = \begin{cases} \epsilon_{ii} \exp[-(\mathrm{R}_{\mathrm{wall}} - R)/\mathrm{R}_{ii}]/(\mathrm{R}_{\mathrm{wall}} - R) & \text{for} \quad R < \mathrm{R}_{\mathrm{wall}} \\ \infty & \text{otherwise,} \end{cases} \tag{6.9}$$

using ϵ_{ii} and R_{ii} of the interaction potentials $V_{ij}(R)$.

For system B (micro-phase separation), there are only minimal changes due to the different wall potential; in the simulational results as well as in the DFT ones (compare figures 6.13 and 6.14). But for sytem A (macro-phase separation), we find a strong sensitivity with respect to the form of the wall potential: in the hard wall case, species 1 is preferred, and in the Yukawa-wall case species 2, as can be seen by comparing figures 6.11 and 6.12.

Other confining geometries could also be interesting, such as parallel walls, where the resulting lamellar ordering of the micro-phase separating mixture causes strong anisotropy regarding the shear properties of the system. In this way, the mixture could act as a lubricant, facilitating relative motion of the walls parallel to each other.

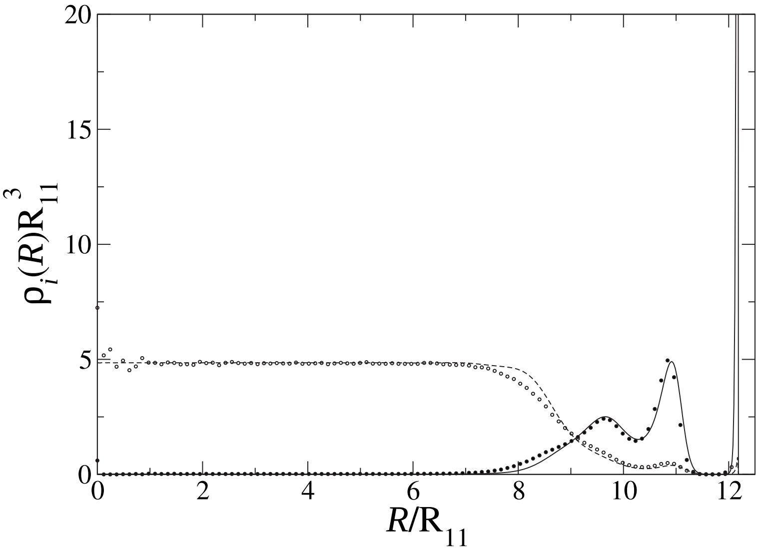

Figure 6.11: Radial density profiles ρ_i for system A with concentration $x = 0.5$ and a total density $\rho\mathrm{R}_{11}^3 = 3.97$ confined in a spherical hard wall potential. The circles denote the MC results, the lines those of DFT. (species 1: full line, full circles; species 2: dashed line, open circles) The DFT results are courtesy of A. J. Archer.

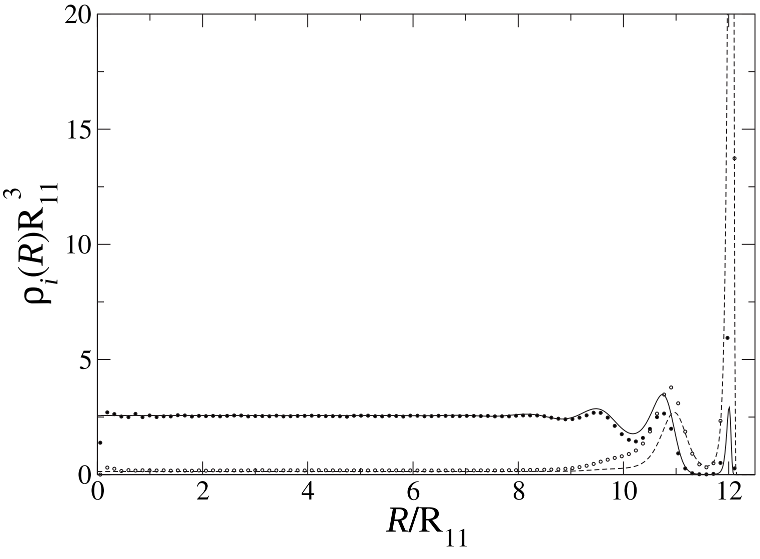

Figure 6.12: Same as figure 6.11 but for a Yukawa-like wall.

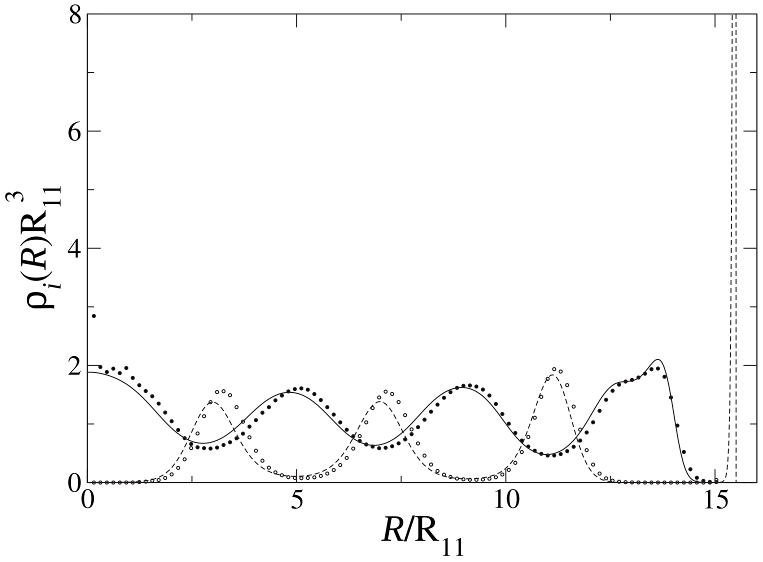

Figure 6.13: Same as figure 6.11 but for system B.

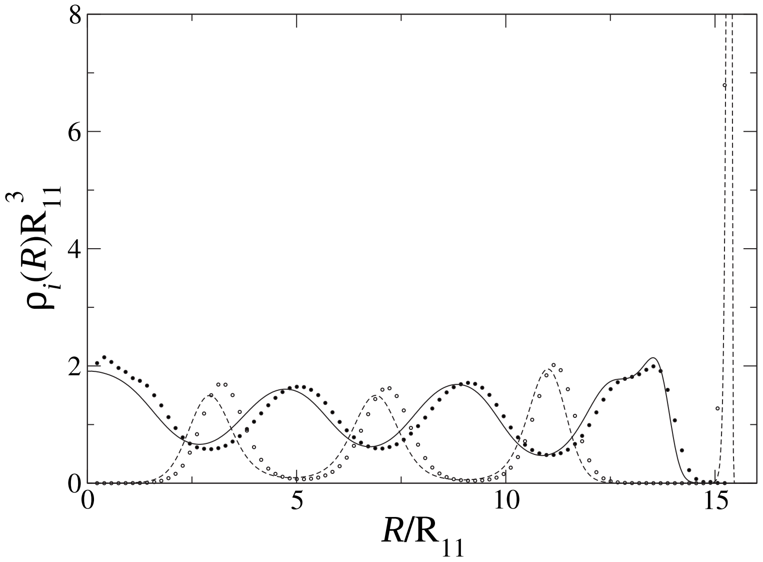

Figure 6.14: Same as figure 6.13 but for a Yukawa-like wall.

Chapter 7

Conclusions

We have introduced a ‘minimal’ model to describe dendrimers of various generations. Our approach takes into account the connectivity and steric interactions of self-avoiding dendrimers in the very simple way, by viewing the monomers as hard spheres connected by ideal threads that have a maximum possible extension. We focused on dendrimers with spacer length $P = 1$ and on athermal solvents in this study, but the generalization to arbitrary P’s and to solvents of varying quality is straightforward. One can introduce a tunable effective attraction of varying shape, depth and range in order to model solvents of decreasing quality. We have shown that the dendrimers are a distinct class of polymeric colloids, possessing a density profile that features a broad plateau of constant density. This makes them clearly distinct from other branched polymeric entities, such as star polymers for which a density profile $\xi(r) \sim r^{-4/3}$ holds, [98] or star-branched polyelectrolytes, in which case a dependence of the form $\xi(r) \sim r^{-2}$ obtains. [60,110] In addition, the height of this plateau was found to be generation-dependent, a feature that causes the size of the dendrimers to grow with the number of monomers slower than the inverse-third power of the latter, as has been observed experimentally. The form factors obtained are also in very good agreement with experiments.

An important property of the models we considered is a strong insensitivity of the results on the details of the microscopic model. This holds both for the bead-thread model, when the contour length is varied by a factor 8 (from 0.05 to 0.40) and for the Lennard-Jones–FENE potential. When lengths are scaled with the radius of gyration of the molecule, results practically collapse on master curves. This has the implication that one cannot determine on the basis of comparisons with scattering data from dilute solutions alone which model is the most realistic for the system at hand. On the other hand, a quantity that most certainly does depend on the model details is the effective interaction (potential of mean force) between two dendrimers.

Having shown that the bead-thread model yields reliable results, we employed it to calculate the interaction potential. By carrying out extensive computer simulations with two different models for dendrimers, and for a variety of parameters within those, we have demonstrated that the effective interaction between their centres of mass can be very well approximated by a Gaussian form. The quantitative characteristics of this Gaussian potential, i. e. its strength and range, can be tuned through a variation of the spacer length and the generation number. Thus, dendrimers are one additional physical system in which the novel family of bounded, ultrasoft and tunable effective interactions can be materialised. Our study has been supplemented by an approximate density-functional theory in which the connections between the monomers have been replaced by a fictitious external potential. This approach captures the main features of the interaction, although the agreement with the simulation results is still not quantitative.

Due to the simplicity of the bead thread model, monomer resolved simulations of concentrated solutions are possible, where correlation functions between the centres of mass of the macromolecules and the individual monomers themselves can be calculated. Moreover, we have carried out simulations employing previously calculated effective interaction potentials. By comparing the real-space correlation functions obtained by the two simulation approaches, we found that many-body effective potentials play a minor role up to the overlap density and they can be altogether ignored for open dendrimers with long bond lengths. Our finding for the scattering intensity, on the other hand, is that the factorisation approximation of this quantity into a form- and a structure factor loses its validity as one approaches the overlap concentration. Structure factors that are obtained from experimental data by dividing the scattering intensity through the form factor can be seriously in error.

It appears, therefore, that the extraction of an accurate structure factor from concentrated dendrimer solutions is extremely difficult as one approaches the overlap concentration. We anticipate that this result is also valid for other ‘polymeric colloids’ such as star-shaped polymers and brushes. One strategy to circumvent this inherent difficulty is to use the labeling technique, in which a small, inner part of the molecule is protonated and the rest is deuterated in such a way that the contrast between the outermost part of the molecule and the solvent vanishes. In this way, only the innermost part of the molecule will have contrast with the solvent and scatter coherently. Thus, one can reach concentrations for the whole system that exceed ρ_*, whereas the labelled parts are still nonoverlapping. Such a technique was successfully applied, e.g., to star polymers [59].

We also have investigated mixtures of dendrimers, finding macroscopic demixing or micro-phase separation, depending on the choice of the dendrimers’ generation numbers and architecture. Here, in contrast to previous studies concerning microphase separation, we do *not* employ arbitrary Gaussian potentials but those obtained from monomer-resolved simulations of dendrimers. Furthermore, we observe pattern formation under confinement, finding a strong sensitivity with respect to the form of the wall potential. The procedure used for calculation of the dendrimer-dendrimer potentials could also be employed to calculate effective dendrimer-wall interaction potentials in MC simulations.

In this thesis, we have restricted ourselves to flexible and neutral dendrimers, always finding dense-core conformations. In view of practical applications, investigation of stiff or charged dendrimers or modified end monomers is of special interest in order to achieve dense shell configurations. Another question are the dynamical properties of dendrimers and the ability of effective interaction potentials to describe it. These are open questions for future work.

Appendix A

Proof of Equation (4.9)

Let us consider, without loss of generality, the force $\mathbf{F}_1 = -\nabla_{\mathbf{R}_1} V_{\text{eff}}(\mathbf{R}_1, \mathbf{R}_2)$ acting on the centre of mass of the first macromolecule. First, let us define the new variables

$$\mathbf{w}_\alpha = \frac{1}{N} \sum_{i=1}^{N} \mathbf{r}_{i\alpha}, \tag{A.1}$$

with $\alpha = 1, 2$. Our starting point is Eq. (4.5) of the main text. Acting with the $\nabla_{\mathbf{R}_1}$-operator on both sides and carrying out the trivial integrations over the momenta on the right-hand side, we obtain

$$\begin{aligned} \mathbf{F}_1 &= k_B T \left\{ \int \mathrm{d}\mathbf{r}_2^N \int \mathrm{d}\mathbf{r}_1^N \delta(\mathbf{R}_2 - \mathbf{w}_2) \nabla_{\mathbf{R}_1} \delta(\mathbf{R}_1 - \mathbf{w}_1) \exp[-\beta(V_{11} + V_{12} + V_{22})] \right\} \\ &\times \left\{ \int \mathrm{d}\mathbf{r}_2^N \int \mathrm{d}\mathbf{r}_1^N \delta(\mathbf{R}_2 - \mathbf{w}_2) \delta(\mathbf{R}_1 - \mathbf{w}_1) \exp[-\beta(V_{11} + V_{12} + V_{22})] \right\}^{-1}. \end{aligned} \tag{A.2}$$

Let Z be the denominator in Eq. (A.2) above. Writing $\nabla_{\mathbf{R}_1} \delta(\mathbf{R}_1 - \mathbf{w}_1) = -\nabla_{\mathbf{w}_1} \delta(\mathbf{R}_1 - \mathbf{w}_1)$ and taking into account that V_{22} does not depend on the coordinates $\{\mathbf{r}_{i1}\}$, $i = 1, 2, \ldots, N$ of the monomers of the first dendrimer, we thus obtain

$$\begin{aligned} \mathbf{F}_1 &= -\frac{k_B T}{Z} \int \mathrm{d}\mathbf{r}_2^N \delta(\mathbf{R}_2 - \mathbf{w}_2) \exp(-\beta V_{22}) \\ &\times \int \mathrm{d}\mathbf{r}_1^N [\nabla_{\mathbf{w}_1} \delta(\mathbf{R}_1 - \mathbf{w}_1)] \exp[-\beta(V_{11} + V_{12})]. \end{aligned} \tag{A.3}$$

The potential energy function V_{11} depends only on the relative coordinates of the monomers of dendrimer 1. On the other hand, V_{12} contains all the interactions between monomers of different dendrimers, thus for a fixed conformation $\{\mathbf{r}_2^N\}$ of the second dendrimer, it can be considered a function of the variables $\{\mathbf{r}_1^N\}$ only.

Let us introduce a transformation from the set of variables $\{\mathbf{r}_{11}, \mathbf{r}_{21}, \dots, \mathbf{r}_{N1}\}$ into the new variables $\{\mathbf{y}_{21}, \mathbf{y}_{31}, \dots, \mathbf{y}_{N1}, \mathbf{w}_1\}$, where

$$\mathbf{y}_{j1} = \mathbf{r}_{11} - \mathbf{r}_{j1}, \qquad j = 2, 3, \dots, N \tag{A.4}$$

and $\mathbf{w}_1$ is given by Eq. (A.1) above. The Jacobian of this transformation is equal to unity and it is straightforward to show that the inverse transformation reads as

$$\begin{aligned} \mathbf{r}_{11} &= \frac{1}{N}\sum_{j=2}^{N} \mathbf{y}_{j1} + \mathbf{w}_1; && \text{(A.5)} \\ \mathbf{r}_{i1} &= \frac{1}{N}\sum_{j=2}^{N} \mathbf{y}_{j1} - \mathbf{y}_{i1} + \mathbf{w}_1, \;\; j = 2, 3, \dots, N. && \text{(A.6)} \end{aligned}$$

The potential energy functions transform as follows:

$$V_{11} \to \tilde{V}_{11}(\mathbf{y}_{21}, \mathbf{y}_{31}, \dots, \mathbf{y}_{N1}), \tag{A.7}$$

i.e., there is no dependence on the variable $\mathbf{w}_1$, whereas for the cross-interaction term we obtain

$$V_{12}(\mathbf{r}_{11}, \mathbf{r}_{21}, \dots, \mathbf{r}_{N1}) \to \tilde{V}_{12}(\mathbf{y}_{21}, \mathbf{y}_{31}, \dots, \mathbf{y}_{N1}, \mathbf{w}_1), \tag{A.8}$$

where the explicit form of the function $\tilde{V}_{12}$ is obtained by substituting the transformations (A.5) and (A.6) in the function V_{12}, explicitly

$$\tilde{V}_{12} = V_{12}\left(\frac{1}{N}\sum_{j=2}^{N} \mathbf{y}_{j1} + \mathbf{w}_1, \frac{1}{N}\sum_{j=2}^{N} \mathbf{y}_{j1} - \mathbf{y}_{21} + \mathbf{w}_1, \dots, \frac{1}{N}\sum_{j=2}^{N} \mathbf{y}_{j1} - \mathbf{y}_{N1} + \mathbf{w}_1\right). \tag{A.9}$$

Under these transformations, Eq. (A.3) takes the form:

$$\begin{aligned} \mathbf{F}_1 &= -\frac{k_B T}{Z}\int \mathrm{d}\mathbf{r}_2^N \delta(\mathbf{R}_2 - \mathbf{w}_2)\exp(-\beta V_{22}) \\ &\times \int \mathrm{d}\mathbf{y}_1^{N-1} \exp(-\beta \tilde{V}_{11}) \\ &\times \int \mathrm{d}^3 w_1 [\nabla_{\mathbf{w}_1} \delta(\mathbf{R}_1 - \mathbf{w}_1)] \exp(-\beta \tilde{V}_{12}), && \text{(A.10)} \end{aligned}$$

where $\int \mathrm{d}\mathbf{y}_1^{N-1}$ is a shorthand for the multiple integral $\int\int \cdots \int \mathrm{d}^3 y_{21} \mathrm{d}^3 y_{31} \dots \mathrm{d}^3 y_{N1}$. In order to evaluate the last integral in Eq. (A.10), we make use of the property of the delta-function

$$\int \mathrm{d}^3 x \nabla_{\mathbf{x}} \delta(\mathbf{x} - \mathbf{a}) f(\mathbf{x}) = -\nabla_{\mathbf{x}} f(\mathbf{x})|_{\mathbf{x}=\mathbf{a}}. \tag{A.11}$$

Applying now the above formula for the last integral of Eq. (A.10), using the chain rule for Eq. (A.9) and the transformations (A.5) and (A.6), we obtain

$$\begin{aligned}\int\ & \mathrm{d}^3 w_1 [\nabla_{\mathbf{w}_1} \delta(\mathbf{R}_1 - \mathbf{w}_1)] \exp(-\beta \tilde{V}_{12}) \\ = \ & \beta \sum_{i=1}^{N} [\nabla_{\mathbf{r}_{i1}} V_{12}(\mathbf{r}_{11}, \mathbf{r}_{21}, \ldots, \mathbf{r}_{N1})] \exp(-\beta V_{12})|_{\mathbf{w}_1 = \mathbf{R}_1}. \end{aligned} \tag{A.12}$$

Reverting to the original variables, rearranging terms in Eq. (A.10), using Eq. (A.12) and reintroducing formally a $\delta(\mathbf{R}_1 - \mathbf{w}_1)$-function to implement the constraint on the centre of mass, we have

$$\begin{aligned}\mathbf{F}_1 \ = \ & \left\{ \int \mathrm{d}\mathbf{r}_2^N \int \mathrm{d}\mathbf{r}_1^N \delta(\mathbf{R}_2 - \mathbf{w}_2) \delta(\mathbf{R}_1 - \mathbf{w}_1) \right. \\ \times \ & \left. \left[- \sum_{i=1}^{N} \nabla_{\mathbf{r}_{i1}} V_{12}(\{\mathbf{r}_{i1}\}, \{\mathbf{r}_{i2}\}) \right] \exp[-\beta(V_{11} + V_{12} + V_{22})] \right\} \\ \times \ & \left\{ \int \mathrm{d}\mathbf{r}_2^N \int \mathrm{d}\mathbf{r}_1^N \delta(\mathbf{R}_2 - \mathbf{w}_2) \delta(\mathbf{R}_1 - \mathbf{w}_1) \exp[-\beta(V_{11} + V_{12} + V_{22})] \right\}^{-1} \end{aligned} \tag{A.13}$$

The term in the square brackets in the numerator of the right-hand side is the sum of the forces exerted on the monomers of dendrimer 1 from all the monomers of dendrimer 2. There is no contribution to the force from internal forces within the dendrimer, as they cancel in pairs. Moreover, Eq. (A.13) makes it manifest that $\mathbf{F}_1$ is the expectation value of the sum of the individual forces under the constraint of keeping the centres of mass fixed at positions $\mathbf{R}_1$ and $\mathbf{R}_2$. This proves Eq. (4.9) of the main text.

Bibliography

[1] Newkome, G. R.; Moorefield, C. N.; Vögtle, F. *Dendrimers and Dendrons*, Wiley WCH: Weinheim, Germany **2001**.

[2] Trollsås, M.; Atthof, B.; Würsch A.; Hedrick, J. L.; Pople, J. A.; Gast, A. P. *Macromolecules* **2000**, *33*, 6423.

[3] Buhleier, E.; Wehner, W.; Vögtle, F. *Synthesis* **1978**, 155.

[4] Newkome, G. R.; Yao, Z.-Q.; Baker, G. R.; Gupta, V. K. *J. Org. Chem* **1985**, *50*, 2003.

[5] Tomalia, D. A.; Baker, H.; Dewald, J. R.; Hall, M.; Kallos, G.; Martin, S.; Roeck, J.; Ryder, J.; Smith, P. *Macromolecules* **1986**, *19*, 2466.

[6] Bosman, A. W.; Janssen, H. M.; Meijer, E. W. *Hem. Rev.* **1999**, *50*, 1665.

[7] Baars, M. W. P. L.; Meijer, E. W. *Top. Curr. Chem.: Dendrimers II* Springer, **2000**, 131.

[8] Boas U.; Heegaard, P. M. H. *Chem. Soc. Rev.* **2004**, *33*, 43.

[9] Gillies, E. R.; Fréchet, J. M. J. *Drug Disc. Today* **2005**, *10*, 35.

[10] Krause, W.; Hackmann-Schlichter, N.; Maier, F. K.; Müller, R. *Top. Curr. Chem.: Dendrimers II* **2000**, 261.

[11] Tomalia, D. A.; Fréchet, J. M. J., editors *Dendrimers and Other Dendritic Polymers*, Wiley: Chichester 2002.

[12] De Gennes, P. G.; Hervet, H. *J. Phys. Lett. (Paris)* **1983**, *44*, L351.

[13] Tomalia, D. A.; Naylor, A. M.; Goddard III, W. A. *Angew. Chem.* **1990**, *102*, 119; *Angew. Chem. Int. Ed. Engl.* **1990**, *29*, 138.

[14] Lescanec R. L.; Muthukumar M. *Macromolecules* **1990**, *23*, 2280.

[15] Boris, D.; Rubinstein, M. *Macromolecules* **1996**, *29*, 7251.

[16] Zook, T. C.; Pickett, G. T. *Phys. Rev. Lett.* **2003**, *90*, 105502.

[17] Ballauff, M.; Likos, C. N. *Angewandte Chemie Intnl. English Ed.* **2004**, *43*, 2998.

[18] Baschnagel, J.; Binder, K.; Doruker, P.; Gusev, A. A.; Hahn, O.; Mattice, W. L.; Müller-Plathe, F.; Murat, M.; Paul, W.; Santos, S.; Suter, U. W.; Tries, V. *Adv. Polym. Sci.* **2000**, *152*, 41.

[19] Likos, C. N. *Physics Reports* **2001**, *348*, 267.

[20] Nielsen, S.O.; Lopez, C.F.; Srinivas, G.; Klein, M.L. *J. Phys.: Condens. Matter* **2004**, *16*, R481.

[21] Naylor, A. M.; Goddard, W. A.; Kiefer, G. E.; Tomalia, A. D. *J. Am. Chem. Soc.* **1989**, *111*, 2339.

[22] Scherrenberg, R.; Coussens, B.; van Vliet, P.; Edouard, G.; Brackman, J.; de Brabander, F.; Mortensen, K. *Macromolecules* **1998**, *31*, 45.

[23] Cavallo, L.; Fraternali, F. *Chem. Eur. J.* **1998**, *4*, 927.

[24] Zacharopoulos, N.; Economou, I. G. *Macromolecules* **2002**, *35*, 1814.

[25] Mazo, M. A.; Shamaev, M. Y.; Balabaev, N. K.; Darinskii, A. A.; Neelov, I. M. *Phys. Chem. Chem. Phys.* **2004**, *6*, 1285.

[26] Allen, M. P.; Tildesley, D. J. *Computer Simulations of Liquids*, Clarendon, Oxford **1987**

[27] D. Frenkel and B. Smit, *Understanding Molecular Simulation* (Academic, San Diego, **1996**).

[28] Murat, M.; Grest, G. S. *Macromolecules* **1996**, *29*, 1278.

[29] Pötschke, D.; Ballauff, M.; Lindner, P.; Fischer, M.; Vögtle, F. *Macromol. Chem. Phys.* **2000**, *201*, 330.

[30] Rosenfeldt, S.; Dingenouts, N.; Ballauff, M.; Lindner, P.; Likos, C. N.; Werner, N.; Vögtle, F. *Macromol. Chem. Phys.* **2002**, *203*, 1995.

[31] Hansen, J. P.; MacDonald, I. R. *Theory of Simple Liquids*, second edition, Academic: New York, **1986**.

[32] Higgins, J. S.; Benoît, H. C. *Polymers and Neutron Scattering*, Clarendon Press: Oxford, **1994**.

[33] Klein, R.; D'Aguanno, B. in *Light Scattering: Principles and Development* (Ed.: W. Brown), Clarendon Press: Oxford, **1996**.

[34] Barrat, J.-L.; Hansen, J.-P. *Basic Concepts for Simple and Complex Liquids*, Cambridge University Press, **2003**.

[35] Harreis, H. M.; Likos, C. N.; Ballauff, M. *J. Chem. Phys.* **2003**, *118*, 1979.

[36] Sheng, Y.-J.; S. Jiang, S.; Tsao, H.-K. *Macromolecules* **2002**, *35*, 7865.

[37] Lue, L.; Prausnitz, J. M. *Macromolecules* **1997**, *30*, 6650.

[38] Verlet, L. *Phys. Rev.* **1967**, *159*, 98.

[39] Hockney, R. W.; Eastwood, J. W. *Computer Simulations Using Particles*, McGraw-Hill, New York **1981**

[40] Milner, S. T.; Witten, T. A.; Cates, M. E. *Macromolecules* **1988**, *21*, 2610.

[41] Wallace E. J.; Buzza, D. M. A.; Read, D. J. *Macromolecules* **2001**, *34*, 7140.

[42] Mansfield, M. L.; Jeong, M. *Macromolecules* **2002**, *35*, 9794.

[43] Rosenfeldt, S.; Dingenouts, N.; Ballauff, M.; Werner, N.; Vögtle, F.; Lindner, P. *Macromolecules* **2002**, *35*, 8098.

[44] Mansfield, M. L.; Klushin, I. *Macromolecules* **1993**, *26*, 4262.

[45] Carl, W. *J. Chem. Soc., Faraday Trans.* **1996**, *92*, 4151-4154.

[46] Chen, Z. Y.; Cui, S.-M. *Macromolecules* **1996**, *29*, 7943.

[47] Lue, L. *Macromolecules* **2000**, *33*, 2266.

[48] Lyulin, A. V.; Davies, G. R.; Adolf, D. B. *Macromolecules* **2000**, *33*, 3294.

[49] Karatasos, K.; Adolf, D. B.; Davies, G. R. *J. Chem. Phys.* **2001**, *115*, 5310.

[50] Timoshenko, E. G.; Kuznetsov, Yu. A.; Connolly, R. *J. Chem. Phys.* **2002**, *117*, 9050.

[51] Giupponi, G.; Buzza, D. M. A. *Macromolecules* **2002**, *35*, 9799.

[52] Rathgeber, S.; Monkenbusch, M.; Kreitschmann, M.; Urban, V.; Brulet, A. *J. Chem. Phys.* **2002**, *117*, 4047.

[53] Mallamace, F.; Canetta, E.; Lombardo, D.; Mazzaglia, A.; Romeo, A.; Monsù Scolaro, L.; Maino, G. *Physica A* **2002**, *304*, 235.

[54] Mansfield, M. L. *Macromolecules* **2000**, *33*, 8043.

[55] Prosa, T. J.; Bauer, B. J.; Amis, E. J. *Macromolecules* **2001**, *34*, 4897.

[56] Nisato, G.; Ivkov, R.; Amis, E. J. *Macromolecules* **2000**, *33*, 4172.

[57] Likos, C. N.; Schmidt, M.; Löwen, H.; Ballauff, M.; Pötschke, D.;Lindner, P. *Macromolecules* **2001**, *34*, 2914.

[58] Likos, C. N.; Rosenfeldt, S.; Dingenouts, N.; Ballauff, M.; Lindner, P.; Werner, N.; Vögtle, F. *J. Chem. Phys.* **2002**, *117*, 1869.

[59] Likos, C. N.; Löwen, H.; Watzlawek, M.; Abbas, B.; Jucknischke, O.; Allgaier, J.; Richter, D. *Phys. Rev. Lett.* **1998**, *80*, 4450.

[60] Jusufi, A.; Likos, C. N.; Löwen, H. *Phys. Rev. Lett.* **2002**, *88*, 018301; *J. Chem. Phys.* **2002**, *116*, 11011.

[61] Jusufi, A.; Dzubiella, J.; Likos, C. N.; von Ferber, C.; Löwen, H. *J. Phys.: Condens. Matter* **2001**, *13*, 6177.

[62] Grosberg, A. Y.; Khalatur, P. G.; Khokhlov, A. R. *Makromol. Chem. Rapid Commun.* **1982**, *3*, 709.

[63] Schäfer, L.; Baumgärtner, A. *J. Phys. (Paris)* **1986**, *47*, 1431.

[64] Krüger, B.; Schäfer, L.; Baumgärtner, A. *J. Phys. (Paris)* **1989**, *50*, 3191.

[65] Dautenhahn, J.; Hall, C. K. *Macromolecules* **1994**, *27*, 5933.

[66] Louis, A. A.; Bolhuis, P. G.; Hansen, J. P.; Meijer, E. J. *Phys. Rev. Lett.* **2000**, *85*, 2522.

[67] Bolhuis, P. G.; Louis, A. A.; Hansen, J. P.; Meijer, E. J. *J. Chem. Phys.* **2001**, *114*, 4296.

[68] Evans, R. *Adv. Phys.* **1979**, *28*, 143; R. Evans, in *Fundamentals of Inhomogeneous Fluids*, ed. by D. Henderson (Dekker, New York, **1992**).

[69] Yethiraj, A.; Fynewever, H.; Shew, C.-Y. *J. Chem. Phys.* **2001**, *114*, 4323.

[70] Yu, Y.-X.; Wu, J. *J. Chem. Phys.* **2002**, *116*, 7094.

[71] Yu, Y.-X.; Wu, J. *J. Chem. Phys.* **2002**, *117*, 2368.

[72] Nordholm, S.; Johnson, M.; Freasier, B. *Aust. J. Chem.* bf 1980, *33*, 2139; Johnson, M.; Nordholm, S. *J. Chem. Phys.* **1981**, *75*, 1953.

[73] Tarazona, P. *Mol. Phys.* **1984**, *52*, 81; Tarazona, P.; Evans, R. *Mol. Phys.* **1984**, *52*, 847.

[74] Carnahan, N. F.; Starling, K. E. *J. Chem. Phys.* **1969**, *51*, 635.

[75] Götze, I. O.; Likos, C. N. *Macromolecules* **2003**, *36*, 8189.

[76] Lang, A.; Likos, C. N.; Watzlawek, M.; Löwen, H. *J. Phys.: Condens. Matter* **2000**, *12*, 5087.

[77] Dijkstra, M.; Brader, J. M.; Evans, R. *J. Phys.: Condens. Matter* **1999**, *11*, 10079.

[78] Dijkstra, M.; van Roij, R.; Evans, R. *Phys. Rev. Lett.* **1998**, *81* 2268; *ibid.* **1999**, **82**, 117.

[79] Dijkstra, M.; van Roij, R.; Evans, R. *Phys. Rev. E* **1999**, *59*, 5744.

[80] Hansen, J. P.; Löwen, H. *Ann. Rev. Phys. Chem.* **2000**, *51*, 209.

[81] Louis, A. A. *J. Phys: Condens. Matter* **2002**, *14*, 9187.

[82] Stillinger, F. H.; Sakai, H.; Torquato, S. *J. Chem. Phys.* **2003**, *117*, 288.

[83] Sakai, H.; Stillinger, F. H.; Torquato, S. *J. Chem. Phys.* **2003**, *117*, 297.

[84] Dijkstra, M.; van Roij, R.; Evans, R. *J. Chem. Phys.* **2000**, *113*, 4799.

[85] Axilrod, B. M.; Teller, E. *J. Chem. Phys.* **1943**, *11*, 229.

[86] Tau, M.; Reatto, L.; Magli, R.; Egelstaff, P. A.; Barrochi, F. *J. Phys: Condens. Matter* **1989**, *1*, 7131.

[87] Krüger, B.; Schäfer, L.; Baumgärtner, A. *J. Phys. (Paris)* **1989**, *50*, 3191.

[88] Louis, A. A.; Bolhuis, P. G.; Hansen, J. P. *Phys. Rev. E* **2000**, *62*, 7961.

[89] Bolhuis, P. G.; Louis, A. A.; Hansen, J. P. *Phys. Rev. E* **2001**, *64*, 021801

[90] Löwen, H.; Allahyarov, E. *J. Phys: Condens. Matter* **1998**, *10*, 4147.

[91] Brunner, M.; Dobnikar, J.; von Grünberg, H. H.; Bechinger, C. *Phys. Rev. Lett.* **2004**, *92*, 078301.

[92] Dobnikar, J.; Brunner, M.; von Grünberg, H. H.; Bechinger, C. *Phys. Rev. E* **2004**, *69*, 031402.

[93] von Ferber, C.; Jusufi, A.; Likos, C. N.; Löwen, H.; Watzlawek, M. *Eur. Phys. J. E* **2000**, *2*, 311.

[94] Götze, I. O.; Harreis, H. M.; Likos, C. N. *J. Chem. Phys.* **2004**, *120*, 7761.

[95] Götze, I. O.; Likos, C. N. *J. Phys.: Condens. Matter* **2005**, *17*, 1777.

[96] Pötschke, D.; Ballauff, M.; Lindner, P.; Fischer, M.; Vögtle, F. *Macromolecules* **1999**, *32*, 4079.

[97] Higgins, J. S.; Benoît, H. C. *Polymers and Neutron Scattering* (Oxford: Clarendon) **1994**.

[98] For an illuminating review on experimental aspects of scattering from polymeric systems see the article: Grest, G. S.; Fetters, L. J.; Huang, J. S.; Richter, D. *Adv. Chem. Phys.* **1996**, *XCIV*, 67.

[99] Likos, C. N.; Löwen, H.; Poppe, A.; Willner, L.; Roovers, J.; Cubitt, B.; Richter, D. 1998 *Phys. Rev. E* **1998**, *58*, 6299.

[100] Krakoviack, V.; Hansen, J. P.; Louis, A. A. *Europhys. Lett.* **2002**, *58*, 53.

[101] Klein, R.; D' Aguanno, B. in *Light Scattering: Principles and Development*, edited by W Brown (Oxford: Clarendon) **1996**.

[102] Pagonabarraga, I.; Cates, M. E. *Europhys. Lett.* **2001**, *55*, 348.

[103] Topp, A.; Bauer, B. J.; Prosa, T. J.; Scherrenberg, R.; Amis, E. J. *Macromolecules* **1999**, *32*, 8923.

[104] Ramzi, A.; Scherrenberg, R.; Brackman, J.; Joosten, J.; Mortensen, K. *Macromolecules* 1998, *31*, 1621.

[105] Archer, A. J.; Evans, R. *Phys. Rev. E* **2001**, *64*, 041501; *J. Phys.: Condens. Matter* **2002**, *14*, 1131; *J. Chem. Phys.* **2003**, *118*, 9726.

[106] Likos, C. N.; Lang, A.; Watzlawek, M.; Löwen, H. *Phys. Rev. E* **2001**, *63*, 031206.

[107] Archer, A. J.; Evans, R. *J. Phys.: Condens. Matter* **2002**, *14*, 12031.

[108] Archer, A. J.; Likos, C. N.; Evans, R. *J. Phys.: Condens. Matter* **2004**, *16*, L297.

[109] Sear, R. P.; Gelbart, W. M. *J. Chem. Phys.* **1999**, *110*, 4582.

[110] Guenoun, P.; Muller, F.; Delsanti, M.; Auvray, L.; Chen, Y. J.; Mays, J. W.; Tirell, M. *Phys. Rev. Lett.* **1998**, *81*, 3872.

[111] Götze, I. O.; Archer, A. J.; Likos, C. N. *J. Chem. Phys.* **2005** in preparation.

Acknowledgment

I would like to thank cordially Christos N. Likos for his excellent support during the past years. I also wish to thank all members of the department for Theoretical Physics II at the Heinrich-Heine-University of Düsseldorf, my family and my friends. Finally, I gratefully acknowledge for finacial support of the Deutsche Forschungsgemeinschaft.